CRC Report No. A-133

IMPROVED TREATMENT OF FIRE EMISSIONS FOR OZONE AND PM2.5 MODELING

Final Report

October 2024

COORDINATING RESEARCH COUNCIL, INC.
5755 NORTH POINT PARKWAY • SUITE 265 • ALPHARETTA, GA 30022

The Coordinating Research Council, Inc. (CRC) is a non-profit corporation supported by the petroleum and automotive equipment industries with participation from other industries, companies, and governmental bodies on research programs of mutual interest. CRC operates through the committees made up of technical experts from industry and government who voluntarily participate. The five main areas of research within CRC are: air pollution (atmospheric and engineering studies); aviation fuels, lubricants, and equipment performance; heavy-duty vehicle fuels, lubricants, and equipment performance (e.g., diesel trucks); light-duty vehicle fuels, lubricants, and equipment performance (e.g., passenger cars); and sustainable mobility (e.g., decarbonization). CRC's function is to provide the mechanism for joint research conducted by industries that will help in determining the optimum combination of products. CRC's work is limited to research that is mutually beneficial to the industries involved. The final results of the research conducted by, or under the auspices of, CRC are available to the public.

Prepared for:

Coordinating Research Council
5755 North Point Parkway, Suite 265
Alpharetta, GA 30022

Prepared by:

Ramboll Americas Engineering Solutions, Inc.
7250 Redwood Blvd., Suite 105
Novato, CA 94945

August 2024
1690031817_Conv

CRC PROJECT A-133 FINAL REPORT

Improved Treatment of Fire Emissions for Ozone and PM2.5 Modeling

CRC PROJECT A-133 FINAL REPORT IMPROVED TREATMENT OF FIRE EMISSIONS FOR OZONE AND $PM_{2.5}$

Ramboll
7250 Redwood Boulevard
Suite 105
Novato, CA 94945
USA

T +1 415 899 0700
https://ramboll.com

Cover photo by Daniel Roberts, Pixabay

CONTENTS

List of Acronyms and Abbreviations **1**
Executive Summary **4**
1.0 Introduction **6**
1.1 Purpose 6
2.0 Fire Emission Inventories Evaluated **7**
2.1 FINN2.5 7
2.2 GFAS1.2 8
2.3 QFED2.5 8
2.4 FEER1.0 8
2.5 RAVE1.0/RAVE2.0 9
2.6 Fire Chemical Speciation and Secondary Organic Aerosol Issues 9
3.0 Update of FEI Processor and CAMx **10**
3.1 Update of CAMx SOA Module to Treat Semi-Volatility of Fire PM Emissions 10
3.2 FEI Processor Updates 10
4.0 Development of a PGM Database for Evaluating Alternative Fire Emissions **13**
4.1 Model Selection 13
4.2 Episode Selection 13
4.3 Horizontal Modeling Domains 15
4.4 Vertical Layer Structure 17
4.5 Meteorological Inputs 19
4.5.1 WRF Summer 2021 36 km Domain Simulation 19
4.6 Initial Concentration and Boundary Condition Inputs 20
4.7 Anthropogenic Emission Inputs 20
4.8 Natural Emission Inputs 20
4.9 CAMx Ancillary Inputs 21
4.10 Summary of CAMx Options 21
5.0 Case Study of 2021 Western U.S. Wildfires and EMissions Comparison **23**
5.1 2021 Case Study Wildfires 23
5.1.1 2021 California Wildfires 24
5.1.2 2021 Colorado Wildfires 26
5.1.3 2021 Arizona Wildfires 27
5.1.4 2021 Utah Wildfires 27
5.1.5 2021 Oregon Wildfires 27
5.1.6 2021 Washington Wildfires 27
5.1.7 2021 Idaho Wildfires 27
5.1.8 2021 Wyoming Wildfires 28
5.1.9 2021 New Mexico Wildfires 28
5.2 FEI Emissions Comparison 28
6.0 Evaluation of Alternative Fire Emissions **31**
6.1 Testing Database for Alternative Fire Emissions 31

6.2 Model Performance Goals and Benchmarks 31
6.3 Available Aerometric Data for Evaluations 32
6.4 Initial Testing (Phase I) 34
6.4.1 Ozone Evaluation 34
6.4.2 $PM_{2.5}$ Evaluation and Comparison 38
6.4.3 Speciated $PM_{2.5}$ Evaluation and Comparison 41
6.4.4 Final Selection of FEIs for Phases II-V 42
6.5 Further Testing, Evaluation and Optimization (Phases II-V) 42
6.5.1 Phase II: NOx Speciation 42
6.5.2 Phase III: Temporal and Vertical Allocation 44
6.5.3 Phase IV: RAVE2.0 Evaluation 46
6.5.4 Phase V: SOAP3 and Unscaled RAVE2.0 Evaluation 47
7.0 Conclusions and Recommendations 51
8.0 References 53

Appendices

Appendix A: FEI Emissions Comparison Maps and Summaries

Table of Figures

Figure 3-1. Design of the FEI processing tool. 12
Figure 3-2. Map showing RAVE1.0 extent (orange) and 36-km CAMx domain (red). 12
Figure 4-1. Acres burned by wildfires in California 1987-2022. 14
Figure 4-2. Daily ozone AQI for Denver Metro (DM) and North Front Range (NFR) in Colorado (CO), Clark County (CC), Nevada (NV) and Salt Lake (SL) County, Utah (UT) and the years 2016-2023. 15
Figure 4-3. 12US2 12 km and 36US3 36 km grid resolution domains used in EPA's 2016v3 modeling platform. 16
Figure 4-4. 12-km western U.S. and 36US3 36-km grid resolution domains used in this study. 17
Figure 5-1. GFAS1.2 NOx emissions for June – September 2021 across a subsection of the western 12 km CAMx domain, with overlays showing subdomains for ten case study wildfires. Numbers correspond to the fires shown in Table 5-1. 24
Figure 5-2. Time series of acreage burned in California comparing 2021 with 2010-2021 (Source: https://blueskyhq.io/blog/how-wildfires-are-impacting-businesses-globally). 25
Figure 5-3. NOx emissions for June – September 2021 across a subsection of the western 12 km CAMx domain for FINN2.5 (top left), GFAS1.2 (top middle), FEER1.0 (top right), RAVE1.0 (bottom left) and QFED2.5 (bottom middle). 29
Figure 5-4. NOx emissions for the ten case study fires for FEER1.0 (orange), FINN2.5 (grey), GFAS1.2 (yellow), QFED2.5 (light blue), RAVE1.0

(green) and 5-FEI average (dark blue). Emissions for largest four fires shown in left panel; six smallest fires shown in right panel. 30

Figure 6-1. Map of CASTNET site locations. Tribal boundaries shown in yellow. Adapted from CASTNET fact sheet at https://www3.epa.gov/castnet/docs/CASTNET-Factsheet-2021.pdf. 33

Figure 6-2. Map of IMPROVE site locations. Adapted from https://vista.cira.colostate.edu/Improve/improve-program/. 33

Figure 6-3. Scatter plots showing MDA8 ozone model performance for No Fires (top left), RAVE1.0 (top middle), GFAS1.2 (top right), QFED2.5 (bottom left), FEER1.0 (bottom middle), and FINN2.5 (bottom left) at all AQS monitors in 12-km western U.S. modeling domain during June-September 2021. 35

Figure 6-4. Scatter plots showing MDA8 ozone model performance for No Fires (top left), RAVE1.0 (top middle), GFAS1.2 (top right), QFED2.5 (bottom left), FEER1.0 (bottom middle), and FINN2.5 (bottom left) at all CASTNET monitors in 12-km western U.S. modeling domain during June-September 2021. 36

Figure 6-5. Domain-wide and individual state MDA8 ozone NMB (top), NME (middle) and correlation coefficient (bottom) for No Fires (dark blue), RAVE1.0 (orange), GFAS1.2 (grey), QFED2.5 (yellow), FEER1.0 (light blue), and FINN2.5 (green) at all AQS monitors in 12-km domain during June-September 2021. Criteria (black dotted lines) and goals (light blue dotted lines) benchmarks are from Emery et al. (2016). 37

Figure 6-6. Scatter plots showing 24-hour $PM_{2.5}$ performance for No Fires (top left), RAVE1.0 (top middle), GFAS1.2 (top right), QFED2.5 (bottom left), FEER1.0 (bottom middle), and FINN2.5 (bottom left) at all AQS monitors in 12-km domain during June-September 2021. 38

Figure 6-7. Scatter plots showing 24-hour $PM_{2.5}$ performance for No Fires (top left), RAVE1.0 (top middle), GFAS1.2 (top right), QFED2.5 (bottom left), FEER1.0 (bottom middle), and FINN2.5 (bottom left) at all IMPROVE monitors in 12-km domain during June-September 2021. 39

Figure 6-8. Domain-wide and individual state 24-hour $PM_{2.5}$ NMB (top), NME (middle) and correlation coefficient (bottom) for No Fires (dark blue), RAVE1.0 (orange), GFAS1.2 (grey), QFED2.5 (yellow), FEER1.0 (light blue), and FINN2.5 (green) at all AQS monitors in the 12-km domain during June-September 2021. Criteria (black dotted lines) and goal (light blue dotted lines) benchmarks from Emery et al. (2016). 40

Figure 6-9. Speciated $PM_{2.5}$ components ($\mu g/m^3$) for observations (leftmost column) and No Fires, RAVE1.0, GFAS1.2, QFED2.5, FEER1.0, and FINN2.5 CAMx runs at all IMPROVE monitors in California during June-September 2021. 41

Figure 6-10. Scatter plots showing MDA8 ozone performance for RAVE1.0 with rapid NOx speciation (left) and RAVE1.0 with default NOx speciation (right) at all AQS monitors in California during July-August 2021. 43

Figure 6-11. Scatter plots showing 24-hour average $PM_{2.5}$ performance for RAVE1.0 with Sofiev (left) and RAVE1.0 with PBL500 (right) plume top heights at all AQS monitors in California during July-August 2021 (note that the

scale of the axis for the PBL500 scatterplot is twice that for the Sofiev scatterplot). 44

Figure 6-12. Scatter plots showing 24-hour average $PM_{2.5}$ performance for FEER1.0 with RAVE (left) and FEER1.0 with default (right) temporal allocation at all AQS monitors in California during July-August 2021. 45

Figure 6-13. Scatter plots showing 24-hour $PM_{2.5}$ performance for RAVE1.0 (left) and RAVE2.0 with scaled aerosol emissions (right) at all AQS monitors in 12 km domain during July-August 2021. 46

Figure 6-14. Scatter plots showing MDA8 ozone performance for RAVE1.0 (left) and RAVE2.0 with scaled aerosol emissions (right) at all AQS monitors in 12 km domain during July-August 2021. 47

Figure 6-15. Scatter plots showing 24-hour Elemental Carbon (EC) performance for RAVE1.0 (left), RAVE2.0 with SOAP3 (no evaporation of POA to SVOC; center), and RAVE2.0 with SOAP3 (including evaporation of POA to SVOC; right) at all AQS monitors in 12 km domain during July-August 2021. 49

Figure 6-16. Scatter plots showing 24-hour Organic Carbon (OC) performance for RAVE1.0 (left), RAVE2.0 with SOAP3 (no evaporation of POA to SVOC; center), and RAVE2.0 with SOAP3 (including evaporation of POA to SVOC; right) at all AQS monitors in 12 km domain during July-August 2021. 49

Figure 6-17. Scatter plots showing 24-hour $PM_{2.5}$ performance for RAVE1.0 (left), RAVE2.0 with SOAP3 (no evaporation of POA to SVOC; center), and RAVE2.0 with SOAP3 (including evaporation of POA to SVOC; right) at all AQS monitors in 12 km domain during July-August 2021. 50

Table of Tables

Table 2-1. Summary of key characteristics of FEIs to be evaluated. 7

Table 4-1. 35 vertical level (34 layers) structure used in EPA's WRF modeling that was also used for CAMx in this study. 18

Table 4-2. CRC A-133 2021 36 km WRF model configuration and comparison with the WRF configuration used in the EPA 2021 12 km WRF modeling. 20

Table 4-3. CAMx model configuration used in CRC Project A-133 modeling of summer 2021 to evaluate alternative representation of emissions from fires. 22

Table 5-1. Description of the ten case study wildfires used to provide an in-depth comparison of emissions from the five FEIs. 23

Table 5-2. Number of California wildfires and yearly acres burned during 2016-2023 Source: https://www.frontlinewildfire.com/wildfire-news-and-resources/california-wildfires-history-statistics/). 25

Table 6-1. Model Performance Evaluation Metrics. 31

Table 6-2. Recommended benchmarks for photochemical model statistics (Source: Emery et al., 2016). 32

Table 6-3. Configuration for CAMx simulations. 34

LIST OF ACRONYMS AND ABBREVIATIONS

3-D	Three-dimensional
ABI	Advanced Baseline Imager
ACM2	Asymmetric Convective Mixing, version 2
AMET	Atmospheric Model Evaluation Tool
AOD	Aerosol Optical Depth
APCD	Air Pollution Control Department
AQRP	Air Quality Research Program
AQI	Air Quality Index
AQS	Air Quality System
AZ	Arizona
BC	Black Carbon
BCs	Boundary Conditions
BEIS4	Biogenic Emission Inventory System version 4
BELD6	Biogenic Emissions Landcover Database version 6
CA	California
CAM-Chem	Community Atmosphere Model with Chemistry
CAMPD	Clean Air Markets Program Data
CAMx	Comprehensive Air quality Model with extensions
CAMS	Copernicus Atmospheric Monitoring Service
CASNET	Clean Air Status and Trends Network
CB6r4	Carbon Bond version 6, Revision 4
CB6r5	Carbon Bond version 6, Revision 5
CB7r1	Carbon Bond version 7, Revision 1
CC	Clark County
CDPHE	Colorado Department of Health and Environment
CEMS	Continuous Emissions Monitoring System
C-IFS	Composition Integrated Forecasting System
CMAQ	Community Multiscale Air Quality Model
CO	Carbon Monoxide
CO	Colorado
CONUS	CONtinental US
CRC	Coordinating Research Council
CSV	Comma Separated Value file
DM	Denver Metropolitan area
EBI	Euler Backward Iterative solver
EC	Elemental Carbon
ECMWF	European Centre for Medium-Range Forecasts
EPA	Environmental Protection Agency
FDDA	Four Dimensional Data Assimilation
FEER	Fire Energetics and Emissions Research
FEI	Fire Emission Inventory
FINN	Fire INventory from NCAR
FRP	Fire Radiative Power
GEOS	Goddard Earth Observing System
GEOS-5	Goddard Earth Observing System Model, Version 5
GEOS-Chem	Goddard Earth Observing System Chemical global model
GFAS	Global Fire Assimilation System
GFS	Global Forecasting System

GIS	Geographic Information System
GMAO	Global Modeling and Assimilation Office
GOES	Geostationary Operational Environmental Satellite
HRRR-Smoke	High Resolution Rapid Refresh model with smoke
ICs	Initial Conditions
ID	Idaho
IMPROVE	Interagency Monitoring of Protected Visual Environments
IS4FIRES	Integrated monitoring and modelling System for wildland FIRES project
JFSP	Joint Fire Science Program
JPSS	Joint Polar Satellite System
km	kilometer
MDA8	Maximum Daily Average 8-hour
MERRA	Modern-Era Retrospective analysis for Research and Applications
MODIS	MODerate resolution Imaging SpectroRadiometer
MPE	Model Performance Evaluation
MW	Megawatt
NASA	National Aeronautics and Space Administration
NCAR	National Center for Atmospheric Research
netCDF	network Common Data Format
NAA	Non Attainment Area
NAAQS	National Ambient Air Quality Standard
NCAR	National Center for Atmospheric Research
NFR	North Front Range
NLCD	National Land Cover Database
NMB	Normalized mean bias
NME	Normalized mean error (unsigned, or gross)
NOAA	National Oceanic and Atmospheric Administation
NOx	Nitrogen oxides
NPP	National Polar-orbiting Partnership
NRT	Near-Real Time
NV	Nevada
OAI	Ozone Assessment Initiative
OC	Organic Carbon
OMPS	Ozone Mapping and Profiler Suite
OPM	Other Particulate Matter less than 2.5 microns
OR	Oregon
PAN	Peroxyacetyl Nitrate
PBL	Planetary Boundary Layer
PBL500	Planetary Boundary Layer height plus 500 meters
PGM	Photochemical Grid Model
PM	Particulate Matter
$PM_{2.5}$	Particulate Matter less than 2.5 microns
PMDETAIL	Prescribed and Other Fire Emissions: Particulate Matter Deterministic & Empirical Tagging & Assessment of Impacts on Levels
ppb	parts per billion
POC	Primary Organic Carbon
PPM	Piecewise Parabolic Method
PSAT	Particulate Source Apportionment Technology
QFED	Quick Fire Emissions Dataset

RAVE	Regional Advanced baseline imager and Visible infrared imaging radiometer suite fire Emissions
RFNO	Rocky Flats North
s	second
SIP	State Implementation Plan
SL	Salt Lake
SMOKE	Sparse Matrix Operator Kernel Emissions
SOA	Secondary Organic Aerosol
SOAP	Secondary Organic Aerosol thermodynamic Partitioning
SOAP2	Secondary Organic Aerosol thermodynamic Partitioning version 2
SOAP3	Secondary Organic Aerosol thermodynamic Partitioning version 3
SVOC	Semi-Volatile Organic Compound
μg	microgram
US	United States
UT	Utah
VBS	Volatility Basis Set
VIIRS	Visible Infrared Imaging Radiometer Suite
VOC	Volatile organic compounds
WA	Washington
WACCM	Whole Atmosphere Community Climate Model
WRAP	Western Regional Air Partnership
WRF	Weather Research and Forecasting model
WRF-Chem	Weather Research and Forecasting model with Chemistry
YSU	Yonsei University

EXECUTIVE SUMMARY

Smoke from wildfires contribute to elevated $PM_{2.5}$ and ozone concentrations in the U.S. (Jaffe, et al., 2013; Lin et al., 2016; Laing and Jaffe, 2019). Emissions from fires can affect air quality thousands of kilometers downwind. In more recent years (e.g., 2020 and 2021), massive wildfires in California have adversely affected air quality in Utah, Colorado and even as far downwind as the East Coast. 2023 was the highest wildfire year ever in Canada and had large impacts on $PM_{2.5}$ concentrations in Canada and the Midwest and Northeast U.S. Emissions from wildfires can elevate ozone and $PM_{2.5}$ concentrations above the National Ambient Air Quality Standards (NAAQS). With climate change, summers are getting hotter and longer and droughts are more frequent and longer. The western U.S. is experiencing longer fire seasons, and wildfires are becoming more widespread and intense. Thus, wildfires are of increasing importance to $PM_{2.5}$ and ozone concentrations and visibility impairment.

The Coordinating Research Council (CRC) funded Ramboll to conduct Project A-133 to improve the treatment of fire emissions in photochemical grid model (PGM) modeling using several of the new fire emissions datasets that are now available. The focus of this project is the evaluation of Fire Emission Inventories (FEIs) that can be used in near real-time (NRT) or as an alternative to FEIs that are typically used in PGM applications. We describe the improvements in the representation of emissions from fires and photochemical model treatment of fires, the FEIs used, and the models, episodes and domains used to evaluate the FEIs. We then evaluate each of the following CAMx sensitivities against available ozone and $PM_{2.5}$ measurements in several phases:

- Phase I evaluated the five FEIs against each other;
- Phase II evaluated the effects of NOx speciation;
- Phase III evaluated changes to temporal/vertical allocation of the fire emissions;
- Phase IV evaluated an update to Regional ABI and VIIRS fire Emissions version 2.0 (RAVE2.0) FEI; and
- Phase V evaluated an update to Secondary Organic Aerosol Partitioning (SOAP) module in CAMx to treat primarily emitted organic carbon emissions by fires as semi-volatile.

As part of this study, Ramboll updated its Python FEI processor to include RAVE1.0, a new FEI that possesses a unique combination of high temporal and spatial resolution that appears well-suited for high-resolution photochemical modeling. Using this processor, Ramboll developed model-ready fire emissions for all five available fire inventories: 1) RAVE1.0, 2) Global Fire Assimilation System version 1.2 (GFAS1.2), 3) Quick Fire Emissions Dataset version 2.5 (QFED2.5), 4) Fire Energetics and Emissions Research (FEER1.0) and 5) Fire INventory from NCAR (FINN) version 2.5 (FINN2.5) and analyzed CAMx ozone and $PM_{2.5}$ model performance for an active Western U.S. wildfire season during June-September 2021. This analysis revealed superior ozone and $PM_{2.5}$ performance for RAVE1.0 compared to the other four FEIs. We therefore selected RAVE1.0 as the first choice to evaluate further fire emission sensitivities including NOx speciation and vertical allocation. We selected an additional inventory as the second-best performing FEI – FEER1.0 – to evaluate temporal allocation. While the ozone and $PM_{2.5}$ performance impacts from these emission sensitivities were minor, of the alternatives evaluated we recommend the rapid NOx speciation, Sofiev vertical allocation and RAVE landcover-specific temporal allocation.

In April 2024, RAVE1.0 emissions were replaced with a newer version, RAVE2.0 covering summer 2021. This version expands the domain extent from the continental U.S. to North America and makes other improvements including refinements to Fire Radiative Power (FRP) based on updated satellite

measurements. RAVE2.0 contains optional "scaled" emission species for primary $PM_{2.5}$, organic carbon (OC), and black carbon (BC), which the RAVE team developed for NOAA forecasting applications. These aerosol emissions are higher than the equivalent aerosol emission species as provided in the RAVE1.0 product. We used these scaled aerosol emissions species in RAVE2.0 for a new CAMx sensitivity and compared it with the RAVE1.0 simulation. The use of the scaled aerosol emissions in RAVE2.0 led to large $PM_{2.5}$ overestimations compared to RAVE1.0, but ozone performance was similar. We then conducted further testing with RAVE2.0 using the unscaled aerosol emissions and found slightly improved performance compared to RAVE1.0. Finally, we evaluated the impact of SOAP3 evaporative effects on primary organic aerosol (POA) and found the increased secondary organic aerosol (SOA) yield helped reduce underestimations of organic aerosol and $PM_{2.5}$.

Recommendations

The following are the recommended configuration for modeling wildfire emissions in PGM modeling using the near-real time (NRT) and alternative FEIs evaluated in the CRC A-133 study:

- The rapid NOx speciation that speciate fire NOx emissions into less reactive species (e.g., nitric acid and PAN) in addition to NO and NO_2 is recommended over the default fire emissions speciation profile that just speciates fire NOx emissions into NO and NO_2;
- The Sofiev vertical allocation algorithm that uses FRP to calculate plume rise is recommended over the PBL500 vertical allocation scheme;
- The RAVE landcover-specific temporal allocation approach for distributing fire emissions over the diurnal cycle is recommended over the default approach that is constant for all landcover types.
- Of the five FEIs that were initially evaluated, the RAVE1.0 generally produced the best ozone and $PM_{2.5}$ model performance and is recommended with the FEER1.0 producing the second best model performance. The FINN2.5 was the worst performing FEI.
- The RAVE2.0 FEI was released near the end of the study that included scaled $PM_{2.5}$ emissions that were evaluated in CAMx and produced large $PM_{2.5}$ overestimations. We conducted further evaluation of RAVE2.0 using the unscaled $PM_{2.5}$ emissions and found similar performance compared to RAVE1.0. Given the improvements of RAVE2.0, it is recommended over the other FEIs evaluated in this study provided the unscaled $PM_{2.5}$ emissions are used.
- Use SOAP3 available in CAMx v7.30+ with POA fire emissions renamed to POA_BB to characterize the evaporation of POA to semi-volatile organic compounds (SVOC) that form SOA.

Ramboll recommends several activities to improve the FEI processor:

- Investigate further refinements to NOx speciation, vertical and temporal allocation using the latest available fire emissions research.
- Evaluate available FEIs and alternatives in FEI processor for CAMx databases other than summer 2021, including EPA fire emissions as available, and evaluate ozone and $PM_{2.5}$ model performance against observations.
- Develop model-ready fire emissions and modeling platform for summer 2023 using multiple FEIs to evaluate impacts of the Canadian wildfires on the central and eastern U.S.

1.0 INTRODUCTION

Smoke from wildfires contribute to elevated $PM_{2.5}$ and ozone concentrations in the U.S. (Jaffe, et al., 2013; Lin et al., 2016; Laing and Jaffe, 2019). Emissions from fires can affect air quality thousands of kilometers downwind.[1] In more recent years, massive wildfires in California have adversely affected air quality in Utah[2], Colorado[3] and even as far downwind as the East Coast.[4] In 2023, Canada had the largest wildfire season ever resulting in smoke impacts across Canada and the Midwest and Northeast U.S.[5] Emissions from wildfires can elevate ozone and $PM_{2.5}$ concentrations above the National Ambient Air Quality Standards (NAAQS). With climate change, summers are getting hotter and longer, droughts are more frequent and the western U.S. is experiencing longer fire seasons resulting in wildfires becoming more frequent, widespread and intense. Thus, wildfires are of increasing importance to $PM_{2.5}$ and ozone concentrations and visibility impairment.

1.1 Purpose

The Coordinating Research Council (CRC) funded Ramboll to conduct Project A-133 to improve the treatment of fire emissions in Photochemical Grid Model (PGM) modeling using several of the new fire emissions datasets that are now available. We describe the improvements in the representation of emissions from fires and photochemical model treatment of fires, the fire emission inventories (FEIs) used, and the models, episodes and domains used to evaluate the FEIs. We then evaluate each of the FEIs against available ozone and $PM_{2.5}$ measurements (Phase I), changes to NOx speciation (Phase II), changes to temporal/vertical allocation (Phase III), update to the newest FEI (RAVE2.0; Phase IV) and finally, update to treat the volatilization of primary emitted organic carbon $PM_{2.5}$ into gaseous species (SOAP3; Phase V). The focus of this project is the evaluation of FEIs that can be used in near real-time (NRT) or as an alternative to FEIs that are typically used in PGM applications.

[1] https://www.nationalacademies.org/event/09-23-2020/wildland-fires-towards-improved-understanding-and-forecasting-of-air-quality-impacts-a-workshop

[2] https://kslnewsradio.com/1954403/more-smoke-from-california-wildfires-on-its-way-to-utah/

[3] https://www.cpr.org/2021/09/28/colorado-wildfire-smoke-air-quality/

[4] https://www.cnbc.com/2021/07/21/western-wildfire-smoke-reaches-east-coast-hurts-air-quality.html

[5] https://natural-resources.canada.ca/simply-science/canadas-record-breaking-wildfires-2023-fiery-wake-call/25303

2.0 FIRE EMISSION INVENTORIES EVALUATED

Several open land fire emission inventories (FEIs) are available. Historically, the FEIs used the most in U.S. air quality modeling are primarily the Fire INventory from NCAR (FINN[6]) and the SmartFire Blue Sky Framework[7] used in the National Emissions Inventory (NEI). Ramboll has recently developed a literature-based Python FEI processing tool for generating open land FEIs for the CAMx photochemical model (Ramboll, 2022). Before this project, the FEI tool was configured to generate open land fire emission inputs based on four FEI databases:

- Fire Inventory from NCAR version 2.5 (FINN2.5[8])
- Global Fire Assimilation version 1.2 (GFAS1.2[9])
- Quick Fire Emissions Dataset version 2.4 (QFED2.5[10])
- Fire Energetics and Emissions Research version 1.0 (FEER1.0[11])

Key characteristics of the FEIs available in the FEI processor are shown in Table 2-1. The last FEI database in Table 2-1 is the Regional ABI and VIIRS fire Emissions (RAVE1.0[12]) that was added to the FEI processor as part of this study.

Table 2-1. Summary of key characteristics of FEIs to be evaluated.

FEI dataset	Horizontal Resolution	Time-frame	Frequency	Approach	Burned Area/FRP Methodology	Emissions Species	Modeling Applications
FINN2.5	1 km^2	2002–2021	Daily through 2021; previous calendar year available each July	Burned Area	Estimated by active fire counts: 0.75 km^2 for savanna at each fire pixel, 1 km^2 for other types	NOx, VOC, CO, SO2, NH3, OC, $PM_{2.5}$	WACCM real time forecasts; non-US fires in EPA modeling platform
GFAS1.2	0.1°×0.1°	2003–present	Daily	FRP	MODIS	NOx, VOC, CO, SO2, NH3, OC, BC, $PM_{2.5}$	CAMS C-IFS
QFED2.5	0.1°×0.1°	2000–Present	Daily with 1-month lag	FRP	MODIS	NOx, VOC, CO, SO2, OC, BC, $PM_{2.5}$	GEOS-Chem; CAM-chem
FEER1.0	0.1°×0.1°	2003–Present	Daily with 1-month lag	FRP	From GFASv1.2 (Kaiser et al., 2012)	NOx, VOC, CO, SO2, NH3, OC, BC, $PM_{2.5}$	Fire research; climate impacts; Northern Sub-Saharan research
RAVE1.0	3 km^2	2021–Present	Hourly	FRP	GOES, VIIRS	NOx, total VOC, CO, SO2, NH3, OC, BC, $PM_{2.5}$	HRRR-Smoke; CMAQ; WRF-Chem

2.1 FINN2.5

FINN2.5 (Wiedinmyer et al., 2023) emissions are available through the end of 2021. FINN2.5 has the highest 1 km^2 horizontal resolution of all FEIs shown in Table 2-1. In the past, EPA used FINN

[6] https://www2.acom.ucar.edu/modeling/finn-fire-inventory-ncar
[7] https://cfpub.epa.gov/si/si_public_record_report.cfm?Lab=CEMM&dirEntryId=347186
[8] https://www2.acom.ucar.edu/modeling/finn-fire-inventory-ncar
[9] https://www.ecmwf.int/en/forecasts/dataset/global-fire-assimilation-system
[10] https://gmao.gsfc.nasa.gov/research/science_snapshots/global_fire_emissions.php
[11] http://feer.gsfc.nasa.gov/data/emissions/
[12] https://sites.google.com/view/rave-emission

emissions for their modeling platform for all areas outside the U.S. For its 2022 modeling platform and beyond, EPA plans to use FINN2.5 for Mexico and Central America and use the BlueSky Pipeline for Canadian fires[13]. Historically, the FINN2.5 emissions product has only been available as a CSV text file, where fire emissions are represented as points corresponding to the centers of MODIS and/or VIIRS satellite burn scar pixels. NCAR recently distributed FINN2.5 emissions as a global 0.1° (~10 km) gridded netCDF product[14] with a format and structure consistent with the GFAS1.2, QFED2.5 and FEER1.0 products. One limitation of the FINN product is its inability to distinguish fires from gas flaring activity.

2.2 GFAS1.2

GFAS multiplies fire radiative power (FRP) from MODIS Aqua/Terra satellite measurements by land cover-specific conversion factors to obtain dry matter combustion rate estimates. GFAS then employs a sophisticated filtering system that masks spurious FRP signals from volcanoes, gas flaring and other industrial activity. GFAS includes vertical parameters – plume bottom, plume top and mean altitude of maximum injection height (described in Rémy et al., 2017), all of which are derived from a plume rise model. GFAS also provides a separate injection height from IS4FIRES (Rémy et al., 2017). As with the fire emissions, these vertical parameters have daily resolution which correspond to early afternoon. The European Centre for Medium-Range Forecasts (ECMWF) Composition Integrated Forecasting System (C-IFS) of Copernicus Atmosphere Monitoring Service (CAMS) utilizes GFAS1.2 for global real time fire and smoke forecasts. GFAS1.2 is available in near real-time at 0.1° (~10-km) resolution. In the project where Ramboll developed the FEI processor, we found that GFAS1.2 showed considerably fewer fire detections compared to FINN2.5 and QFED2.5 on a select number of days when thick smoke was present.

2.3 QFED2.5

Similar to GFAS, QFED uses FRP measurements from MODIS Aqua/Terra satellites. QFED calculates emissions using scaling factors applied to the FRP measurements. These scaling factors are developed from comparisons of aerosol optical depth (AOD) between NASA's Goddard Earth Observing System (GEOS) model and MODIS measurements across different regions (Darmenov and da Silva, 2015). QFED2.5 applies a sophisticated treatment of cloud obscured land areas and is used in NASA's NRT GEOS model and Modern-Era Retrospective analysis for Research and Applications version 2 (MERRA-2) reanalyses (Randles et al., 2017). NCAR's Community Atmosphere Model with chemistry (CAM-chem) also utilizes QFED and QFED is an optional FEI for GEOS-Chem. QFED2.5 emissions are available for the entire previous calendar month and have 0.1° (~10 km) resolution.

2.4 FEER1.0

FEER1.0 uses GFAS1.2 FRP data and multiplies by emission coefficients to obtain smoke aerosol emissions (Ichoku and Ellison, 2014). These emission coefficients were formulated from a detailed analysis of MODIS AOD and winds from NASA's MERRA reanalysis dataset (Rienecker et al., 2011). Scaling factors for chemical species including OC, BC, NOx, VOC, SO_2 and CO are then applied to the smoke aerosol emissions to obtain emissions for these species. Fire research, climate impacts and Northern Sub-Saharan research all utilize FEER emissions[15]. As with QFED2.5, FEER1.0 emissions are available for the entire previous calendar month and have 0.1° (~10 km) resolution.

[13] Personal communication, Jeff Vukovich, US EPA

[14] https://rda.ucar.edu/datasets/ds312.9/

[15] https://feer.gsfc.nasa.gov/data/emissions/

2.5 RAVE1.0/RAVE2.0

The RAVE1.0 product utilizes a new algorithm to generate hourly 3 km^2 horizontal resolution fire emissions by fusing temporally resolved GOES Advanced Baseline Imager (ABI) FRP and fine spatial-resolution (375 m) FRP from the Visible Infrared Imaging Radiometer Suite (VIIRS) on the Joint Polar Satellite System (JPSS) satellites (Li et al., 2022). Hourly emissions are produced from land cover and ecoregion-specific FRP diurnal cycles using 5-minute GOES ABI FRP measurements. RAVE's combination of high temporal and spatial resolution is unique and thus appears well-suited for high resolution photochemical modeling. One drawback compared to the other FEIs is that only total VOC (unspeciated) emissions are provided in the RAVE1.0 product. Therefore, we used landcover-dependent VOC speciation profiles used by FINN[16] for RAVE1.0 in the FEI processor. The RAVE1.0 product was available as a near real-time product that covered North America and a "re-processed" historical product that covered the continental U.S. only. For this study, we used the re-processed RAVE1.0 emissions and supplemented them with GFAS1.2 emissions for portions of the CAMx 36 km domain that the RAVE1.0 extent did not cover.

As of April 2024, the re-processed RAVE2.0 emissions were made available for summer 2021. We therefore generated RAVE2.0 emissions for the July – August 2021 sensitivity period. These RAVE2.0 emissions now cover North America, include refinements to FRP based on updated satellite measurements and contain optional "scaled" emission species for primary $PM_{2.5}$, organic carbon (OC), and black carbon (BC), which the RAVE team developed for NOAA forecasting applications[17]. We used these scaled aerosol emissions species in the RAVE2.0 fire emissions for the CAMx sensitivity described in Section 6.5.3. These aerosol emissions are higher than the equivalent aerosol emission species as provided in the RAVE1.0 product. As of June 2024, the re-processed RAVE2.0 emissions are available for all of 2021 and for April-December of 2022[18]. RAVE1.0 emissions are no longer available, so we prioritized RAVE2.0 evaluation to understand how this product differs from RAVE1.0.

2.6 Fire Chemical Speciation and Secondary Organic Aerosol Issues

The default PM speciation profiles for open land fires fail to account for the volatility properties of the PM emissions and the processing of the NO_X emissions within fire plumes as they are diluted and begin to react in the free atmosphere. Primary PM organic carbon (POC) emissions are semi-volatile and tend to partially evaporate as diluted in the atmosphere to become gaseous semi-volatile organic compounds (SVOC) that can subsequently react further downwind. Thus, current modeling of wildfire emissions frequently overstates PM concentrations near the fires because it doesn't account for the evaporation of the PM emissions as they dilute. The Volatility Basis Set (VBS) SOA module can treat this early evaporation of primary POC but can be costly to apply.

Default NO_X speciation profiles for wildfires in the SMOKE emissions model speciate the emitted NO_X into NO and NO_2. However, rapid processing of the NO_X emissions in wildfire plumes can quickly convert NO_X into less reactive nitrogen species (e.g., HNO_3, organic nitrates, PAN, etc.). For example, a GEOS-Chem application used aircraft measurements of nitrogen species in wildfire plumes to speciate the wildfire NO_X emissions and found lower predicted ozone concentrations and better agreement with the aircraft measured nitrogen species (Alvarado et al., 2010).

[16] https://github.com/NCAR/finn/blob/master/v2.5_emissions_code/NMOCfrac_byGenVeg_MOZ.csv

[17] Personal communication, Fangjun Li

[18] https://mft.sdstate.edu/public/folder/uvorilnmm0sgb8e_jbjizq/NorthAmerica

3.0 UPDATE OF FEI PROCESSOR AND CAMX

The CAMx secondary organic aerosol thermodynamic partitioning (SOAP) module was updated to include the semi-volatility of primary organic carbon (POC) emitted from open land fires. We updated the Python-based FEI processor as follows:

- Inclusion of the RAVE FEI.
- Updated speciation profiles.
- Updated Sofiev plume rise algorithm.

3.1 Update of CAMx SOA Module to Treat Semi-Volatility of Fire PM Emissions

Fire primary organic carbon (POC) emissions are semi-volatile and partially evaporate as they are diluted in the atmosphere to become gaseous semi-volatile compounds (SVOC) that can react and condense into particles downwind. This can result in PGMs overstating the near-source $PM_{2.5}$ impacts of emissions from fires. CAMx includes a detailed Volatility Basis Set (VBS; Donahue et al., 2006; Robinson et al., 2007; Koo et al., 2014) aerosol module that treats the semi-volatility of different types of POC emissions and their various levels of volatility as they react. For a Joint Fire Science Program (JFSP[19]) study (PMDETAIL[20]) we modeled the fire PM emission volatility using the VBS module in CAMx and found that accounting for the semi-volatility of the fire POC emissions greatly reduced the near-source $PM_{2.5}$ impacts of fires but also affected the spatial distribution of fire $PM_{2.5}$ impacts farther downwind (Posner et al., 2019; Theodoritsi et al., 2020). However, the VBS module treats many families of volatility types so is quite computationally expensive and is currently incompatible with the CAMx probing tools, such as the Particulate Source Apportionment Technology (PSAT).

Compared to VBS, modifying the CAMx secondary organic aerosol scheme (SOAP2; Strader et al., 1999; Malecha et al., 2018) is substantially more computationally efficient and should yield similar accuracy of wildfire PM emissions volatility as simulated by VBS. We identify this modified SOAP2 mechanism as "SOAP3" (Huang et al., 2024) and it includes the addition of 5 chemical species: POA_BB (primary OA from fires) and two $PM_{2.5}$ SOA and Condensable Gas (CG) pairs (SOA5/CG5 and SOA6/CG6). Speciating fire emissions as POA_BB rather than POA activates the scheme for a particular source and the partitioning of emissions between POA_BB/SOA5/SOA6 occurs inside CAMx so that the fire PM is treated as semi-volatile. A more advanced question is whether SOA5 and SOA6 undergo chemical aging that increases or/and decreases PM mass, which was not addressed in the SOAP3 update.

3.2 FEI Processor Updates

An overview of the FEI processor design is provided in Figure 3-1. We updated the processor to include the RAVE1.0 FEI. FINN2.5, FEER1.0, GFAS1.2 and QFED2.5 are all global products with 0.1° resolution. We therefore designed the FEI processor to regrid FEI emissions from this 0.1° latitude-longitude grid to the target CAMx modeling domains grid resolution using a lookup table produced by a GIS intersection preprocessing step. In contrast, RAVE1.0 emissions have 0.03° (~ 3 km) resolution, so we generated new GIS lookup tables to map the RAVE1.0 emissions to the target CAMx modeling domains. Further, the RAVE1.0 product (orange box in Figure 3-2) does not cover the entirety of the 36 km CAMx domain (36US3; red box in Figure 3-2). We therefore need to "stitch" RAVE1.0 emissions with those from another FEI to cover the full 36 km extent of the CAMx domain. Our prior CAMx model

[19] https://www.firescience.gov/ords/prd/jf_jfsp/jf_jfsp/r/jfspublic/home

[20] https://www.wrapair2.org/pdf/PMDETAIL_Attachment_1_Technical%20Proposal11_18_2011final.pdf

performance evaluation revealed superior ozone and $PM_{2.5}$ performance in Mexico and Central America for the FRP-based FEIs (FEER1.0, GFAS1.2 and QFED2.5) as compared to the burned area FEI – FINN2.5. We stitched RAVE1.0 emissions with GFAS1.2 emissions in the regions of the 36 km CAMx domain not covered by RAVE1.0 (Canada, Mexico and Central America). By contrast, the RAVE2.0 emissions cover most of North America, including the entirety of the 36 km CAMx domain. Therefore, no such stitching is needed for RAVE2.0.

The FEI processor includes chemical species mapping files that map chemical species from the FEI to the species used in the chemical mechanism in CAMx. The previous version of the tool provided species mapping from the FINN2.5, FEER1.0, GFAS1.2, and QFED2.5 FEIs to the CB6r4 and CB7 chemical mechanisms. As part of this study, we updated the chemical species mapping files to include the RAVE FEI. As mentioned previously, RAVE includes only total VOC (unspeciated). Therefore, we used landcover-dependent VOC speciation profiles used by FINN in a separate VOC speciation mapping file. We also developed a duplicate set of chemical species mapping files that contain the POA_BB species to work with the new SOAP3 scheme as described above.

The FEI processor's temporal allocation schemes distribute daily fire emissions to hourly emissions using a defined diurnal profile. There are currently two options in the FEI processor: 1) default: constant diurnal profile for all landcover types and 2) RAVE landcover: applies landcover-specific diurnal profiles developed from 5-minute FRP measurements by the RAVE team[21]. Because the RAVE product contains hourly emissions, the temporal allocation step is bypassed for the RAVE FEI.

The last step in the FEI processor defines the top of the smoke plume (injection height) using one of two options: 1) PBL500 adds 500 m to the PBL height; or 2) Sofiev that uses a modified version of the injection height parameterization defined in Sofiev et al. (2012) that depends on FRP, PBL height and meteorological stability parameters. GFAS1.2 includes daily FRP, which we allocate to hourly FRP using the landcover-dependent FRP diurnal profiles developed by the RAVE team[22]. Because the RAVE product includes hourly FRP, we use this hourly FRP directly in the calculation of plume injection height in the Sofiev scheme.

[21] https://sites.google.com/view/rave-emission/diurnal-cycles?authuser=1

[22] https://sites.google.com/view/rave-emission/diurnal-cycles?authuser=1

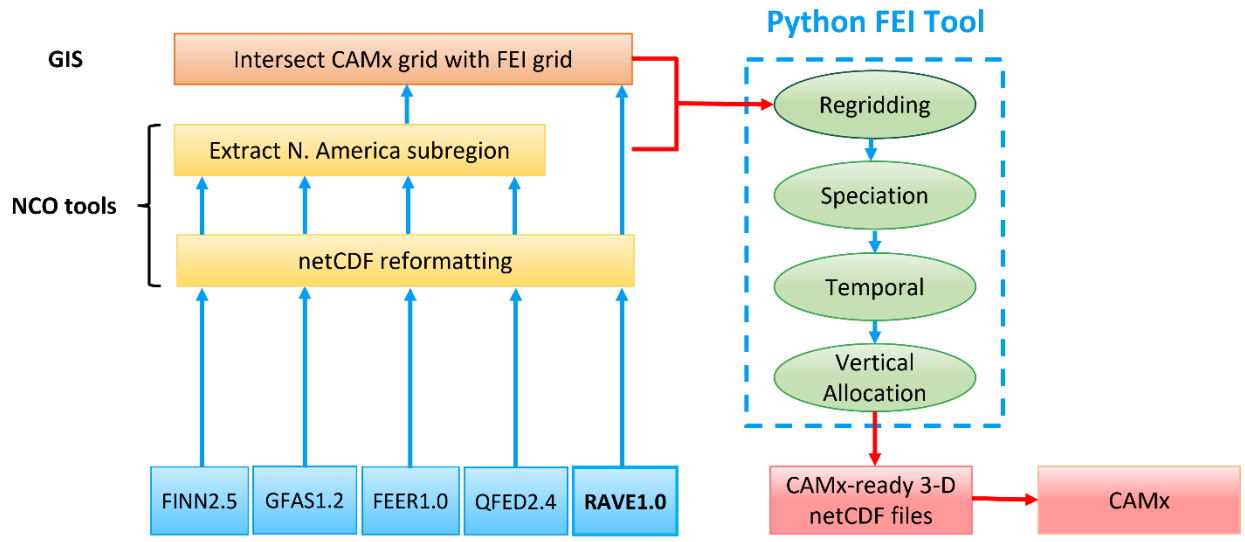

Figure 3-1. Design of the FEI processing tool.

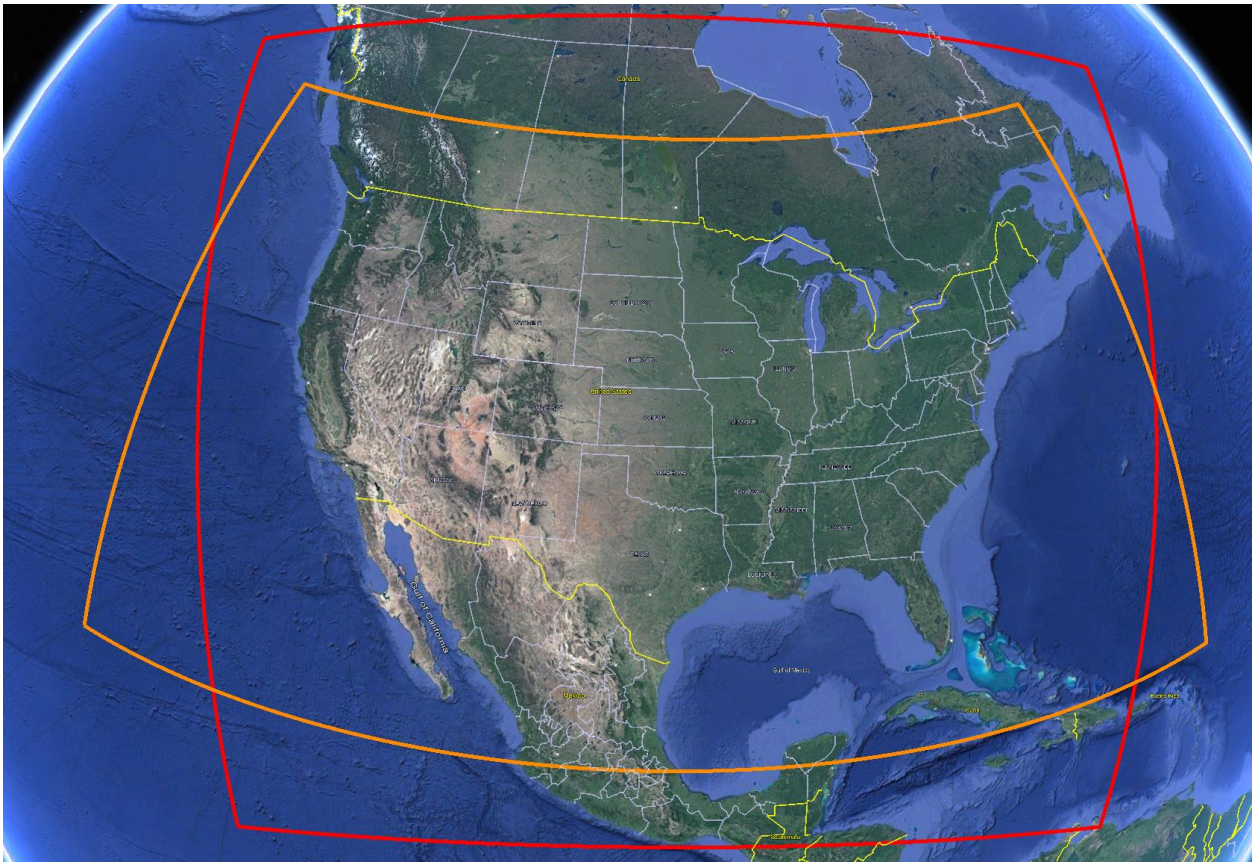

Figure 3-2. Map showing RAVE1.0 extent (orange) and 36-km CAMx domain (red).

4.0 DEVELOPMENT OF A PGM DATABASE FOR EVALUATING ALTERNATIVE FIRE EMISSIONS

This chapter discusses the procedures for developing a photochemical grid model (PGM) database for testing and evaluation of alternative emissions inventories for fires.

4.1 Model Selection

The CAMx PGM model was selected because the FEI processor is currently designed to generate emissions for CAMx and Ramboll's familiarity with the code allows the efficient implementation of semi-volatile primary organic carbon (POC) emissions from fires in the CAMx SOAP secondary organic aerosol (SOA) module (i.e., SOAP3). The WRF meteorological model was used as it is the current standard model for developing PGM meteorological inputs. Output from the WACCM global chemistry model was used for boundary conditions (BCs).

4.2 Episode Selection

In order to include RAVE1.0 FEI in the evaluation, the modeling period needs to be 2021 or newer, which means modeling years of either 2021 or 2022. We began the fire emissions processing and CAMx modeling in 2023, we could not select that year. Since one of the air pollutants of interest is ozone and most wildfires typically occur in the summer and fall, we selected the model summer months for the testing of alternative FEIs. The summer of 2021 was selected as the modeling period over 2022 for the following reasons:

- 2021 was a high wildfire year in the western states, with 2022 being relatively low wildfire year of recent years.
- Ozone concentrations in the western states were higher in 2021 than 2022.
- EPA has 2021 12 km CONUS domain WRF meteorological data that at the time of the project initiation in 2023 was not yet available for 2022.
- The re-processed RAVE FEI was not available for 2022 at project initiation.

In California, 2020 was the worst wildfire year on record and 2021 was the second worst as shown in Figure 4-1. 2022 was a relatively low wildfire year in California due to a combination of well-timed precipitation and favorable wind conditions. 2022 also had more summer monsoon activity in other western states that suppressed wildfires (e.g., Colorado).

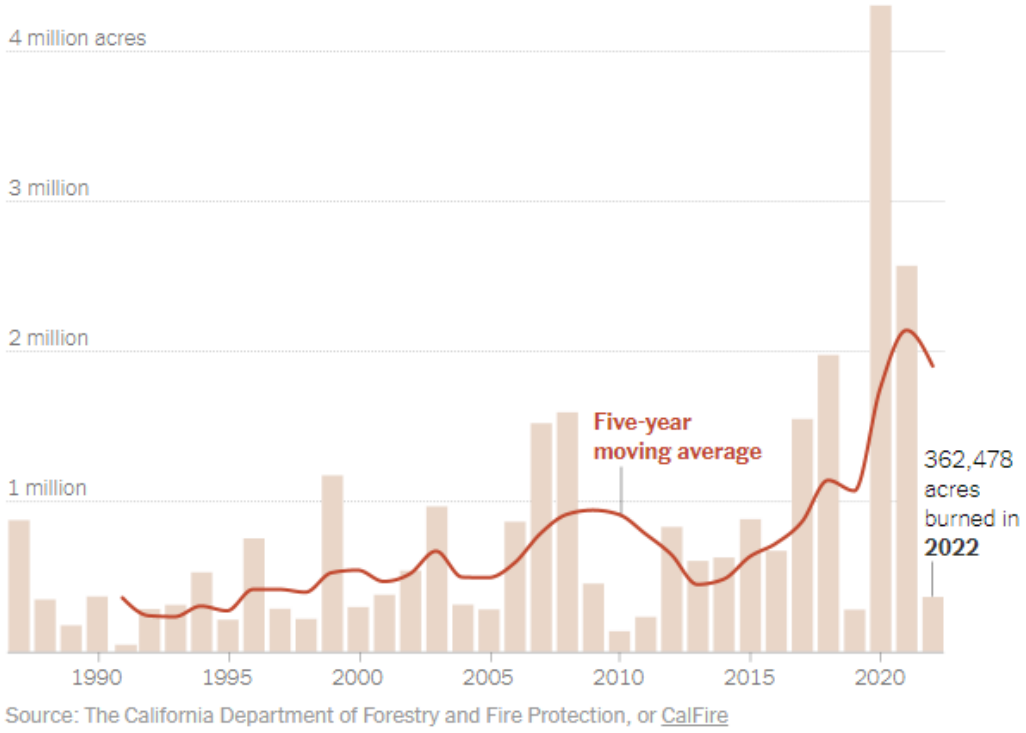

Figure 4-1. Acres burned by wildfires in California 1987-2022.

Figure 4-2 displays the daily ozone Air Quality Index (AQI) for 2016-2023 for several regions in the western states outside of California (Colorado, Nevada and Utah). Maximum Daily Average 8-hour (MDA8) ozone concentrations that are above the 70 ppb 2015 ozone NAAQS are indicated by orange and red, with red indicating MDA8 ozone above the 84 ppb 1997 ozone NAAQS. The ozone concentrations during summer 2021 were some of the highest and most frequent occurring exceedances at these four key ozone nonattainment areas in the western states.

An examination of the observed MDA8 ozone concentrations at these four key areas in the west reveals few exceedances of the ozone NAAQS before June or after September so we selected a June 1 – September 30, 2023 modeling episode with a 15-day spin-up period starting from mid-May.

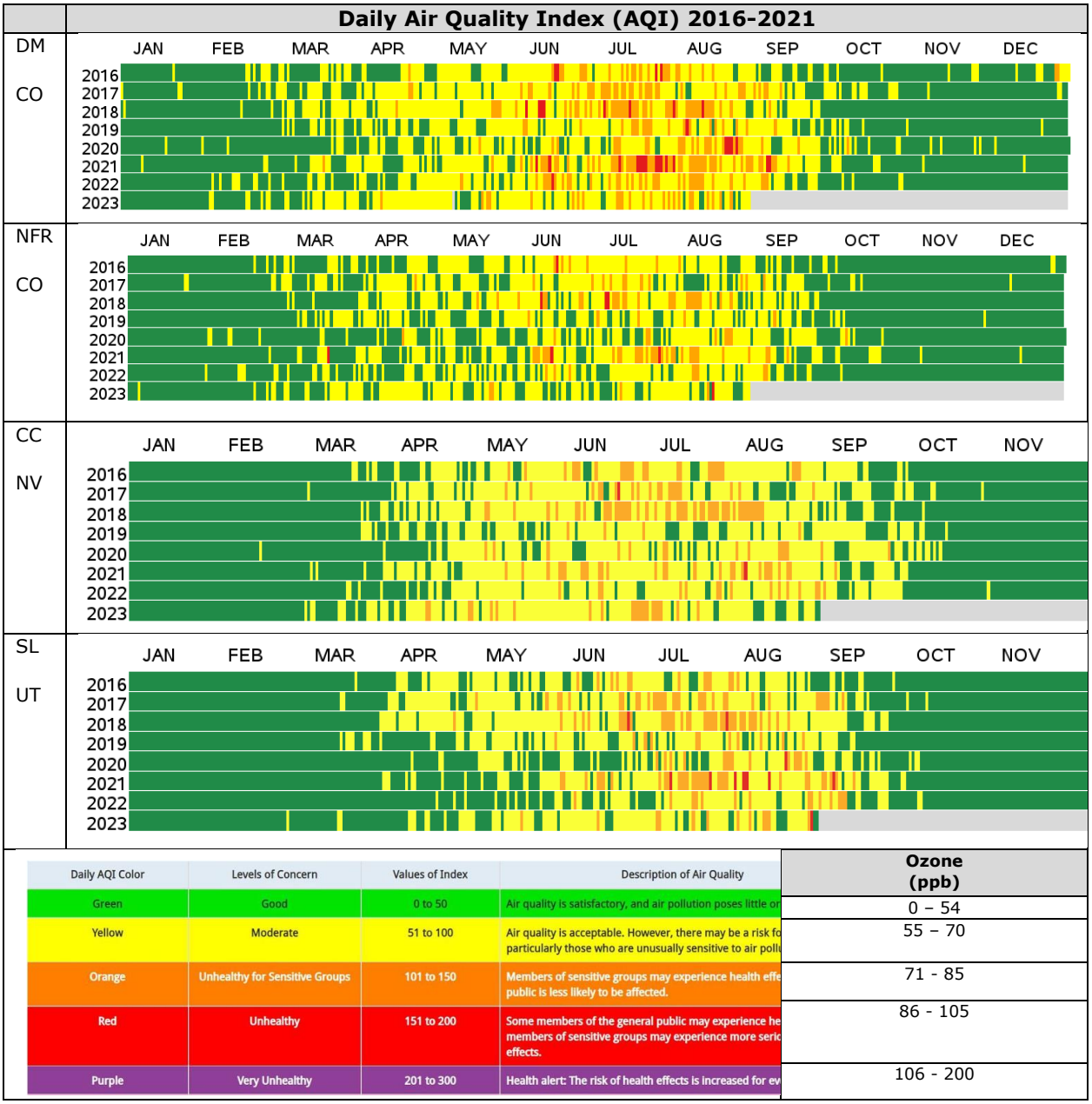

Figure 4-2. Daily ozone AQI for Denver Metro (DM) and North Front Range (NFR) in Colorado (CO), Clark County (CC), Nevada (NV) and Salt Lake (SL) County, Utah (UT) and the years 2016-2023.

4.3 Horizontal Modeling Domains

We want to leverage the available data from EPA's modeling platforms as much as possible with the 2016v3 platform being the latest version (EPA, 2023a). The EPA 2016v3 platform uses a 12-km grid resolution domain (12US2) that covers all of the continental U.S. (CONUS) contiguous 48 states and a 36-km grid resolution domain (36US3) that is larger covering most of North America as shown in Figure 4-3. Since our focus is on modeling ozone and $PM_{2.5}$ from wildfires in the western U.S. and the predominant wind direction is from west to east, we used a 12-km grid resolution domain covering just the western states embedded in the 36-km 36US3 domain instead of the CONUS 12-km domain used in the EPA platform. This is similar to what the Western Regional Air Partnership (WRAP) used for

the Round 2 Regional Haze SIP modeling that used a 12-km Western US domain. Thus, for CRC Project A-133 we use the EPA 36 km 36US3 domain and a 12-km domain that is similar in extent to the 12WUS2 12 km domain used by WRAP (see Figure 4-4 for both domains). CAMx was run using one-way grid nesting between the 36-km and 12-km domains for the initial round (Phase I) of CAMx sensitivity simulations that compare the different FEIs against each other. All remaining CAMx sensitivity simulations were run for the 12-km domain only, with boundary conditions extracted from the Phase I 36-km results.

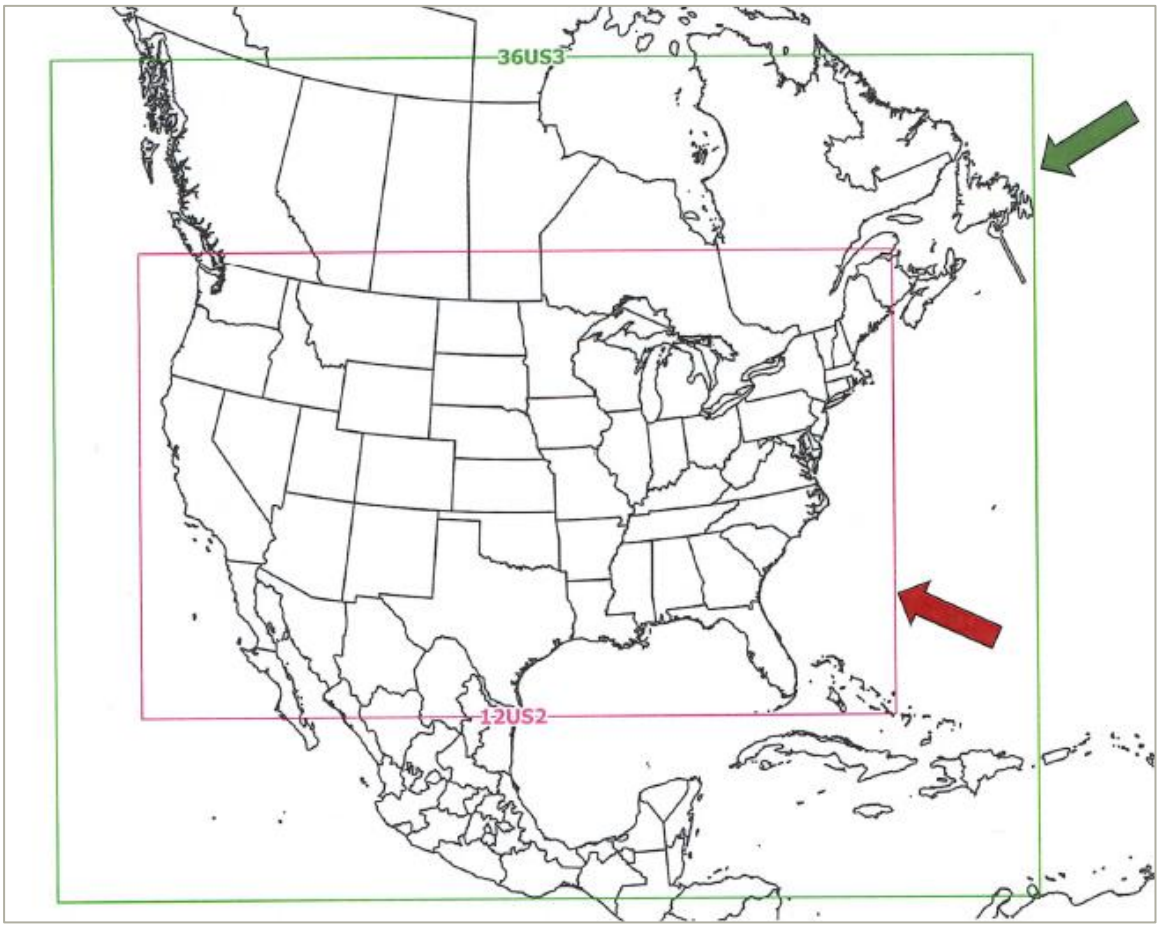

Figure 4-3. 12US2 12 km and 36US3 36 km grid resolution domains used in EPA's 2016v3 modeling platform.

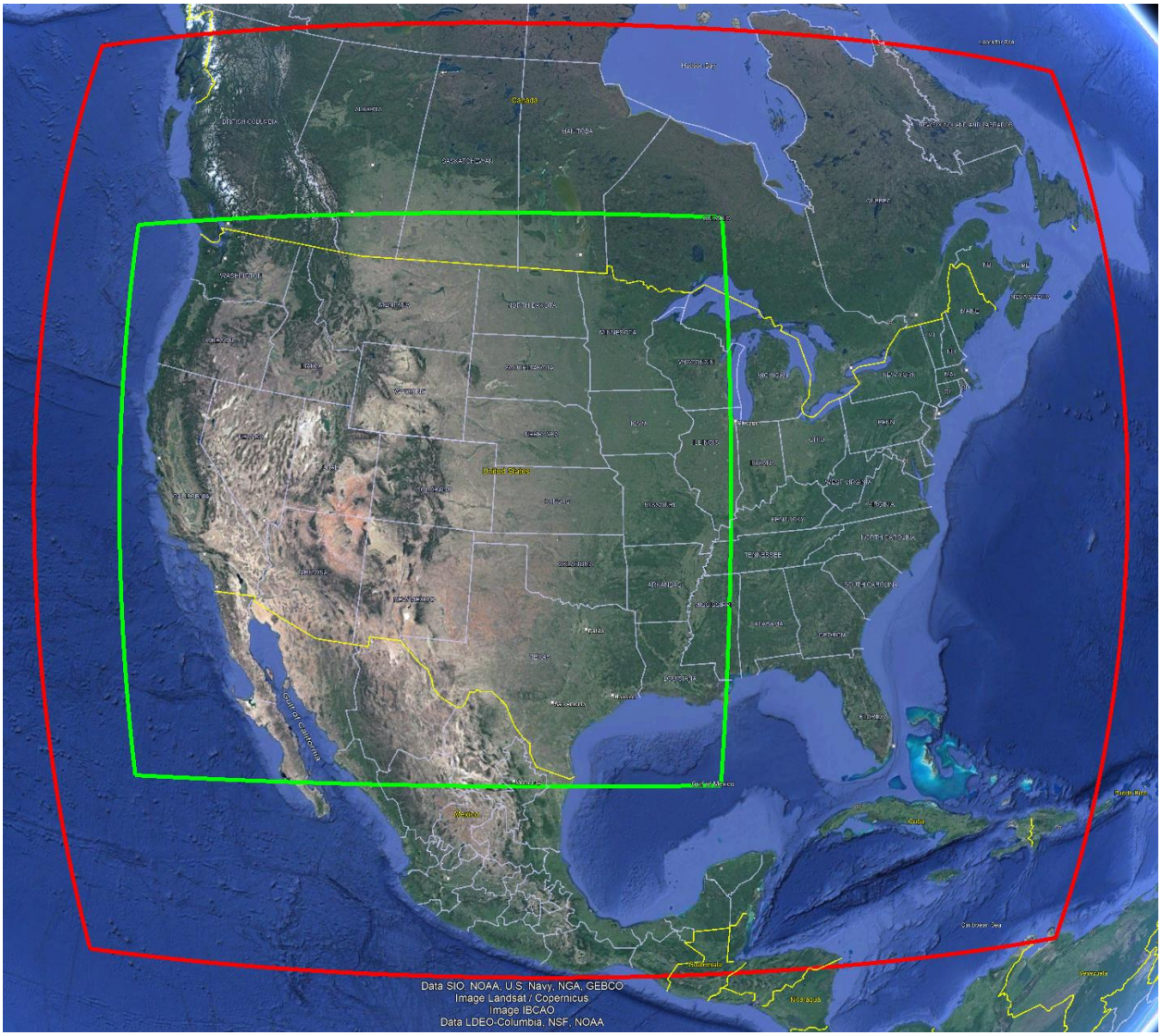

Figure 4-4. 12-km western U.S. and 36US3 36-km grid resolution domains used in this study.

4.4 Vertical Layer Structure

The CAMx vertical layer structure is defined by the vertical levels used in the 2021 WRF simulations. EPA runs WRF with 35 vertical levels from the surface to 50 mb height as shown in Table 4-1. CAMx has the same vertical structure as WRF and uses 34 vertical layers with the lowest layer 1 being 19 m thick. Although the WRFCAMx processor has the capability to do layer collapsing to reduce the number of vertical layers used in CAMx than in WRF, layer collapsing was not used as the higher vertical resolution may be needed to adequately simulate meteorological conditions in the high terrain areas of the western U.S.

Table 4-1. 35 vertical level (34 layers) structure used in EPA's WRF modeling that was also used for CAMx in this study.

WRF Layer	Height (m)	Pressure (mb)	Sigma
35	17,556	5000	0.000
34	14,780	9750	0.050
33	12,822	14500	0.100
32	11,282	19250	0.150
31	10,002	24000	0.200
30	8,901	28750	0.250
29	7,932	33500	0.300
28	7,064	38250	0.350
27	6,275	43000	0.400
26	5,553	47750	0.450
25	4,885	52500	0.500
24	4,264	57250	0.550
23	3,683	62000	0.600
22	3,136	66750	0.650
21	2,619	71500	0.700
20	2,226	75300	0.740
19	1,941	78150	0.770
18	1,665	81000	0.800
17	1,485	82900	0.820
16	1,308	84800	0.840
15	1,134	86700	0.860
14	964	88600	0.880
13	797	90500	0.900
12	714	91450	0.910
11	632	92400	0.920
10	551	93350	0.930
9	470	94300	0.940
8	390	95250	0.950
7	311	96200	0.960
6	232	97150	0.970
5	154	98100	0.980
4	115	98575	0.985
3	77	99050	0.990
2	38	99525	0.995
1	19	99763	0.9975
Surface	0	100000	1.000

4.5 Meteorological Inputs

The CAMx meteorological inputs for the summer 2021 modeling episode and the 36/12 km domains are based on output from the Weather Research Forecasting (WRF) model. We obtained WRF 2021 12-km CONUS domain output from EPA that was processed by WRFCAMx to generate CAMx meteorological inputs for the 12-km domain and summer 2021 modeling period. EPA routinely performs annual WRF CONUS 12-km domain simulations to support their modeling platform and other program development. EPA's WRF modeling uses similar configurations with updates to newer versions of the model and physics options as available. EPA's WRF CONUS 12 km simulations use analysis fields from the 12 km resolution North American Mesoscale Forecast System (NAM) as boundary condition (BC) inputs and also in the four-dimensional data assimilation (FDDA) to nudge the WRF meteorological variables to the NAM fields that are based in part on observations.

In the past (e.g., for 2016v3 platform), EPA has run WRF for a 36 km domain larger than the 36US3 domain but used the 28-km resolution Global Forecast System (GFS) for BC and FDDA as the 12-km NAM fields do not go far enough north for the 36US3 domain. However, EPA did not perform a WRF 36-km domain simulation for the 2021 period so Ramboll performed a WRF 2021 36-km simulation under this project to generate CAMx 36-km meteorological inputs for the 36US3 domain (Figure 4-4).

4.5.1 WRF Summer 2021 36 km Domain Simulation

Table 4-2 summarizes the 36-km WRF configuration for this study compared with the EPA 12 km WRF configuration. Given that this WRF modeling task is outside the scope of the original study, we chose a WRF configuration that closely matches other studies utilizing WRF at in the Western U.S., such as the WRAP Regional Haze[23] and the New Mexico Ozone Assessment Initiative (OAI[24]). These studies all showed reasonable model performance and therefore this WRF configuration provides the best option given the lack of resources for multiple WRF simulations and detailed model performance evaluation. In addition to the physics configuration differences in our 36 km and EPA's 12 km WRF 2021 simulations shown in Table 4-2 below, EPA also applied soil temperature and moisture nudging using the Pleim-Xiu Land Surface Model. This procedure is labor and time intensive and so we decided not to apply this nudging technique for this study.

[23] https://www.wrapair2.org/reghaze.aspx

[24] https://www.wrapair2.org/NMOAI.aspx

Table 4-2. CRC A-133 2021 36 km WRF model configuration and comparison with the WRF configuration used in the EPA 2021 12 km WRF modeling.

WRF Option	CRC A-133	EPA
Domains run	36 km	12 km
Vertical Coordinate	Hybrid	Hybrid
Microphysics	Thompson	Morrison 2
LW Radiation	RRTMG	RRTMG
SW Radiation	RRTMG	RRTMG
Sfc Layer Physics	MM5 similarity	Pleim-Xiu
LSM	Noah	Pleim-Xiu
PBL scheme	Yonsei University (YSU)	ACM2
Cumulus	Multi-scale Kain Fritsch	Kain-Fritsch
BC, IC Analysis Nudging Source	36 km GFS	12 km NAM
Analysis Nudging	On	On
Obs Nudging	None	None
Sea Sfc Temp	FNMOC	FNMOC

4.6 Initial Concentration and Boundary Condition Inputs

We initialized CAMx in mid-May 2021 and ran for 15 days to wash out the influence of the initial concentrations (IC) before analyzing the results on June 1, 2021. Initial and boundary conditions (ICs/BCs) for the CAMx 36US3 36 km domain were based on output from the Whole Atmosphere Community Climate Model (WACCM) global chemistry transport model. WACCM has a horizontal grid resolution of 1.25° x 0.9° (~100 km) with 88 vertical levels. WACCM utilizes meteorological fields from the NASA Global Modeling and Assimilation Office (GMAO) Goddard Earth Observing System Model, Version 5 (GEOS-5) model and anthropogenic emissions from the latest Copernicus Atmosphere Monitoring Service (CAMS) inventory.

4.7 Anthropogenic Emission Inputs

Anthropogenic emission inputs were based mainly on EPA's 2016v3 modeling platform (EPA, 2023a,b). The exception to this is for emissions from large (> 25 MW) Electrical Generating Units (EGUs) whose hourly NO_X and SO_2 emissions are based on 2021 hourly Continuous Emissions Monitoring Systems (CEMS) measurements that are available from EPA's Clean Air Markets Program Data (CAMPD) website. The 2016v3 platform has emissions processed for the 12-km and 36-km domains and the 2016, 2023 and 2026 emission years. The 2016v3 platform 2023 36/12 km emissions were processed by source sector to obtain monthly average weekday, Saturday and Sunday hourly emissions for the 36US3 and 12-km domains. The new 36/12 km domain emissions by source sector were backcast from 2023 to 2021 for mobile sources using MOVES national adjustments applied to model-ready files.

4.8 Natural Emission Inputs

Biogenic emissions for the summer 2021 and 36/12 km domains were based on the BEIS4/BELD6 biogenic emissions model using the WRF 2021 36/12 km output as input. Lightning NOx (LNOx) emissions and sea salt, dimethyl sulfide and halogen emissions from the ocean were generated using

the 2021 36/12 km WRF output and CAMx LNOx and Oceanic processors available on the CAMx website. Multiple open land fire emissions were developed using the FEI processor discussed in Section 3.

4.9 CAMx Ancillary Inputs

Total atmospheric ozone column data are needed to derive clear-sky photolysis rate inputs for CAMx. These data are available every 24-hours from the Ozone Mapping and Profiler Suite (OMPS) aboard the joint NASA/NOAA Suomi National Polar-orbiting Partnership (Suomi NPP) satellite and are distributed on an HTTP site supported by the National Aeronautics and Space Administration (NASA; 2023). This ozone data is processed for the CAMx parent domain by the O3MAP processor. The O3MAP outputs are then used by the TUV[25] radiative transfer and photolysis model, developed and distributed by the National Center of Atmospheric Research (NCAR; 2011), to provide the air quality model with a multi-dimensional lookup table of clear-sky photolysis rates. CAMx internally adjusts clear-sky rates for the presence of clouds and aerosols using a fast in-line version of TUV.

Fractional landuse for CAMx was passed through the WRFCAMx preprocessor from the 2011 National Land Cover Dataset (NLCD[26]) used by EPA in their WRF simulation. The Multi-Resolution Land Characteristics Consortium developed the NLCD dataset and is based on observations from the Landsat Thematic Mapper (Homer et al., 2015). NLCD contains 20 landuse categories specific to the Continental U.S. and MODIS landuse categories elsewhere (Ran et al., 2015).

4.10 Summary of CAMx Options

Table 4-3 displays a summary of the options used in the CAMx summer 2021 36/12 km simulations. The latest publicly available version of CAMx version 7.20 (v7.20) posted May 2, 2022 was used with the SOAP2 secondary organic aerosol module for the initial CAMx simulations with separate simulations run with the updated SOAP3 SOA module to isolate the effects of treating the semi-volatility of primary emitted carbon (POC) from fires. The Plume-in-Grid module was not used as its primary purpose is to better simulate the near source chemistry and dispersion of large NO_X emissions point source plumes, whereas this study is focusing on better simulation of emissions from fires. The CB6r5 gas-phase chemistry, coarse/fine aerosol treatment, Zhang dry deposition scheme and PPM advection solver were used.

[25] https://www2.acom.ucar.edu/modeling/tropospheric-ultraviolet-and-visible-tuv-radiation-model

[26] https://www.mrlc.gov/data/nlcd-2011-land-cover-conus

Table 4-3. CAMx model configuration used in CRC Project A-133 modeling of summer 2021 to evaluate alternative representation of emissions from fires.

Science Options	CAMx	Comment
Model Codes	CAMx v7.20 CAMx v7.30	Released May 2022 With SOAP3, June 2024
Horizontal Grid Mesh	36 km 36US3; 12 km	
36 km grid	172 x 148 cells	Same as EPA's 2016 Modeling Platform
12 km grid	225 x 213 cells	Similar to WRAP 2014 platform regional haze modeling
Vertical Grid Mesh	34 vertical layers	Layer 1 = 19 m. Model top 50 mb.
Grid Interaction	36/12 km one-way nesting	36 km used for BCs in 12 km simulations
Initial Conditions	~15-day spin-up end of May	Jun-Sep 2021 Episode
Boundary Conditions	2021 WACCM	
Emissions		
Baseline Emissions	Estimated 2021 emissions	2021 EGU from hourly CEMs
Sub-grid-scale Plumes	Plume-in-Grid not used	Focus on fire impacts
36/12 km Anthro. Emissions	2023 36/12 km backcast to 2021 except EGU 2021 hourly CEMS	2023 36/12 km from EPA 2016v3 platform
36/12 km Biogenic Emissions	BEIS4/BELD6	With 2021 WRF data
36/12 km Fire Emissions	From FEI Processor	See Chapters 3 and 5
36/12 km Natural Emissions	CAMx Lightning NOx and Oceanic emissions processors	With 2021 WRF data
Chemistry		
Gas Phase Chemistry	CB6r5	Updated CB6 chemistry revision 5
Aerosol Scheme	Course/Fine	
Secondary Organic Aerosol	SOAP2 and SOAP3	SOAP3 updated semi-volatile treatment of POC from fires
Meteorology		
…Source of WRF	EPA WRF/NAM 2021 12 km; CRC A-133 WRF/GFS 2021 36 km	
Meteorological Processor	WRFCAMx	Use YSU vertical diffusion coefficient
Horizontal Diffusion	Spatially varying	K-theory with Kh grid size dependence
Vertical Diffusion	YSU Kv formulation	Minimum Kv 0.1 to 1.0 m^2/s
Diffusivity Lower Limit	Kv_min = 0.1 to 1.0 m^2/s	Depends on percent urban landuse
Deposition Schemes		
Dry Deposition	Zhang dry deposition scheme	(Zhang et. al, 2001; 2003)
Wet Deposition	CAMx -specific formulation	rain/snow/graupel
Numerics		
Gas Phase Chemistry Solver	Euler Backward Iterative (EBI)	EBI fast and accurate solver
Vertical Advection Scheme	Piecewise Parabolic Method (PPM) scheme	New in CAMx v7.20
Horizontal Advection Scheme	Piecewise Parabolic Method (PPM) scheme	Colella and Woodward (1984)
Integration Time Step	Wind speed dependent	1-5 min (12 km), 5-15 min (36 km)

5.0 CASE STUDY OF 2021 WESTERN U.S. WILDFIRES AND EMISSIONS COMPARISON

This chapter presents a comparison of emissions across the five available FEIs for ten case study wildfires that occurred in the western U.S. during the Summer 2021 CAMx modeling period.

5.1 2021 Case Study Wildfires

We identified 10 case study wildfires that occurred during June-August 2021 in the western U.S. that were used to compare the NO_X, VOC, CO and $PM_{2.5}$ emissions from the five FEIs in detail. We summarize key characteristics of these fires in Table 5-1 and describe each in detail in the sections that follow. With a historic drought and record-breaking heat waves, 2021 was an intense year for wildfires across the U.S., burning over 7 million acres.[27] Although this was less acreage burned than the previous year[28], the lack of precipitation during the 2020-2021 winter[29] resulted in many wildfires in 2021 starting earlier than previous years. Megafires burning more than 100,000 acres are becoming more normal.[30]

In many cases, these case study wildfires are several wildfires within a similar geographic area, such as occurs when multiple wildfires are ignited by dry lightning. Figure 5-1 shows the June – September 2021 GFAS1.2 NOx fire emissions gridded to the CAMx 12-km domain. The white boxes highlight the ten case study wildfires (adjacent numbers match the leftmost column in Table 5-1). We selected wildfires with a wide range of sizes and locations (different fuel types) to better understand the differences of the emissions estimates between the FEIs across a range of conditions.

Table 5-1. Description of the ten case study wildfires used to provide an in-depth comparison of emissions from the five FEIs.

No.	Name	Acres Burned	Duration	Location (counties)
1	Dixie	963,309	Jul 13 – Oct 21	Butte, Lassen, Plumas, Shasta, Tehama (CA)
2a 2b	Monument River Complex	223,124 199,343	Jul 30 – Oct 25 July 30 – Oct 25	Trinity (CA) Siskiyou (CA)
3	Caldor	221,835	Aug 15 – Sep 18	El Dorado, Amador, Alpine (CA)
4	French	26,535	Aug 18 – Oct 19	Kern (CA)
5	Oil Springs	12,613	Jun 18 – Jul 10	Rio Blanco (CO)
6a 6b	Telegraph Mescal	180,757 72,250	Jun 4 – Jul 5 Jun 1 – Jun 18	Pinal, Gila (AZ) Gila (AZ)
7	Rafael	78,065	Jun 18 – Jul 15	Yavapai, Coconino (AZ)
8	Bootleg	413,717	Jul 8 – Aug 14	Klamath, Lake (OR)
9	Cedar Creek	55,572	Jul 11 – Aug 15	Okanagan (WA)
10	Snake Fire Complex	109,444	Jul 7 – Aug 15	Nez Perce (ID), Wallowa (OR), Asotin (WA)

[27] https://www.ncei.noaa.gov/access/monitoring/monthly-report/fire/202113
[28] https://www.ncei.noaa.gov/access/monitoring/monthly-report/fire/202013
[29] https://www.theguardian.com/us-news/2021/feb/11/california-dry-weather-drought-wildfire-agriculture
[30] https://education.nationalgeographic.org/resource/megafire/

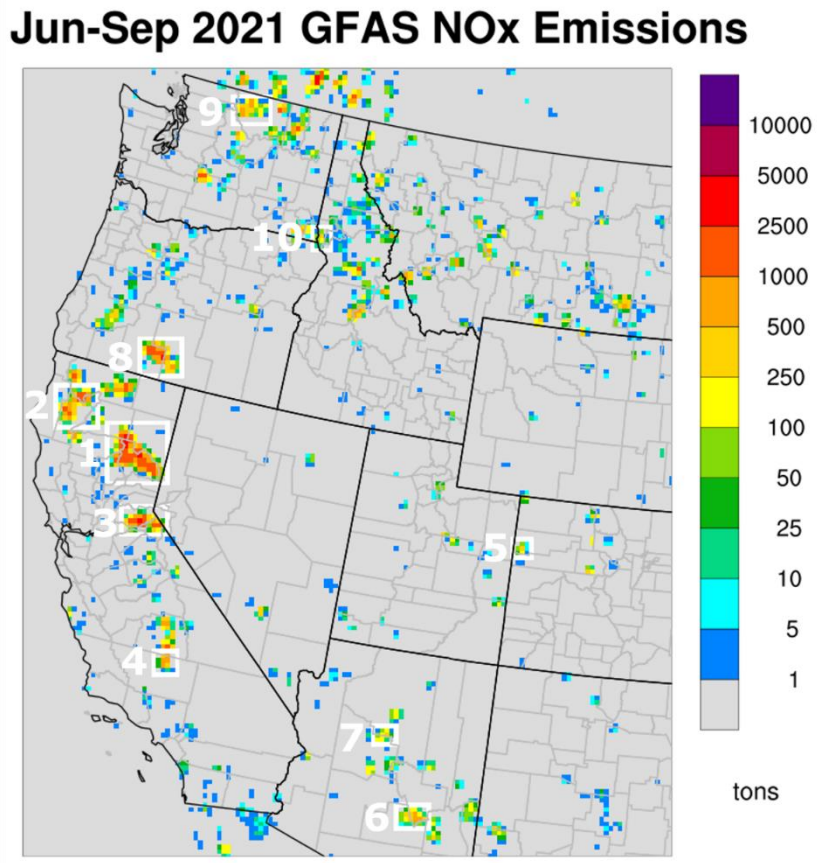

Figure 5-1. GFAS1.2 NOx emissions for June – September 2021 across a subsection of the western 12 km CAMx domain, with overlays showing subdomains for ten case study wildfires. Numbers correspond to the fires shown in Table 5-1.

5.1.1 2021 California Wildfires

2021 had more acres burned in California than any other year besides 2020 (see Figure 5-2). California had approximately 7,000 wildfires in 2021, that burned approximately 2.6 million acres (Table 5-2).

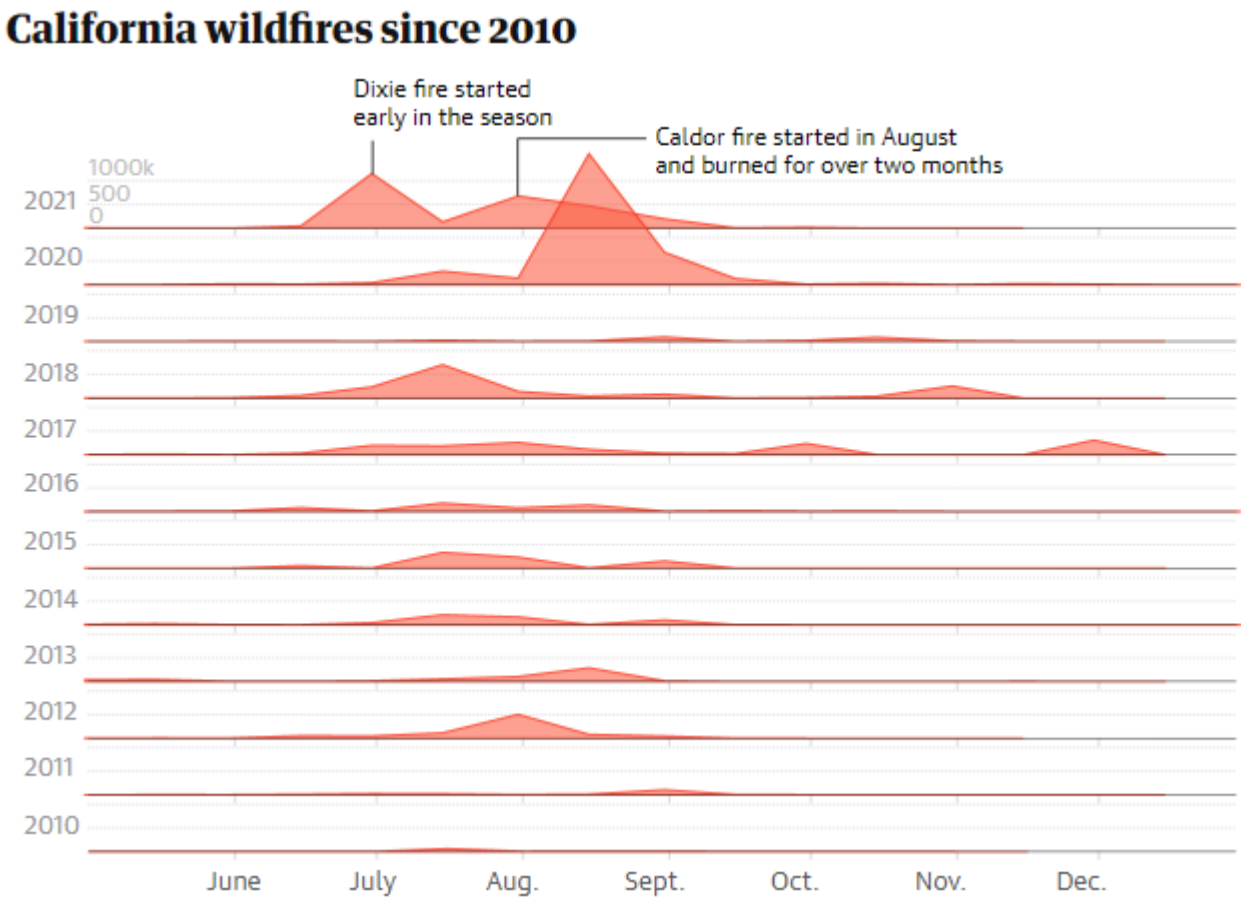

Figure 5-2. Time series of acreage burned in California comparing 2021 with 2010-2021 (Source: https://blueskyhq.io/blog/how-wildfires-are-impacting-businesses-globally).

Table 5-2. Number of California wildfires and yearly acres burned during 2016-2023 Source: https://www.frontlinewildfire.com/wildfire-news-and-resources/california-wildfires-history-statistics/).

Year	Number	Acres Burned
2016	6,954	669,534
2017	9,270	1,599,640
2018	7,948	1,975,086
2019	7,148	277,285
2020	8,648	4,304,379
2021	7,396	2,569,386
2022	7,477	363,939
2023	7,084	343,025

Below are a few notable 2021 California wildfires that are used as case studies in our evaluation of the five FEIs. Most of the California fires ended around October 25, but since our modeling episode covers June-September 2021, the analysis of the FEI emissions ends on September 30, 2021.

1. Dixie Fire: July 13 – October 25, 2021

The Dixie Fire was the second largest wildfire in California history (after 2020 August Complex Fire) burning over three months and almost a million acres, which is approximately 35% of the acres

burned in 2021 California. Smoke from the Dixie Fire caused unhealthy air quality across the western states, including Utah and Colorado. On August 4, 2021, $PM_{2.5}$ levels spiked to over 3 times the 24-hour $PM_{2.5}$ NAAQS in Salt Lake City. The Dixie Fire began on July 13 when a large tree fell on a PG&E powerline in the Feather River Canyon. High winds in mid-August contributed to the spread of the fire.

2. Monument-River Complex Fires: Jul 30 – October 25

Lightning strikes at the end of July started numerous wildfires in Northern California. The Monument and River Complex Fires were the 2nd and 4th biggest 2021 wildfires in California and are used to represent these lightning-caused wildfires (other nearby fires active at the same time are the Antelope, Lava, McFarland and McCash Fires). The Monument Fire burned in the Shasta-Trinity National Forest in Trinity County for three months. The River Complex fire was in the Klamath Forest in Siskiyou County on the border with Trinity County just north of the Monument Fire. Smoke from these fires impacted air quality in the Sacramento Valley and San Francisco Bay Area.

3. Caldor Fire: August 15 – September 18

The Caldor Fire is the third largest 2021 wildfire in California and believed to have been started by lightning and burned mainly in the El Dorado National Forest and adjacent regions. It was the second fire to cross the crest of the Sierra Mountains (after the Dixie Fire that did it the previous week) and threatened South Lake Tahoe. It started slowly and was given little attention due to resources being focused on other wildfires and then exploded into a large wildfire under high winds starting on August 16.

4. French Fire: Aug 18 – Oct 24

The French Fire was started by lightning and burned in Kern County in the Sierra Nevada foothills. It grew rapidly, fanned by high winds in mid-August.

5.1.2 2021 Colorado Wildfires

2021 was one of the smokiest years in Colorado ever and had some of the highest ozone levels in the Denver area in a decade due to meteorological conditions very conducive to ozone formation combined with ozone precursors from wildfires. However, the smoke did not come from local wildfires in Colorado but from wildfires in California, Arizona and the Pacific Northwest. The Denver Metro/North Front Range (DM/NFR) ozone nonattainment area (NAA) recorded ozone exceedances of the 2015 70 ppb ozone NAAQS on 66 of the 122 days from June 1 to September 30 with 62 of those days flagged by the state (CDPHE/APCD) as potentially being influenced by smoke from wildfires. In July 2021, the Rocky Flats North (RFNO) monitor had 22 days with exceedances of the 2015 ozone NAAQS. NOAA estimates without incoming smoke and ozone precursors from wildfires there would have been only 10 ozone exceedances at RFNO in July 2021. Unlike 2020, which was the largest wildfire season in Colorado ever burning 665,454 acres, 2021 was a relatively light wildfire year for Colorado (42,202 acres) so we selected the largest Colorado wildfire during our June-August 2021 modeling period for a case study wildfire in Colorado.

5. Oil Springs Fire: June 18 – July 10

The Oil Springs fire started by lightning just north of Grand Junction in western Rio Blanco County, Colorado. Rio Blanco County is west of the DM/NFR NAA on the border with Utah. It is a relatively smaller fire (12,613 acres) taking up a third of a 12 km grid cell and is included as a case study fire to also examine smaller fires as well as its relatively closer proximity to the Denver ozone NAA.

5.1.3 2021 Arizona Wildfires

2021 was a high wildfire year in Arizona with almost 2,000 fires burning 524,428 acres fueled by drought, high temperatures and dry lightning.

6. Telegraph Fire and Mescal Fires: June 4 – July 5

The Telegraph Fire started on June 4, 2021, and burned in Gila and Pinal Counties for about a month. It is believed to be human-caused and was the 6th largest wildfire in Arizona history. The Mescal Fire started on June 1 and burned 72,250 acres in Gila County.

7. Rafael Fire: June 18 – July 15

The Rafael fire burned 78,065 acres on the border of Yavapai and Coconino Counties and was started on June 18 by lightning.

5.1.4 2021 Utah Wildfires

2021 was a low wildfire year for Utah so we did not select any case study fires in Utah.

5.1.5 2021 Oregon Wildfires

In 2021, Oregon had over a thousand wildfires that burned over a half million acres with by far the largest 2021 Oregon wildfire selected for case study.

8. Bootleg Fire: July 6 - August 15

The Bootleg Fire was started by lightning and was the second largest U.S. wildfire in 2021 behind only the Dixie Fire in California. It burned 413,765 acres and was the third largest wildfire in Oregon history. The smoke from the Bootleg Fire travelled all the way to the east coast. The heat and smoke from the Bootleg Fire generated its own weather including pyrocumulus and pyrocumulonimbus clouds some reaching as high as 45,000 feet (14 km) and bringing lightning strikes and precipitation and even tornados.

5.1.6 2021 Washington Wildfires

The Washington 2021 wildfire season begin early in March and ended in early October after precipitation. Approximately 500,000 acres burned as compared to 840,000 acres in 2020.

9. Cedar Creek Fire: July 11 - August 15

The Cedar Creek Fire represent a series of wildfires that occurred at the same time in Okanagan County on the border with Canada. Although the Cedar Creek fire burned approximately 55,000 acres the combined acres burned in Okanagan County from all of the fires was ~350,000 acres. The fires started by lightning and caused smoke in eastern Washington and the Puget Sound areas.

5.1.7 2021 Idaho Wildfires

In 2021, wildfires in Idaho burned 433,734 acres with about half due to natural and half due to human causes.

10. Snake River Complex Fire: July 7 – August 15

The Shovel Creek Fire was the largest 2021 wildfire in Idaho (90,594 acres) that with the nearby Shovel Creek Fire along with adjacent Hood River Fire (12,422 acres) and Captain John Creek Fire (6,533 acres) are referred to as the Snake River Complex Fire which combined burned 109,444 acres in western Idaho on the border of Washington and Idaho.

5.1.8 2021 Wyoming Wildfires

Although summer temperatures were higher than normal in Wyoming, wildfires were average with the two largest were the Crater Ridge Fire (~7,700 acres) and Deer Creek grass fire (~5,300 acres). Thus, no case study fires were selected for Wyoming.

5.1.9 2021 New Mexico Wildfires

2021 was a low wildfire year in New Mexico (121,277 acres burned), especially compared to 2022 (899,453 acres) so no case studies were defined in New Mexico.

5.2 FEI Emissions Comparison

In Figure 5-3, we present spatial maps similar to Figure 5-1 showing the June – September 2021 total NOx emission from the FINN2.5 (top left), GFAS1.2 (top middle), FEER1.0 (top right), RAVE1.0 (bottom left) and QFED2.5 (bottom middle) FEIs. In general, we find similar spatial patterns – but differing magnitudes – among the four non-RAVE FEIs, especially for the ten case study fires. The RAVE1.0 plot (bottom left panel of Figure 5-3) shows substantially more fire detections than the other four FEIs. The RAVE FEI also shows fires in desert areas of southeast California and southwest Arizona. It is likely that at least some of the satellite-based fire detections in these areas are erroneous and caused by highly reflective surfaces (e.g. solar farms)[31]. Figure 5-4 shows bar charts of total NOx emissions for each of the ten case study wildfires (clusters) by individual FEI (bars in each cluster). In addition to the five FEIs, we display the five-FEI average as a separate bar to identify potential outliers more easily. Because there is a substantial range in emissions across the ten case study fires, we display the four largest fires in the left panel and the six smallest fires in the right panel of Figure 5-4. QFED2.5 NOx emissions are lower than the FEI average for large fires. Otherwise, we find no clear outlier FEIs (substantially different than five-FEI average) across all fires. We provide spatial maps and case study fire emissions charts similar to those shown in Figure 5-3 and Figure 5-4 for VOC, $PM_{2.5}$ and CO emissions in Appendix A. We summarize findings from these maps and charts as follows:

- FINN2.5 VOC emissions are substantially higher than the 5-FEI average for Northern California and Washington fires.
- QFED VOC emissions are lowest of all FEIs for larger fires.
- $PM_{2.5}$ emissions show better agreement across the FEIs than for NOx or VOC.
- GFAS1.2 $PM_{2.5}$ emissions are lower than the 5-FEI average for most fires.
- QFED $PM_{2.5}$ emissions are higher than the 5-FEI average for all fires.

[31] https://gsweb18.umd.edu/sites/default/files/2022-07/Ivan_NOAA_GOFC_Fire_070822%20final.pdf

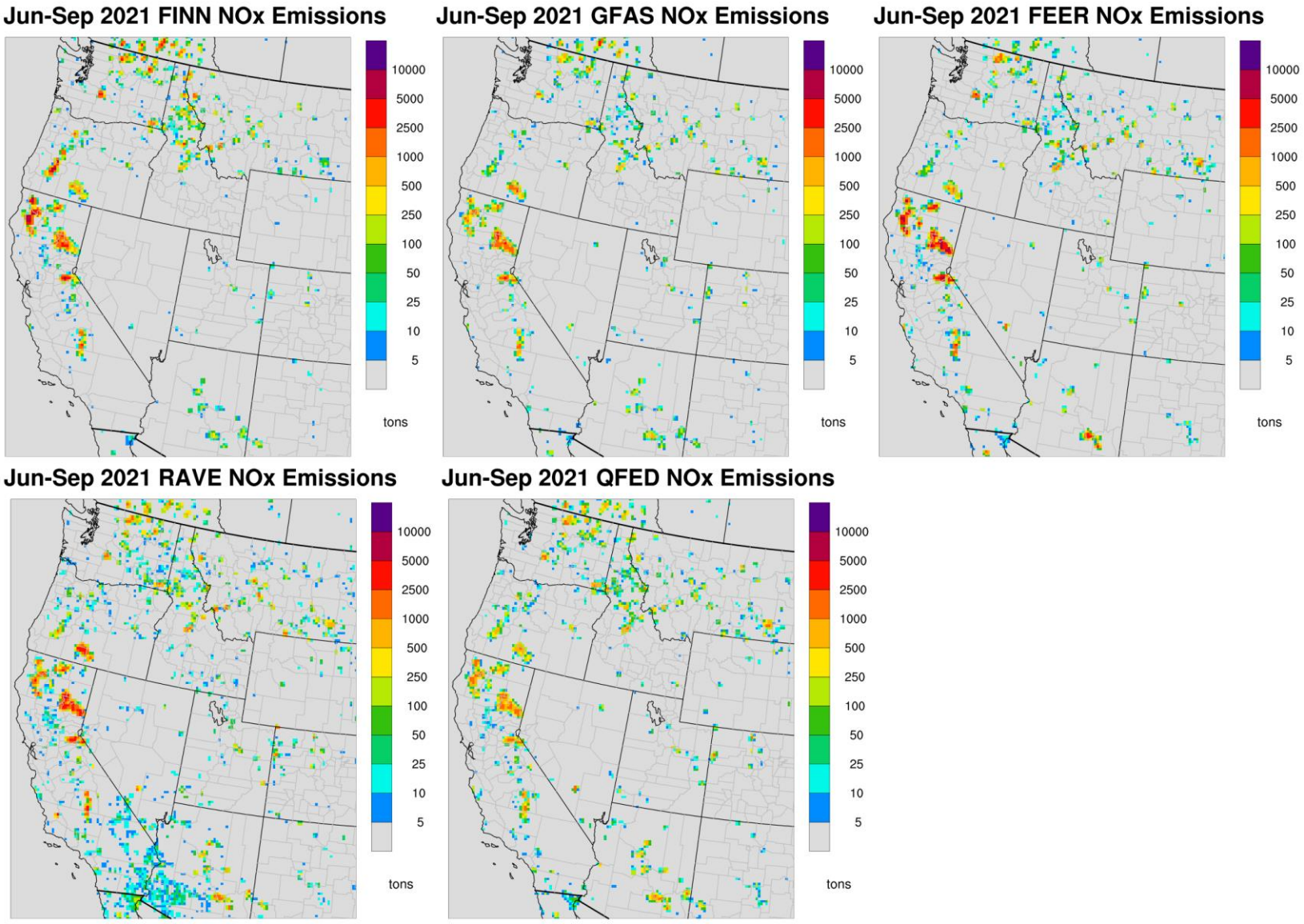

Figure 5-3. NOx emissions for June – September 2021 across a subsection of the western 12 km CAMx domain for FINN2.5 (top left), GFAS1.2 (top middle), FEER1.0 (top right), RAVE1.0 (bottom left) and QFED2.5 (bottom middle).

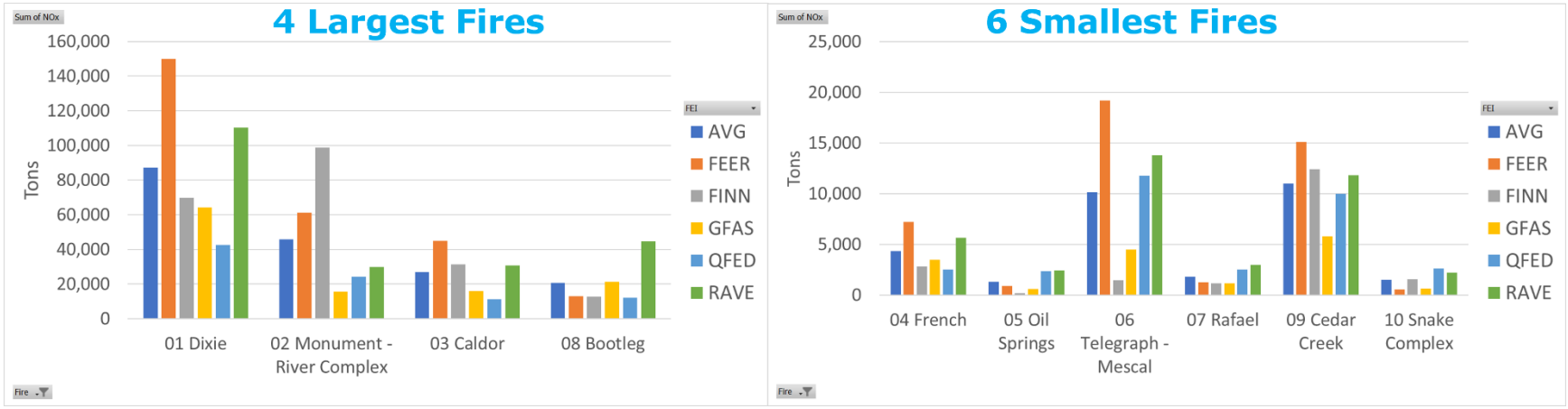

Figure 5-4. NOx emissions for the ten case study fires for FEER1.0 (orange), FINN2.5 (grey), GFAS1.2 (yellow), QFED2.5 (light blue), RAVE1.0 (green) and 5-FEI average (dark blue). Emissions for largest four fires shown in left panel; six smallest fires shown in right panel.

6.0 EVALUATION OF ALTERNATIVE FIRE EMISSIONS

As noted in Chapter 3, there are 5 alternative fire emission inventories (FEI) that can potentially be evaluated. The FEI processor contains two plume rise algorithms (PBL500 and Sofiev), a default and alternative (RAVE) diurnal temporal distributions, default and new (rapid) NOx speciation, and treatment of fire primary organic carbon (POC) emissions as inert or semi-volatile. This results in 80 separate combinations of alternative fire that all cannot be evaluated. We therefore designed a condensed set of simulations described and evaluated in the sections that follow.

6.1 Testing Database for Alternative Fire Emissions

We configured the Atmospheric Model Evaluation Tool (AMET) to evaluate CAMx for the June – August 2021 modeling period. AMET matches the model output at grid cells that collocate with observational sites for one or more monitoring networks. AMET also performs species mappings to match the modeled species to those from corresponding observations. These model and observation pairings are then used to analyze the model's performance using a variety of statistical and graphical techniques. Table 6-1 summarizes key statistical measures that were used to quantify model performance. We focused the evaluation on ozone, total $PM_{2.5}$ mass and speciated $PM_{2.5}$ concentrations. After an initial evaluation conducted in Phase I for the entire June – September 2021 4-month episode, we identified a shorter period – July-August 2021 – that had smoke impacts from numerous, large fires across the Western U.S. for focused analysis for the remaining phases.

Table 6-1. Model Performance Evaluation Metrics.

Metric	Definition
Mean observation value	The average observed concentration
Mean simulation value	The average simulated concentration
Normalized bias (NMB)	$\sum_{l=1}^{N}(S_l - O_l)/O_l \cdot 100\%$
Normalized error (NME)	$\sum_{l=1}^{N}\lvert S_l - O_l\rvert/O_l \cdot 100\%$
Where, N is the number of data pairs, and S_l and O_l are the simulated and observed values at site *l*, respectively, over a given time interval	

6.2 Model Performance Goals and Benchmarks

EPA first proposed the use of ozone model performance goals in their 1991 ozone modeling guidance (EPA, 1991) with goals for bias (≤±15%) and error (≤35%). Since then, EPA has lessened the emphasis on the use of model performance goals as some users focused on achieving the model performance goals and not whether the model was correctly simulating atmospheric processes that led to the high ozone concentrations. However, model performance goals are still useful for interpreting model performance and putting the model performance into context. Boylan and Russell (2006) extended the performance goals to PM species and visibility. Simon et al. (2012) summarized the model performance statistics of 69 PGM applications from 2006 to 2012 and although they found significant variability, they were able to isolate model performance statistical levels for the best performing models.

Emery et al., (2016) built off the work of Simon et al. (2012) including additional PGM model applications and recommended a set of PGM model performance goals and criteria based on the variability of past model performance. "Goals" indicate statistical values that about a third of the top performing past PGM applications have met and should be viewed as the best a model can be expected to achieve. "Criteria" indicates statistics values that about two thirds of past PGM applications have met and should be viewed as what most models have achieved. We compare the CAMx 2021 simulations for the various fire configurations model performance statistics for normalized mean bias (NMB) and normalized mean error (NME) against the model performance goals and criteria summarized by Emery et al., (2016) that are given in Table 6-2.

Table 6-2. Recommended benchmarks for photochemical model statistics (Source: Emery et al., 2016).

Species	NMB		NME		r	
	Goal	Criteria	Goal	Criteria	Goal	Criteria
1-hr & MDA8 Ozone	<±5%	<±15%	<15%	<25%	>0.75	>0.50
24-hr $PM_{2.5}$, SO_4, NH_4	<±10%	<±30%	<35%	<50%	>0.70	>0.40
24-hr NO_3	<±15%	<±65%	<65%	<115%	NA	NA
24-hr OC	<±15%	<±50%	<45%	<65%	NA	NA
24-hr EC	<±20%	<±40%	<55%	<75%	NA	NA

6.3 Available Aerometric Data for Evaluations

Air quality observation data from the following monitoring networks operating in 2021 were used in the CAMx 12 km model performance evaluation.

EPA AQS Surface Air Quality Data: Data files containing hourly-averaged concentration measurements at a wide variety of state and EPA monitoring networks were available in the Air Quality System (AQS[32]) database. For this study, we evaluated hourly ozone and 24-hour average $PM_{2.5}$ mass and speciated $PM_{2.5}$ concentrations at AQS monitoring stations.

CASTNET Network: The Clean Air Status and Trends Network (CASTNET[33]) collects ozone, NO_2, SO_2 and $PM_{2.5}$ concentrations across 99 sites throughout the U.S. (see map in Figure 6-1). For this study, we used hourly ozone concentrations from the CASTNET monitors for model performance evaluation.

IMPROVE Monitoring Network: The Interagency Monitoring of Protected Visual Environments (IMPROVE[34]) network collects 24-hour average $PM_{2.5}$ and PM_{10} mass and speciated $PM_{2.5}$ concentrations at several sites on a 1:3 day sampling frequency, including most Class I areas. We provide a map of IMPROVE monitoring stations in Figure 6-2.

[32] https://www.epa.gov/aqs

[33] https://www3.epa.gov/castnet/docs/CASTNET-Factsheet-2021.pdf

[34] https://vista.cira.colostate.edu/Improve

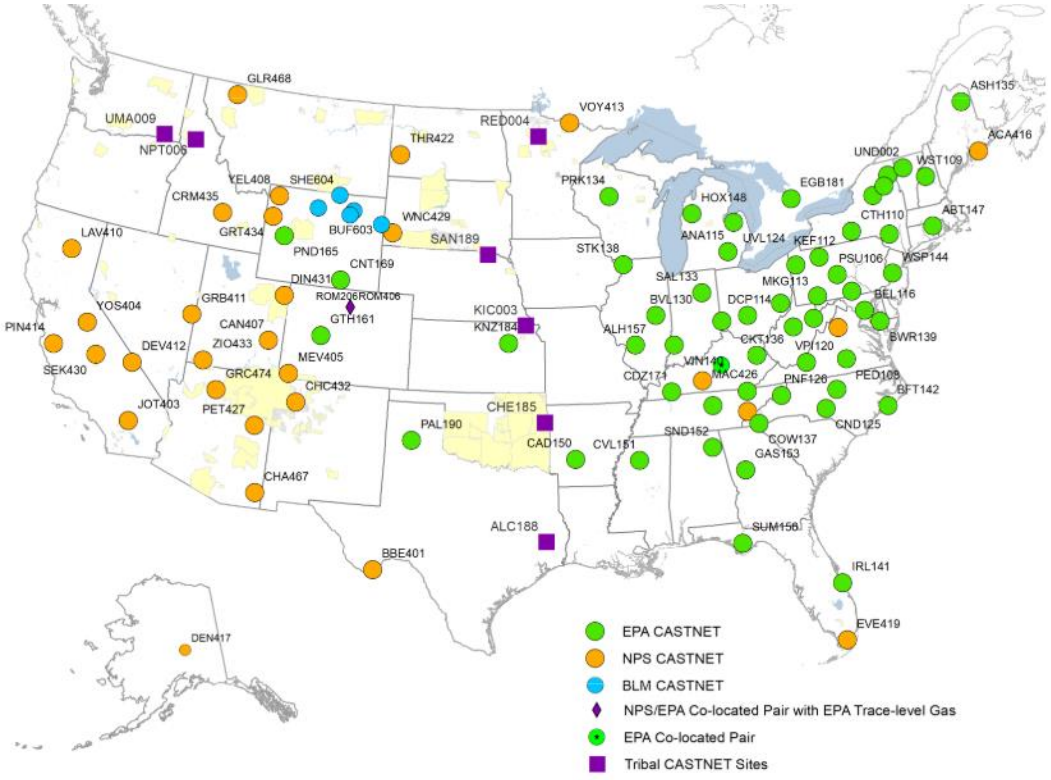

Figure 6-1. Map of CASTNET site locations. Tribal boundaries shown in yellow. Adapted from CASTNET fact sheet at https://www3.epa.gov/castnet/docs/CASTNET-Factsheet-2021.pdf.

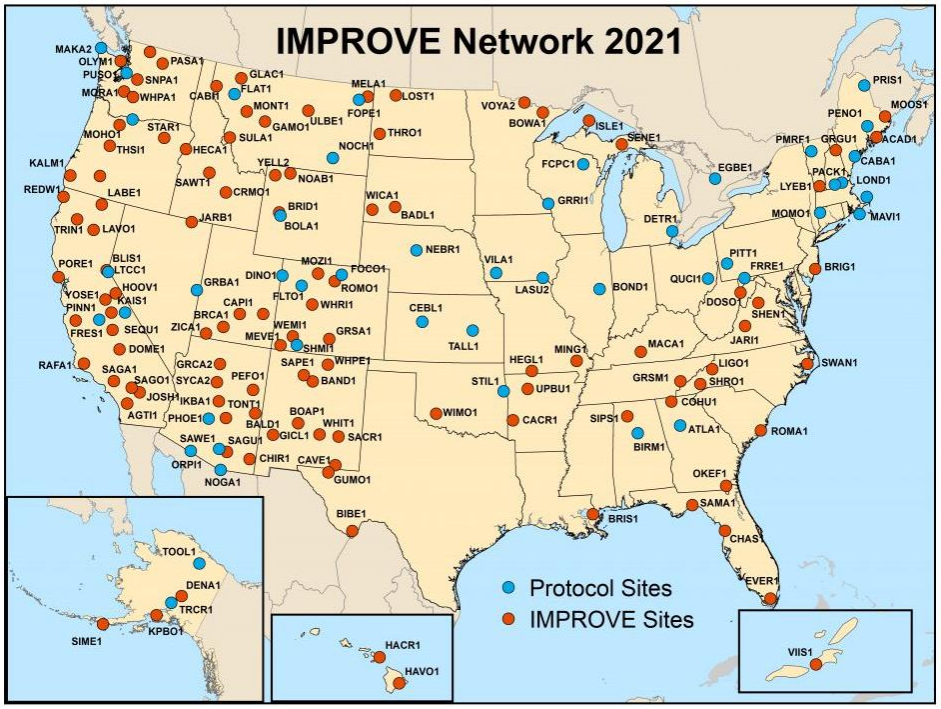

Figure 6-2. Map of IMPROVE site locations. Adapted from https://vista.cira.colostate.edu/Improve/improve-program/.

6.4 Initial Testing (Phase I)

We detail the configuration of our CAMx simulations (Phases I-V) in Table 6-3. In Phase I, we examined the impacts of the FEIs themselves. For this initial set of runs, we apply the same NOx speciation (rapid), SOAP version (SOAP2; inert POC), temporal allocation (RAVE) and plume rise algorithm (Sofiev). These simulations utilized a one-way nested approach where the 3-D outputs from the 36-km simulation were used to generate boundary conditions for the 12-km simulation. Because the RAVE1.0 FEI does not cover the full extent of the CAMx 36-km domain, we used GFAS1.2 emissions for the grid cells in the 36 km domain where RAVE1.0 emissions do not exist. In Phase I we evaluated and analyzed the CAMx model results for the five FEIs to determine which two FEIs provide the best representation of the observed $PM_{2.5}$, speciated $PM_{2.5}$ and ozone air quality that would be used in subsequent phases of the study.

Table 6-3. Configuration for CAMx simulations.

Phase	Run	Domains	FEI	Temporal	Vertical	NOx Speciation	SOAP version
I	run0	36/12 km	None	N/A	N/A	N/A	SOAP2
I	run1	36/12 km	RAVE1.0	N/A	Sofiev	rapid	SOAP2
I	run2	36/12 km	GFAS1.2	RAVE	Sofiev	rapid	SOAP2
I	run3	36/12 km	QFED2.5	RAVE	Sofiev	rapid	SOAP2
I	run4	36/12 km	FEER1.0	RAVE	Sofiev	rapid	SOAP2
I	run5	36/12 km	FINN2.5	RAVE	Sofiev	rapid	SOAP2
II	run6	12 km	RAVE1.0	N/A	Sofiev	default	SOAP2
III	run7	12 km	RAVE1.0	N/A	PBL500	rapid	SOAP2
III	run8	12 km	FEER1.0	default	Sofiev	rapid	SOAP2
IV	run9	12 km	RAVE2.0 (scaled PM)	N/A	Sofiev	rapid	SOAP2
V	run10	12 km	RAVE2.0 (unscaled PM)	N/A	Sofiev	rapid	SOAP3 with EVAP
V	run11	12 km	RAVE2.0 (unscaled PM)	N/A	Sofiev	rapid	SOAP3 without EVAP

6.4.1 Ozone Evaluation

In Figure 6-3, we show scatter plots of MDA8 ozone performance for No Fires (top left), RAVE1.0 (top middle), GFAS1.2 (top right), QFED2.5 (bottom left), FEER1.0 (bottom middle), and FINN2.5 (bottom left) at all AQS monitors in 12 km domain spanning the entire June-September 2021 modeling period. The No Fires run achieves the performance goal for both bias (NMB: -4%) and error (NME: 15%). All five simulations with fire emissions show NME that stays the same (FINN2.5: 15%) or is slightly improved (all other FEIs: 14%). Bias performance is slightly more varied, but all FEIs show improved ozone performance from the No Fires run with NMB varying between -2% (QFED2.5) and +2% (FINN2.5). In between, RAVE1.0, GFAS1.2 and FEER1.0 all show good distribution across the 1:1 line, with similar numbers of occurrences of large underestimates and overestimates, which explains the near zero bias.

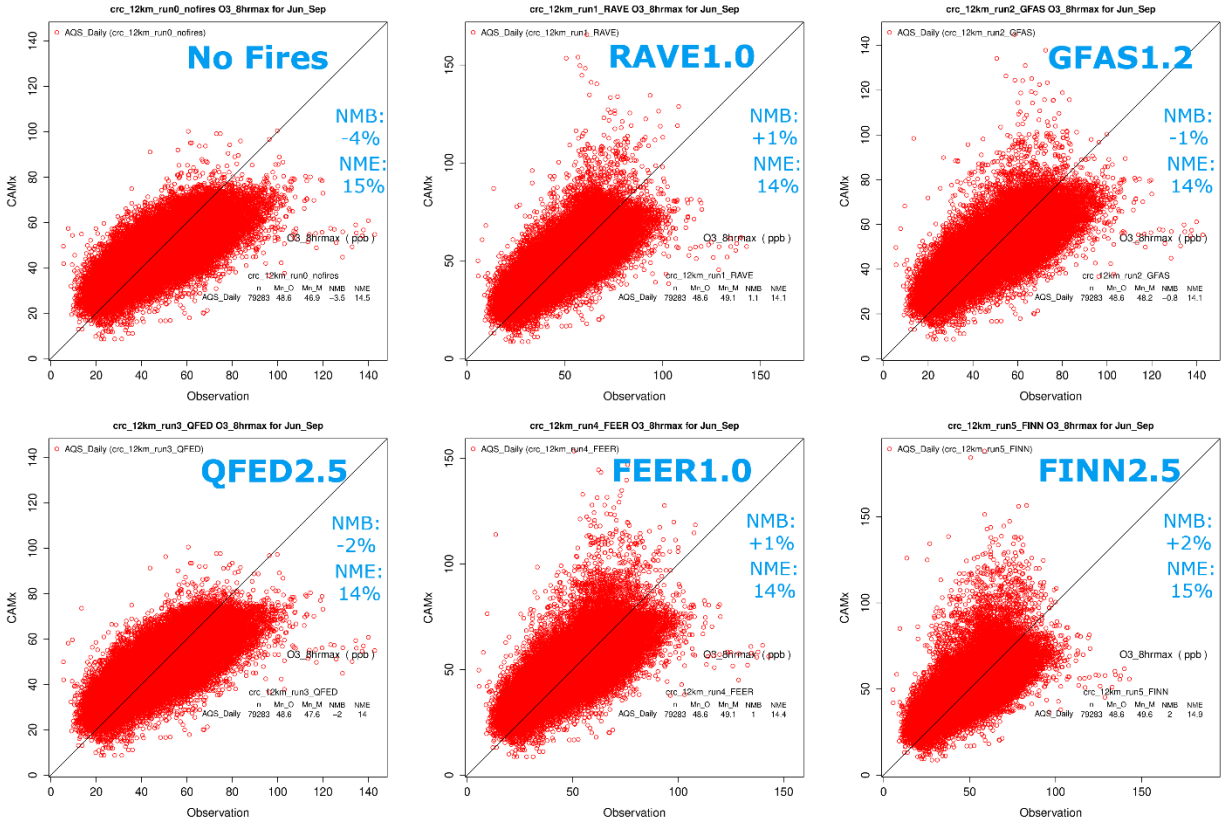

Figure 6-3. Scatter plots showing MDA8 ozone model performance for No Fires (top left), RAVE1.0 (top middle), GFAS1.2 (top right), QFED2.5 (bottom left), FEER1.0 (bottom middle), and FINN2.5 (bottom left) at all AQS monitors in 12-km western U.S. modeling domain during June-September 2021.

Figure 6-4 shows a similar set of scatter plots, but for the CASTNET monitors instead of the AQS monitors. As shown in Figure 6-1, the CASTNET monitors are located mostly in rural areas, compared to the AQS monitors which are located mostly in or near urban/suburban areas. The No Fires run shows a more pronounced negative bias (NMB: -7%) compared to the AQS monitors (-4%), which lies between the goal and criteria benchmarks. The No Fires error, however, shows slightly better performance (NME: 14%) compared to performance at the AQS monitors (15%). All FEIs show improvements in both bias and error statistics at CASTNET monitors compared to the No Fires run. RAVE1.0 has the smallest bias (NMB: -0.2%), while GFAS1.2 and QFED2.5 have the smallest error (NME: 12%).

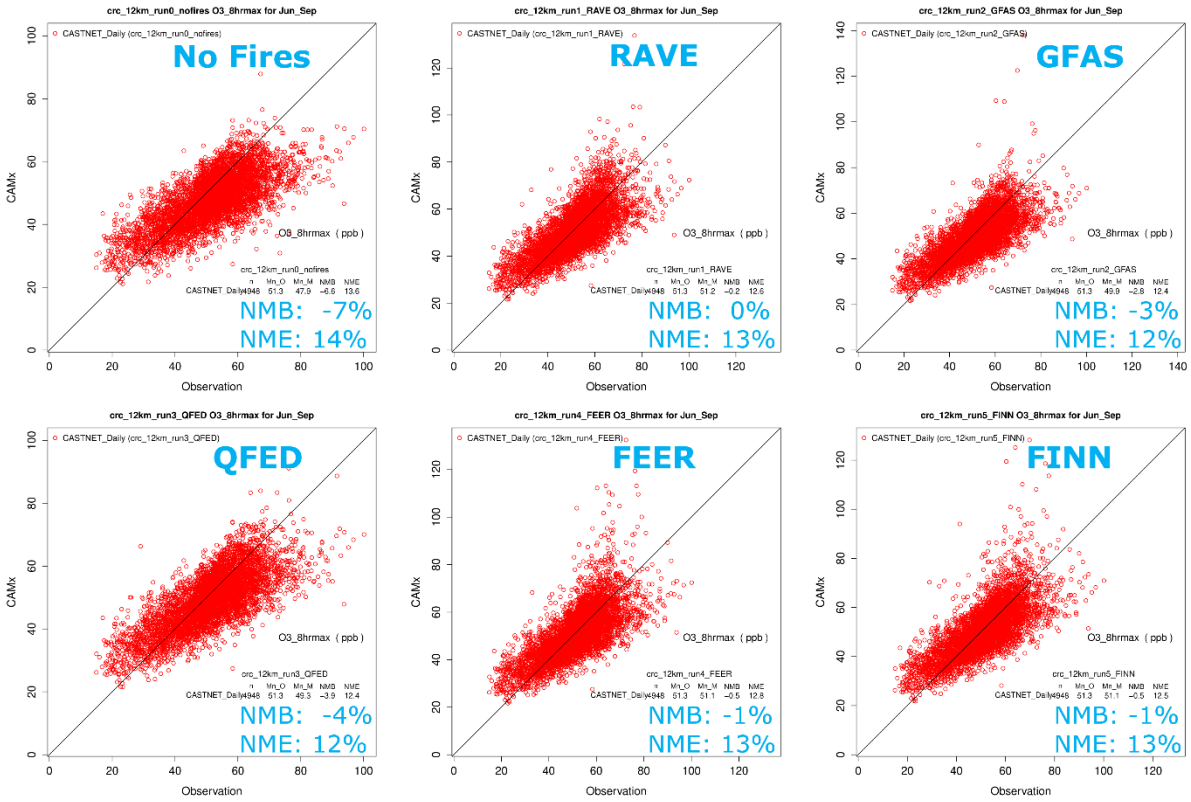

Figure 6-4. Scatter plots showing MDA8 ozone model performance for No Fires (top left), RAVE1.0 (top middle), GFAS1.2 (top right), QFED2.5 (bottom left), FEER1.0 (bottom middle), and FINN2.5 (bottom left) at all CASTNET monitors in 12-km western U.S. modeling domain during June-September 2021.

In Figure 6-5, we present the 12-km western U.S. domain-wide and individual state MDA8 ozone NMB (top), NME (middle) and correlation coefficient (bottom) for No Fires (dark blue), RAVE1.0 (orange), GFAS1.2 (grey), QFED2.5 (yellow), FEER1.0 (light blue), and FINN2.5 (green) at all AQS monitors in 12 km domain during June-September 2021. The MDA8 ozone criterion (black dotted lines) and goal (light blue dotted lines) benchmarks from Emery et al. (2016) are also shown on the figures. All runs (No Fires and all FEI runs) achieve the ozone criteria benchmarks for bias and error for each individual state. In California and Oregon, negative biases in the No Fires run are improved by all FEIs. Only FINN2.5 shows a positive bias for these two states, and for Oregon, this bias is higher than in the No Fires run. For most of the western states shown in Figure 6-5, the large negative ozone biases in the No Fires run are substantially improved by adding fire emissions, though the relative performance between the FEI simulations varies by state. Relative error performance in California and Oregon reveals that the FEI runs show similar error as the No Fires run, except for FINN2.5, which has slightly higher errors. For states with lower fire activity where impacts from more distant fires are likely (e.g. Idaho, Montana, Wyoming, North Dakota), all FEI runs show smaller errors than the No Fires run. Correlation performance is more varied. For example, all FEI runs show worse correlation than the No Fires run in California (FINN2.5 has the lowest correlation). However, the FEI runs show better correlation than the No Fires run in Washington.

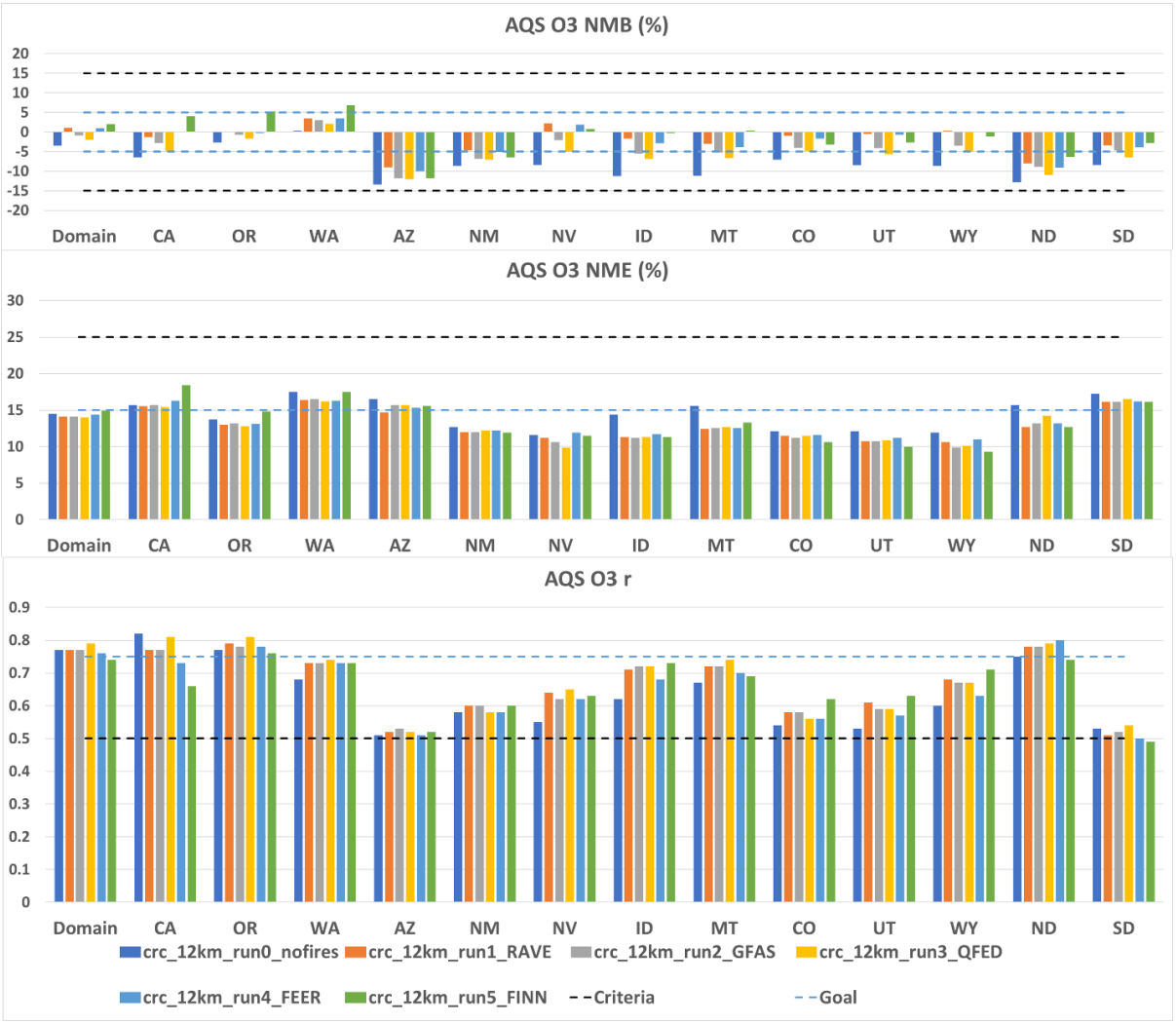

Figure 6-5. Domain-wide and individual state MDA8 ozone NMB (top), NME (middle) and correlation coefficient (bottom) for No Fires (dark blue), RAVE1.0 (orange), GFAS1.2 (grey), QFED2.5 (yellow), FEER1.0 (light blue), and FINN2.5 (green) at all AQS monitors in 12-km domain during June-September 2021. Criteria (black dotted lines) and goals (light blue dotted lines) benchmarks are from Emery et al. (2016).

6.4.2 $PM_{2.5}$ Evaluation and Comparison

Figure 6-6 shows scatter plots like those in Figure 6-3, but for 24-hour $PM_{2.5}$ performance. The No Fires run has substantial negative bias (NMB: -58%) and error (NME: 66%) that fall outside of the criteria benchmarks (NMB: < ±30%; NME < 50%). All FEI runs improve bias relative to the No Fires run, with NMB ranging from -40% (GFAS1.2) to +6% (FINN2.5). All FEI runs except FINN2.5 improve error, with RAVE1.0 (NME: 50%) and FEER1.0 (NME: 53%) showing the smallest error close to the error criterion benchmark. Examination of the individual model-observation pairs reveals some very large overestimations for all FEIs that range from hundreds to thousands of ug/m^3 for a small set of days. QFED2.5 and FINN2.5 show the largest and most frequent $PM_{2.5}$ overestimates, with both of these FEIs show relatively few underestimates, which explains the positive biases (QFED2.5 NMB: +3%; FINN2.5 NMB: +6%) for these runs. Although the inclusion of fire emissions reduces the underestimation bias in the No Fires simulation (-58% No Fires versus +6% to -40% with fires), we suspect that the poor performance may also be due to inaccurate emissions and/or boundary conditions.

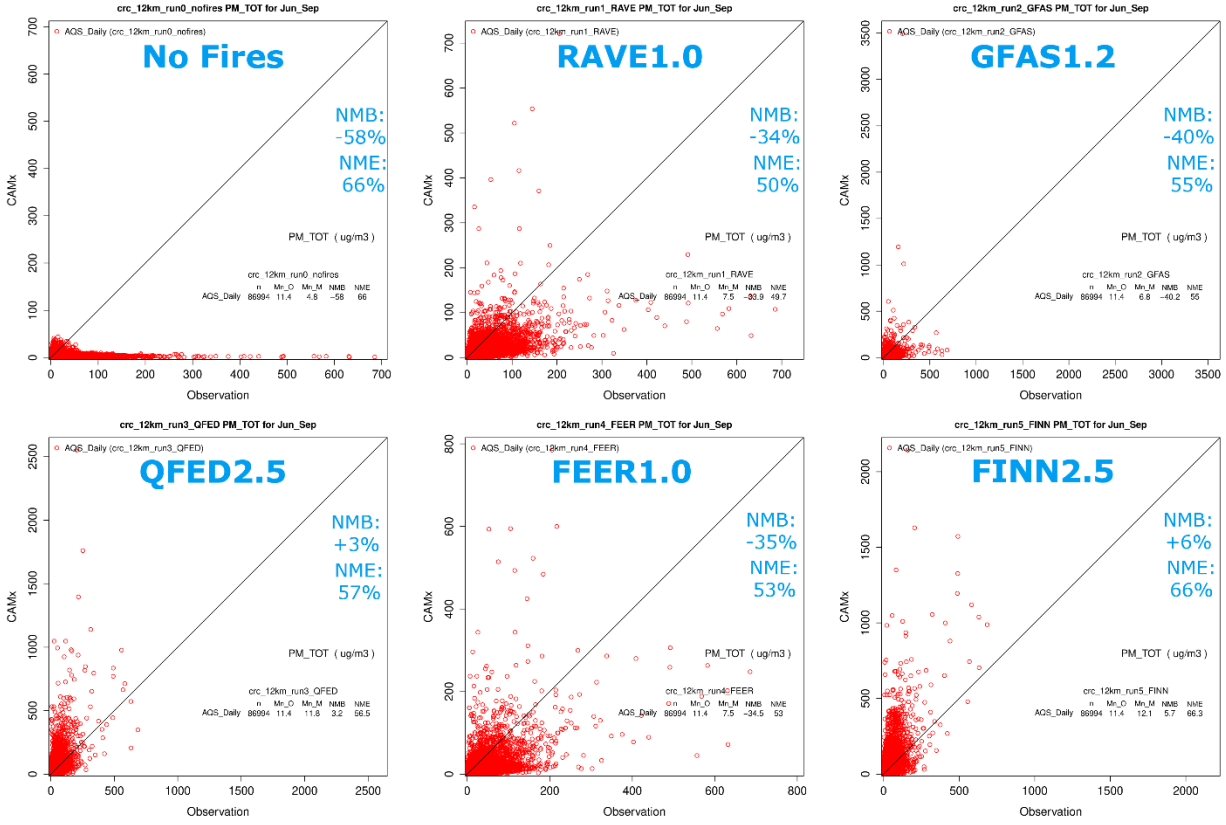

Figure 6-6. Scatter plots showing 24-hour $PM_{2.5}$ performance for No Fires (top left), RAVE1.0 (top middle), GFAS1.2 (top right), QFED2.5 (bottom left), FEER1.0 (bottom middle), and FINN2.5 (bottom left) at all AQS monitors in 12-km domain during June-September 2021.

Figure 6-7 shows a similar set of scatter plots as Figure 6-6 but for the IMPROVE monitors instead of the AQS monitors. As shown in Figure 6-2, the IMPROVE monitors are located mostly in or near Class I areas instead of in or near the more urban/suburban locations where AQS monitors tend to be sited. The No Fires run shows a more pronounced negative bias (NMB: -70%) at the IMPROVE monitors compared to the AQS monitors (-58%). Similarly, the No Fires error is more pronounced (NME: 75%) compared to performance at the AQS monitors (66%). All FEIs show improvements in both bias and error statistics at IMPROVE monitors compared to the No Fires run. While FINN2.5 shows the smallest bias (NMB: +3%), it also has the largest error (NME: 71%) of the FEI runs, representing only a modest improvement over the No Fires run. QFED2.5 has the next lowest bias (NMB: +14%), but it has the second largest error of the FEI runs (NME: 66%). Both FINN2.5 and QFED2.5 both show large $PM_{2.5}$ overestimations and considerably fewer underestimations. RAVE1.0, GFAS1.2 and FEER1.0 all show a better distribution of pairings across the 1:1 line, with RAVE displaying the best bias (NMB: -34%) and error (NME: 51%) of this group that are approximately right at the $PM_{2.5}$ bias and error benchmarks.

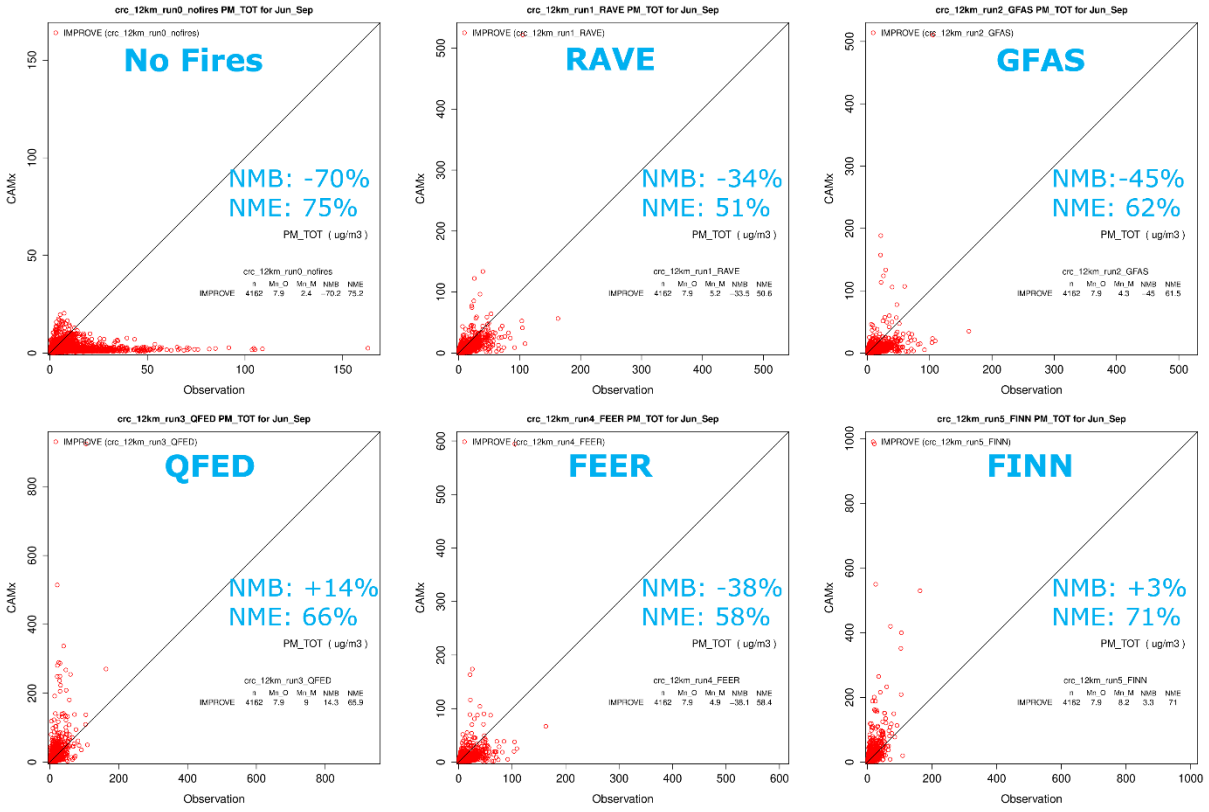

Figure 6-7. Scatter plots showing 24-hour $PM_{2.5}$ performance for No Fires (top left), RAVE1.0 (top middle), GFAS1.2 (top right), QFED2.5 (bottom left), FEER1.0 (bottom middle), and FINN2.5 (bottom left) at all IMPROVE monitors in 12-km domain during June-September 2021.

In Figure 6-8, we present the same domain-wide and individual state bar charts as in Figure 6-5, but for 24-hour average $PM_{2.5}$ instead of MDA8 ozone. In California and Washington, the large negative $PM_{2.5}$ biases in the No Fires run turn into large positive biases for FINN2.5. QFED2.5 with FINN2.5 also showing substantial positive $PM_{2.5}$ biases in Oregon. Performance across the remaining three FEIs (RAVE1.0, GFAS1.2 and FEER1.0) in these three states varies, but both bias and error improve relative to the No Fires run. Similar to the ozone statistics charts, the FEI runs generally improve $PM_{2.5}$ bias and error relative to the No Fires run for the states that are impacted more from downwind smoke rather than local wildfire activity. Unsurprisingly, $PM_{2.5}$ correlation is quite poor and sometimes negative at the state level (California and Washington) for the No Fires run. Again, relative performance between the FEI runs varies, but for nearly all states shown in the chart, the FEI runs substantially improve correlation from the No Fires run. The large discrepancy between the domain-wide correlation and individual states is explained by the numerous monitors in other states not shown in the chart, including central and midwestern states that experienced much smaller impacts from wildfires in summer 2021 compared to the western U.S. states shown in Figure 6-8.

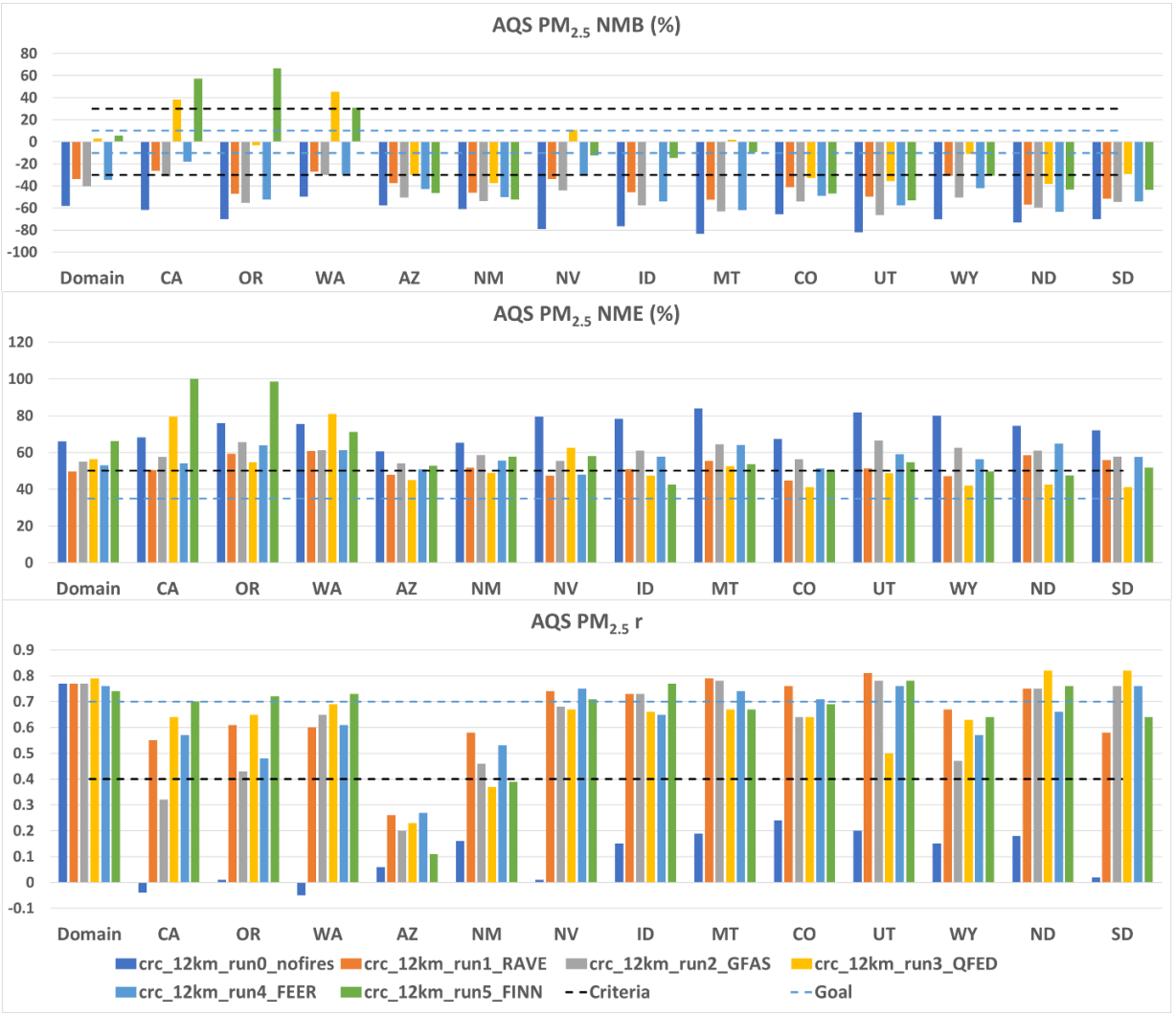

Figure 6-8. Domain-wide and individual state 24-hour $PM_{2.5}$ NMB (top), NME (middle) and correlation coefficient (bottom) for No Fires (dark blue), RAVE1.0 (orange), GFAS1.2 (grey), QFED2.5 (yellow), FEER1.0 (light blue), and FINN2.5 (green) at all AQS monitors in the 12-km domain during June-September 2021. Criteria (black dotted lines) and goal (light blue dotted lines) benchmarks from Emery et al. (2016).

6.4.3 Speciated $PM_{2.5}$ Evaluation and Comparison

As discussed in the previous section, domain wide $PM_{2.5}$ performance varies substantially from the statewide performance (see Figure 6-8). For the speciated $PM_{2.5}$ evaluation and comparison, we focus on California because wildfires were active for long periods across much of the state, and $PM_{2.5}$ performance varies substantially among the FEIs. Figure 6-9 shows the speciated $PM_{2.5}$ components ($\mu g/m^3$) for observed concentrations and the No Fires and the five FEI CAMx simulations, averaged over all IMPROVE monitors in California during June-September 2021. The large $PM_{2.5}$ overestimations in Figure 6-8 for QFED2.5 and FINN2.5 are mostly due to organic carbon (OC) and Other PM (OPM)[35]. QFED2.5 VOC emissions are the smallest of the FEIs, so most of the OC overestimation must result from directly emitted OC. On the other hand, FINN2.5 VOC emissions were substantially higher than the other FEIs, particularly in California, though information about relative contributions from primary and secondary OC is not readily available for the observed OC. QFED2.5 and FINN2.5 also overestimate OPM, which is the combination of CAMx species FPRM (fine primary aerosol), FCRS (fine crustal aerosol), and NA and CL (sea salt). Of these OPM species, only FPRM is present in the fire emissions. In the FEI processor, FPRM emissions are mapped from the difference between primary $PM_{2.5}$ emissions minus the sum of elemental and organic carbon emissions. QFED2.5 concentrations of elemental carbon (EC), nitrate (NO3) and sulfate (SO4) are all overestimated, but none exceed 1 $\mu g/m^3$. FINN2.5 EC and SO4 are both only slightly overestimated (by 0.2 and 0.1 $\mu g/m^3$, respectively), but NO3 is overestimated by 1.3 $\mu g/m^3$ (0.4 $\mu g/m^3$ observed vs. 1.7 $\mu g/m^3$ predicted). RAVE1.0, GFAS1.2 and FEER1.0 all show considerably better agreement with observations.

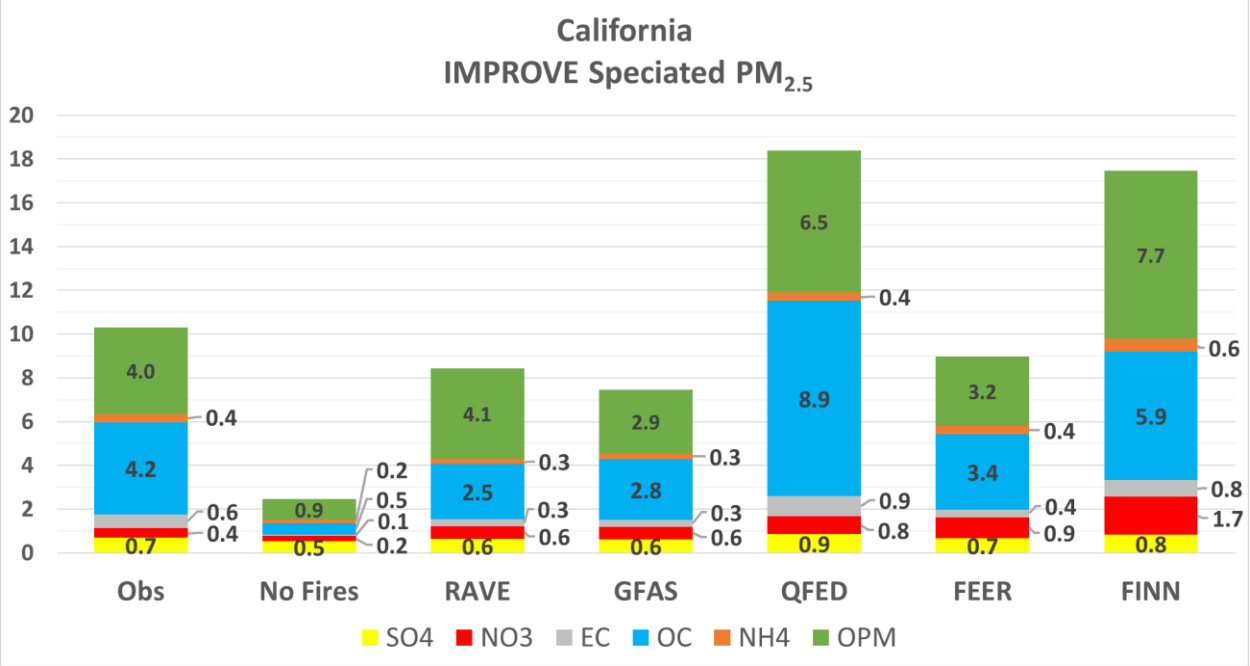

Figure 6-9. Speciated $PM_{2.5}$ components ($\mu g/m^3$) for observations (leftmost column) and No Fires, RAVE1.0, GFAS1.2, QFED2.5, FEER1.0, and FINN2.5 CAMx runs at all IMPROVE monitors in California during June-September 2021.

[35] OPM = Total $PM_{2.5} - NO_3 - SO_4 - NH_4 - EC - OC$

6.4.4 Final Selection of FEIs for Phases II-V

Our evaluation of ozone and $PM_{2.5}$ model performance presented in the previous sections finds that RAVE1.0 exhibits the best agreement with observations, while FINN2.5 displays the poorest agreement with observations. QFED2.5 shows large $PM_{2.5}$ overestimations. Finally, while FEER1.0 and GFAS1.2 show similar ozone performance, FEER1.0 shows slightly better agreement with $PM_{2.5}$ observations compared to GFAS1.2. Therefore, we selected RAVE1.0 and FEER1.0 for further testing in Phases II-V described below.

6.5 Further Testing, Evaluation and Optimization (Phases II-V)

Phase II, III, IV and V examined the impacts of NOx speciation, temporal/vertical allocation, the newly available RAVE2.0 emissions and SOAP3, respectively. To be computationally efficient so that more sensitivity tests could be examined, simulations in each of these phases cover the July-August 2021 period only, when the largest wildfires in the Western U.S. were active rather than the entire June – September, 2021 episode used in Phase I.

6.5.1 Phase II: NOx Speciation

In Phase II, we use the RAVE1.0 FEI to examine the impact of NOx speciation. For all FEI simulations in Phase I, we utilized a realistic (rapid) NOx to NOy conversion in smoke plumes, an approach obtained from the 2015 Texas Air Quality Research Program (AQRP) Fires project (McDonald-Buller et al., 2015). In Phase II, we developed an alternate set of RAVE1.0 fire emissions using a more traditional 90:10 split of $NO:NO_2$ that is typically used in emissions processing (e.g., default fire NOx speciation in the SMOKE[36] emissions processing system). As expected, differences between the two simulations are minor in regions not impacted by wildfire smoke. The change in NOx speciation impacts nitrate and therefore $PM_{2.5}$ concentrations, but the magnitudes of these impacts are small. We therefore chose to focus our evaluation on ozone performance in California. Figure 6-10 shows scatter plots of MDA8 ozone performance for RAVE1.0 with rapid NOx speciation (left panel) and RAVE1.0 with default ($NO:NO_2$ split of 90:10; right panel) at all AQS monitors in California during July-August 2021. The ozone impacts between the two runs are minor, with bias improving slightly (rapid NOx: -2.6%; default NOx: -1.4%) and error degrading slightly (rapid NOx: 16.5%; default NOx: 17.0%).

[36] https://www.cmascenter.org/smoke/

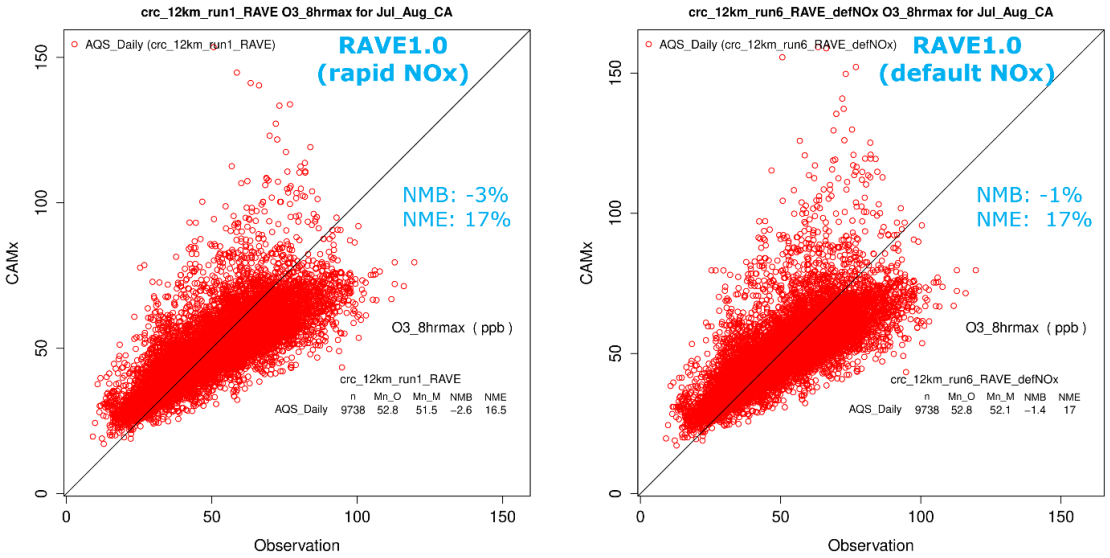

Figure 6-10. Scatter plots showing MDA8 ozone performance for RAVE1.0 with rapid NOx speciation (left) and RAVE1.0 with default NOx speciation (right) at all AQS monitors in California during July-August 2021.

6.5.2 Phase III: Temporal and Vertical Allocation

In Phase III, we examined the impact of different vertical and temporal allocation schemes available in the FEI processor. For the vertical allocation, the FEI processor defines the top of the smoke plume (injection height) using one of two options: 1) PBL500: adds 500 m to the PBL height or 2) Sofiev: uses a modified version of the injection height parameterization defined in Sofiev et al. (2012) that depends on FRP, PBL height and meteorological stability parameters. GFAS1.2 includes daily FRP, which we allocate to hourly FRP using the landcover-dependent FRP diurnal profiles developed by the RAVE team[37]. Because the RAVE product includes hourly FRP, we use this hourly FRP directly in the calculation of plume injection height in the Sofiev scheme. In Phase I, all FEI runs utilized the Sofiev plume top heights. In Phase III, we developed an alternate set of RAVE1.0 fire emissions that utilized the PBL500 plume top heights. As in Phase II, impacts from changes to the vertical allocation are minor away from wildfires. Therefore, we focus our evaluation on California monitors. Figure 6-11 shows scatter plots of 24-hour average $PM_{2.5}$ performance for RAVE1.0 with Sofiev (left) and RAVE1.0 with PBL500 (right) plume top heights at all AQS monitors in California during July-August 2021. While the PBL500 scheme decreases bias (Sofiev NMB: -26%; PBL500 NMB: -9%), it degrades error (Sofiev NME: 53%; PBL500 NME: 60%). Examination of the scatter plots show more frequent substantial $PM_{2.5}$ overestimations in the PBL500 run compared to Sofiev. The Sofiev algorithm calculates plume top heights well into the free troposphere for fires with the highest intensity (FRP; Ramboll, 2023). The PBL500 scheme sets plume top heights to 500 m above the PBL height for all fires, including the most intense fires. This results in more smoke near the surface for the largest fires in the PBL500 scheme resulting in large PM2.5 overestimations for the highest modeled daily concentrations. We recommend using the Sofiev vertical allocation for more realistic characterization vertical allocation of fire emissions.

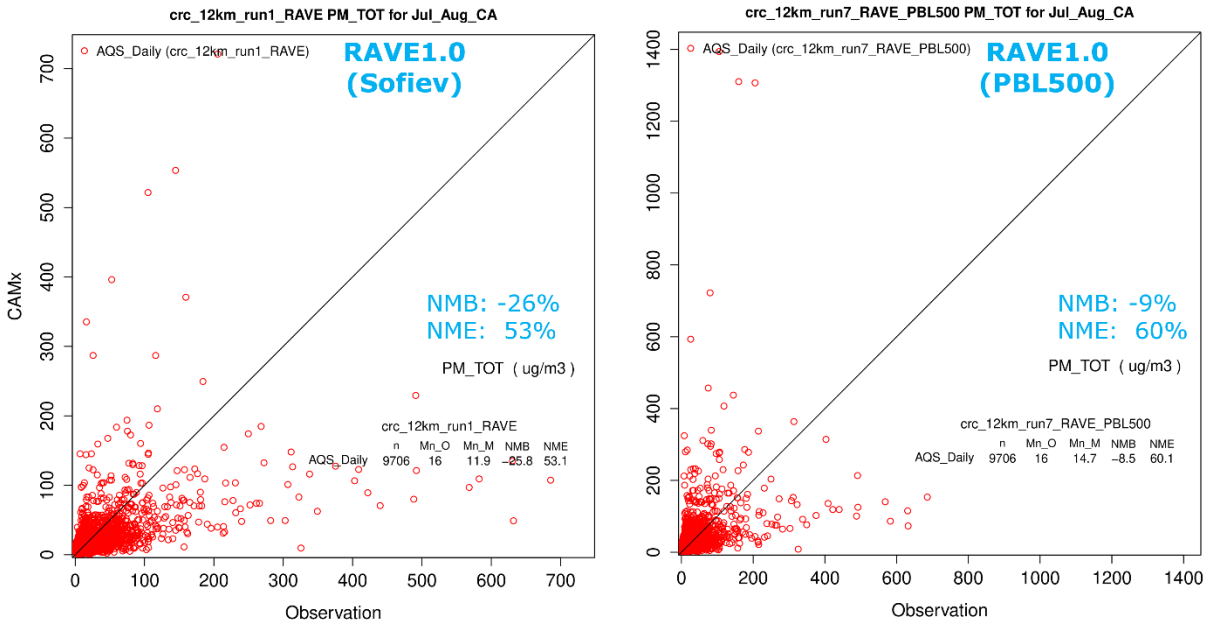

Figure 6-11. Scatter plots showing 24-hour average $PM_{2.5}$ performance for RAVE1.0 with Sofiev (left) and RAVE1.0 with PBL500 (right) plume top heights at all AQS monitors in California during July-August 2021 (note that the scale of the axis for the PBL500 scatterplot is twice that for the Sofiev scatterplot).

[37] https://sites.google.com/view/rave-emission/diurnal-cycles?authuser=1

The FEI processor's temporal allocation schemes distribute daily fire emissions to hourly emissions using a defined diurnal profile. There are currently two options in the FEI processor: 1) default: constant diurnal profile for all landcover types and 2) RAVE landcover: applies landcover-specific diurnal profiles developed from 5-minute FRP measurements by the RAVE team[38]. Because the RAVE product contains hourly emissions, the temporal allocation step is bypassed for RAVE. In Phase I, all FEI runs used the RAVE landcover-based temporal allocation. In Phase III, we developed an alternate set of FEER1.0 fire emissions that used the default (fixed) diurnal profile for all landcover types. Figure 6-12 shows scatter plots of 24-hour average $PM_{2.5}$ performance for FEER1.0 with the RAVE temporal allocation (left) and FEER1.0 with default (fixed) temporal allocation (right) at all AQS monitors in California during July-August 2021. The default temporal allocation appears to have more frequent large $PM_{2.5}$ underestimates, but also reduces some of the larger $PM_{2.5}$ overestimates. This results in a degradation in bias (RAVE temporal NMB: -15%; default temporal NMB: -25%), but slight improvement in error (RAVE temporal NME: 57%; default temporal NME: 54%). We recommend tracking the development of the landcover-specific diurnal profiles by the RAVE team, as these are likely to be refined in the future. Further testing with alternate FEIs and time periods could also help to better understand the strengths and weaknesses of each temporal allocation option and highlight areas for improvement.

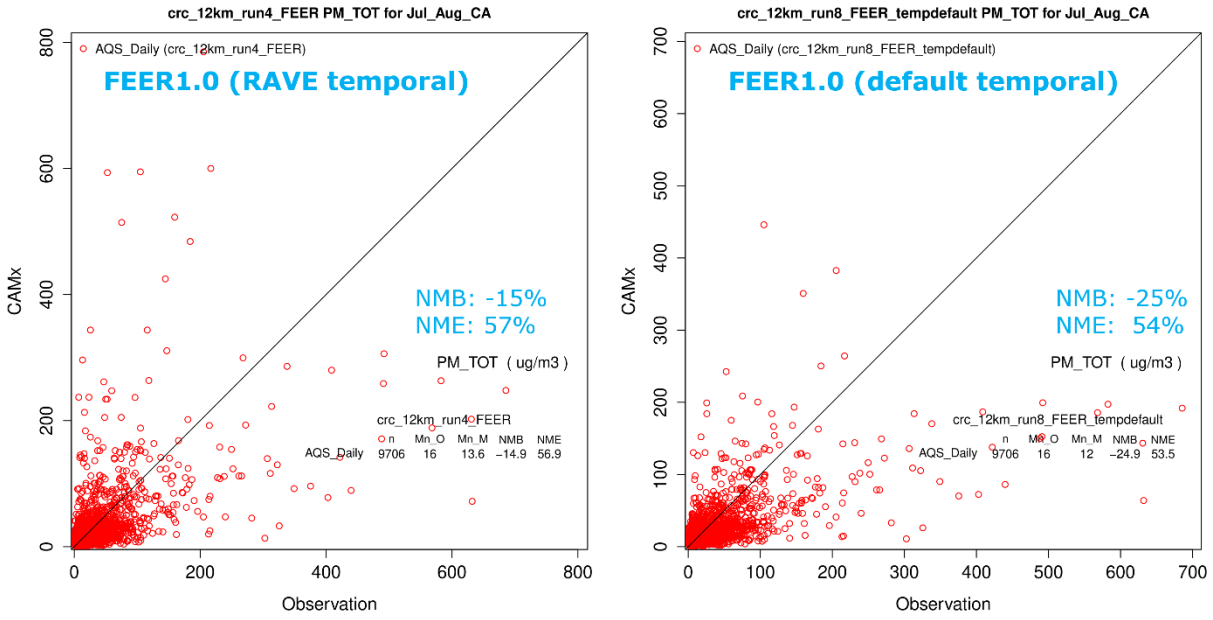

Figure 6-12. Scatter plots showing 24-hour average $PM_{2.5}$ performance for FEER1.0 with RAVE (left) and FEER1.0 with default (right) temporal allocation at all AQS monitors in California during July-August 2021.

[38] https://sites.google.com/view/rave-emission/diurnal-cycles?authuser=1

6.5.3 Phase IV: RAVE2.0 Evaluation

In May 2024, all re-processed RAVE1.0 emissions were updated to RAVE2.0. One advantage of RAVE2.0 is that it covers nearly all North America and the entirety of the CAMx 36 km domain. However, due to the timing of the RAVE2.0 release, we could only process and evaluate RAVE2.0 emissions for the CAMx 12 km domain. As with Phases II and III, we generated RAVE2.0 emissions for the July – August 2021 sensitivity period. RAVE2.0 emissions contain optional "scaled" emission species for primary $PM_{2.5}$, organic carbon (OC), and black carbon (BC), which the RAVE team developed for NOAA forecasting applications. We used these scaled aerosol emissions species in the RAVE2.0 fire emissions for the CAMx sensitivity simulation. These aerosol emissions are higher than the equivalent aerosol emission species as provided in the RAVE1.0 product. Figure 6-13 shows scatter plots of 24-hour average $PM_{2.5}$ concentrations for the RAVE1.0 FEI run (left panel) and the RAVE2.0 FEI run (right panel) across all AQS monitors during July – August 2021. The agreement with observations is made much poorer by updating to RAVE2.0 with the scaled aerosol emissions. In Figure 6-14, we present the same scatter plots, but for MDA8 ozone. The bias and error statistics do not change much, which suggests that the emissions species other than the scaled aerosol emissions did not change substantially from RAVE1.0. The downward shift in the highest MDA8 ozone concentrations predicted by the model from RAVE1.0 to RAVE2.0 is likely the result of smoke shading from the increased aerosol loading in the RAVE2.0 run that reduces photolysis rates. We recommend using the original, unscaled aerosol emissions with the RAVE2.0 FEI that are comparable to the RAVE1.0 FEI that produced the best model performance.

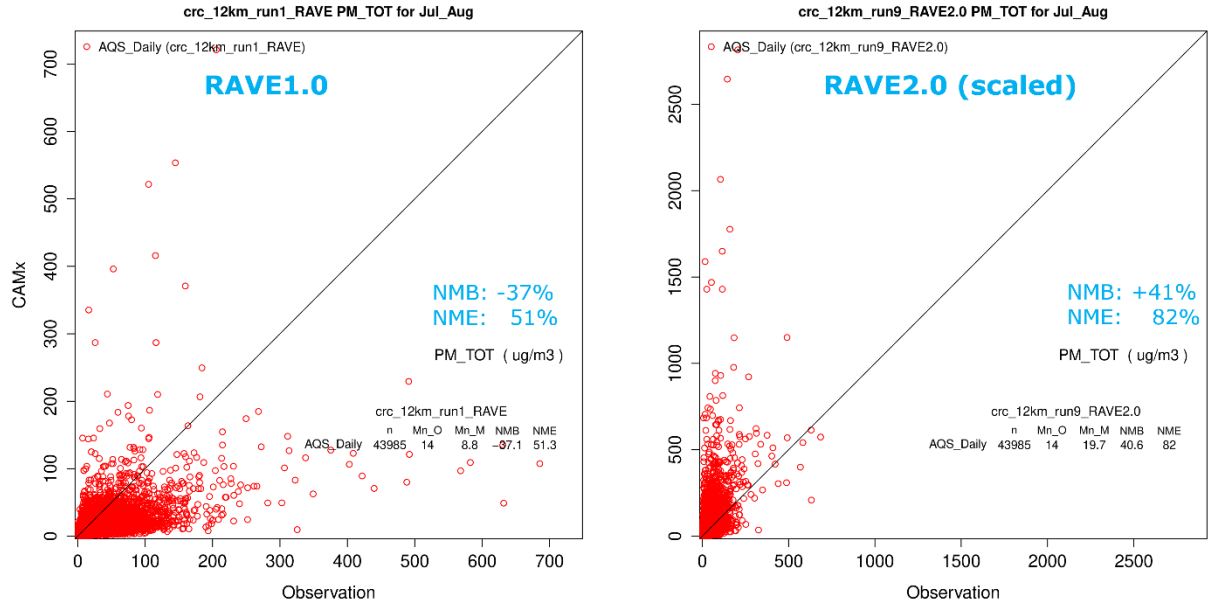

Figure 6-13. Scatter plots showing 24-hour $PM_{2.5}$ performance for RAVE1.0 (left) and RAVE2.0 with scaled aerosol emissions (right) at all AQS monitors in 12 km domain during July-August 2021 (note that the scale of the axis for the RAVE2.0 plot is over 3 times that of the RAVE1.0 plot).

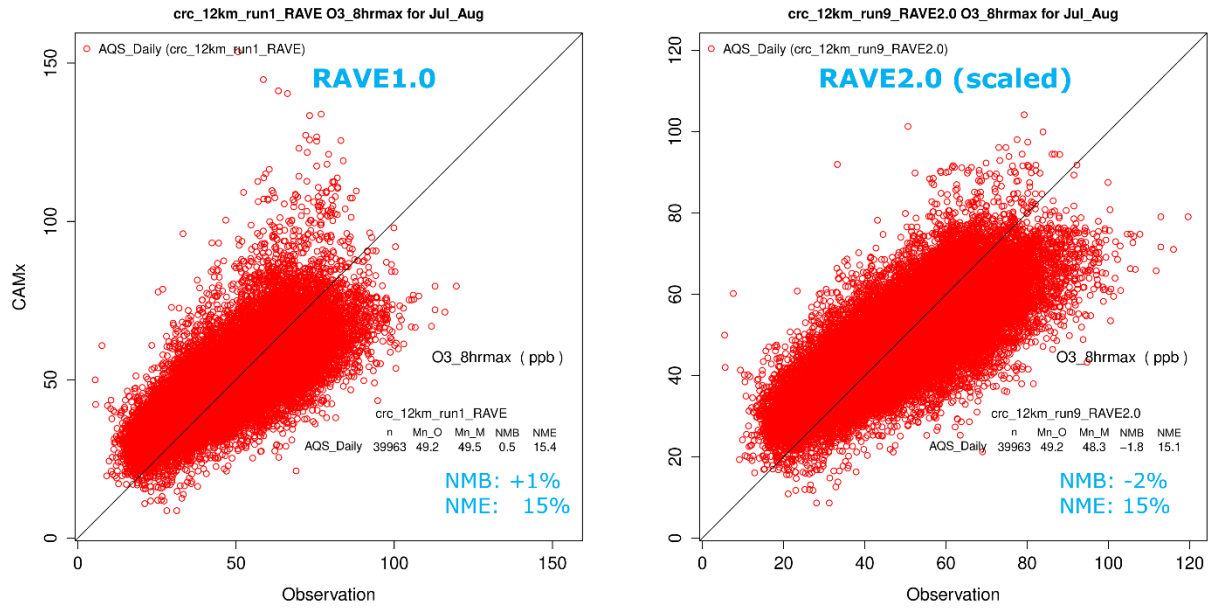

Figure 6-14. Scatter plots showing MDA8 ozone performance for RAVE1.0 (left) and RAVE2.0 with scaled aerosol emissions (right) at all AQS monitors in 12 km domain during July-August 2021.

6.5.4 Phase V: SOAP3 and Unscaled RAVE2.0 Evaluation

For Phase V, we generated RAVE2.0 emissions for the July – August 2021 sensitivity period using the unscaled emission species for primary $PM_{2.5}$, organic carbon (OC), and black carbon (BC) due to the poor $PM_{2.5}$ performance we found when using the scaled PM emission species. We also mapped the primary organic aerosol emissions (model species "POA") to "POA_BB" for compatibility with the new SOAP3 scheme in CAMx. We did not rename POA species for anthropogenic source sectors, so they were not treated by SOAP3 for these simulations and therefore the SOAP3 evaporative effects we evaluated are limited to biomass burning only.

We then used these updated RAVE2.0 fire emissions for two CAMx sensitivity simulations: 1) CAMx v7.30 with SOAP3, excluding evaporation of POA to SVOC (run11 in Table 6-3); and 2) CAMx v7.30 with SOAP3, including evaporation of POA to SVOC (run10 in Table 6-3). In the following figures, we evaluate performance for elemental carbon (EC) to evaluate emissions updates from RAVE1.0 to unscaled RAVE2.0. We examined organic carbon (OC) and $PM_{2.5}$ performance to evaluate both RAVE2.0 emissions updates and SOAP3 evaporative effects. Additionally, we evaluated MDA8 ozone and other speciated $PM_{2.5}$ impacts (nitrate, ammonium, sulfate, and other $PM_{2.5}$) as part of Phase V, but they are all small, as expected, and not shown in this report.

Figure 6-15 shows scatter plots of 24-hour average Elemental Carbon (EC) concentrations for the RAVE1.0 FEI run (run1; left panel), the RAVE2.0 FEI run with SOAP3 excluding evaporation of POA to SVOC (run11; center panel), and RAVE2.0 FEI run with SOAP3 including evaporation of POA to SVOC (run10; right panel) across all AQS monitors in the 12 km domain during July – August 2021. We chose to examine EC because it is not affected by the SOAP3 updates. Comparing the left (run1) and center (run11) panels, the agreement with observations is made slightly better by updating to RAVE2.0 with the unscaled aerosol emissions. The center (run11) and right (run10) panels show nearly identical results because the evaporation of POA to SVOC does not affect EC, as expected.

Figure 6-16 shows the same scatter plots as in Figure 6-15, but for Organic Carbon (OC). Comparing the left (run1) and center (run11) panels, we find that RAVE2.0 (NMB: -15%; NME: 52%) exhibits better agreement with observations compared to RAVE1.0 (NMB: -47%; NME: 58%). While run11 uses SOAP3, it does not include evaporation of POA to SVOC and the resulting increased SOA yield from this process. Therefore, the better agreement in run11 must be due to differences resulting from the RAVE1.0 to RAVE2.0 emissions update, non-evaporative updates from SOAP2 to SOAP3, other updates from CAMx v7.20 to v7.30 or some combination of these factors. Comparing the center (run11) panel with the right (run10) panel, we find further improvement in bias (run11 NMB: -15%; run10: NMB -3%) and slight degradation in error (run11 NME: 52%; run10 NME: 55%) from including the evaporative effects of POA to SVOC.

Figure 6-17 shows the same scatter plots as in the previous figures, but for $PM_{2.5}$ concentrations. Comparing the left (run1) and center (run11) panels, we find that RAVE2.0 (NMB: -31%; NME: 50%) exhibits better agreement with observations compared to RAVE1.0 (NMB: -57%; NME: 51%). Comparing the center (run11) panel with the right (run10) panel, we find further improvement in bias (run11 NMB: -31%; run10: NMB -19%) and similar error (run11 NME: 50%; run10 NME: 51%) from including the evaporative effects of POA to SVOC.

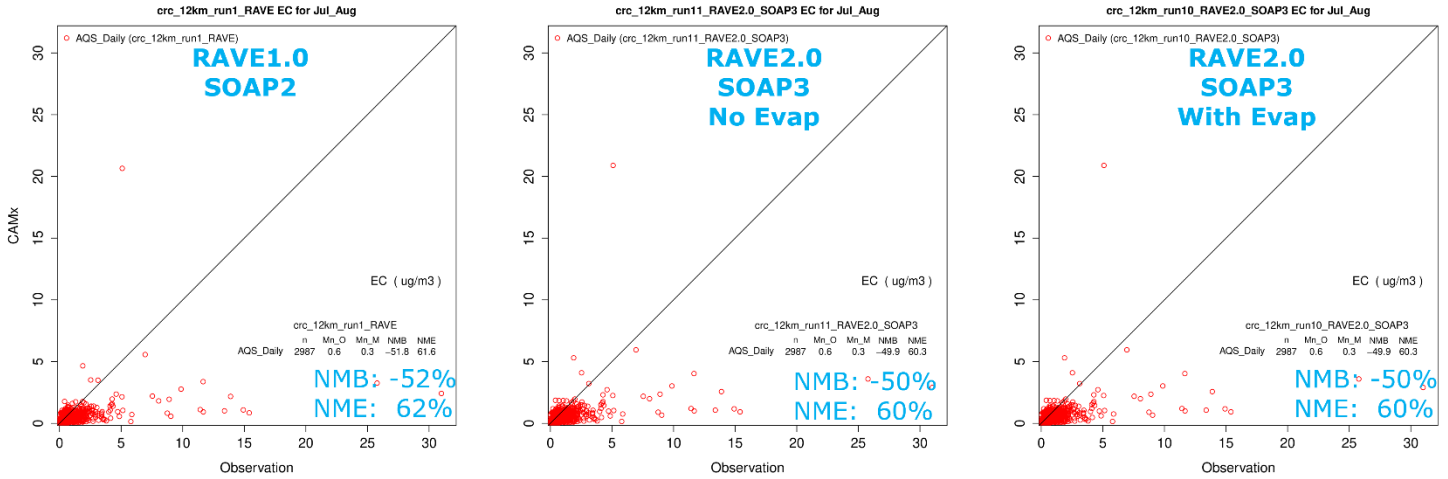

Figure 6-15. Scatter plots showing 24-hour Elemental Carbon (EC) performance for RAVE1.0 (left), RAVE2.0 with SOAP3 (no evaporation of POA to SVOC; center), and RAVE2.0 with SOAP3 (including evaporation of POA to SVOC; right) at all AQS monitors in 12 km domain during July-August 2021.

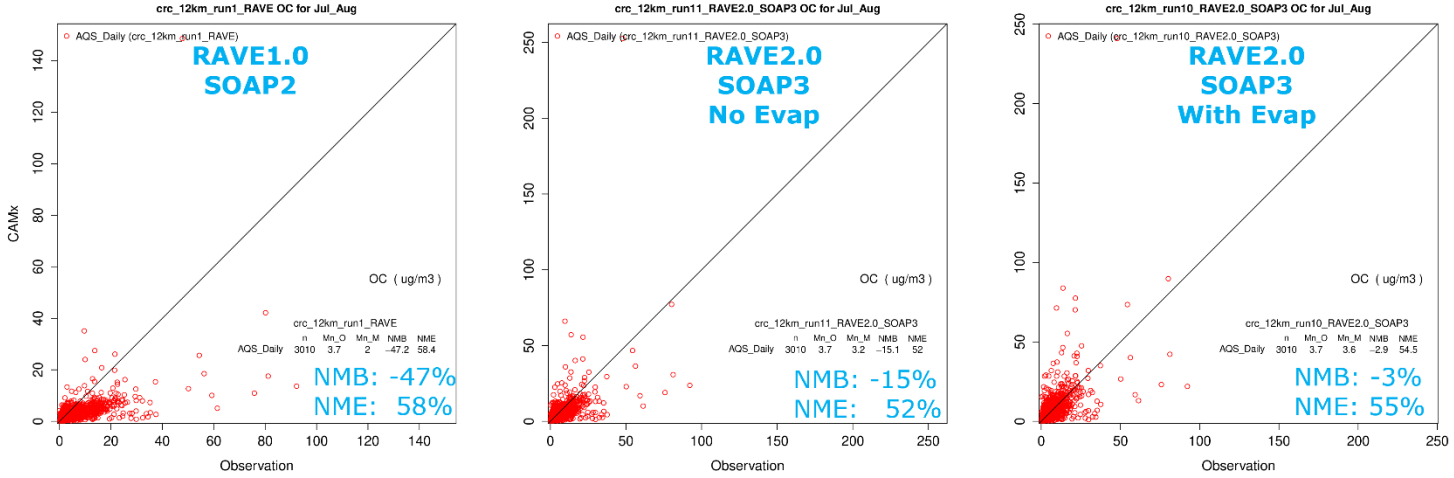

Figure 6-16. Scatter plots showing 24-hour Organic Carbon (OC) performance for RAVE1.0 (left), RAVE2.0 with SOAP3 (no evaporation of POA to SVOC; center), and RAVE2.0 with SOAP3 (including evaporation of POA to SVOC; right) at all AQS monitors in 12 km domain during July-August 2021.

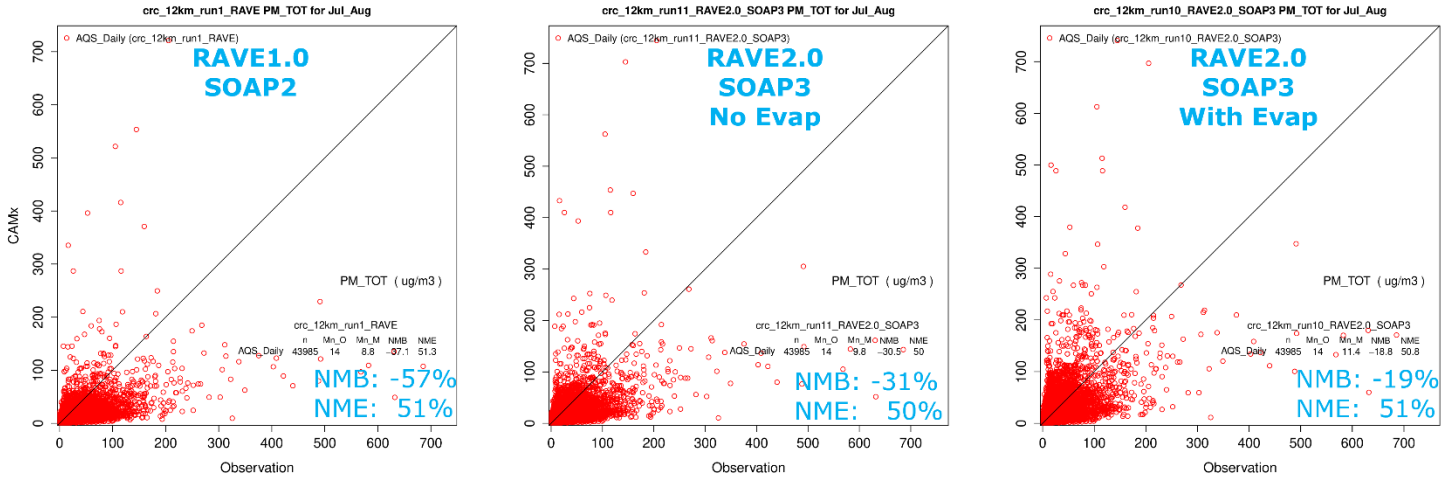

Figure 6-17. Scatter plots showing 24-hour $PM_{2.5}$ performance for RAVE1.0 (left), RAVE2.0 with SOAP3 (no evaporation of POA to SVOC; center), and RAVE2.0 with SOAP3 (including evaporation of POA to SVOC; right) at all AQS monitors in 12 km domain during July-August 2021.

7.0 CONCLUSIONS AND RECOMMENDATIONS

As part of this study, Ramboll updated its Python FEI processor to include RAVE1.0, a new FEI that possesses a unique combination of high temporal and spatial resolution that appears well-suited for high-resolution photochemical modeling. Using this processor, Ramboll developed model-ready fire emissions for all five available fire inventories (RAVE1.0, GFAS1.2, QFED2.5, FEER1.0 and FINN2.5) and analyzed CAMx ozone and $PM_{2.5}$ model performance during the active Western U.S. wildfire season during June-September 2021. This analysis revealed superior ozone and $PM_{2.5}$ performance for RAVE1.0 compared to the other four FEIs. We therefore selected RAVE1.0 as the first choice to evaluate further fire emission sensitivities including NOx speciation and vertical allocation. We selected an additional inventory as the second-best performing FEI – FEER1.0 – to evaluate temporal allocation. While the ozone and $PM_{2.5}$ performance impacts from these emission sensitivities were minor, of the alternatives evaluated we recommend the rapid NOx speciation, Sofiev vertical allocation and RAVE landcover-specific temporal allocation.

In April 2024, RAVE1.0 emissions were replaced with a newer version, RAVE2.0 covering summer 2021. This version expands the domain extent from the continental U.S. to North America and makes other improvements including refinements to FRP based on updated satellite measurements. RAVE2.0 contains optional "scaled" emission species for primary $PM_{2.5}$, organic carbon (OC), and black carbon (BC), which the RAVE team developed for NOAA forecasting applications. These aerosol emissions are higher than the equivalent aerosol emission species as provided in the RAVE1.0 product. We used these scaled aerosol emissions species in RAVE2.0 for a new CAMx sensitivity and compared it with the RAVE1.0 simulation. The use of the scaled aerosol emissions in RAVE2.0 led to large $PM_{2.5}$ overestimations compared to RAVE1.0, but ozone performance was similar. We then conducted further testing with RAVE2.0 using the unscaled aerosol emissions and found slightly improved performance compared to RAVE1.0. Finally, we evaluated the impact of SOAP3 evaporative effects on primary organic aerosol (POA) and found the increased secondary organic aerosol (SOA) yield helped reduce underestimations of organic aerosol and $PM_{2.5}$.

The following are the recommended configuration for modeling wildfire emissions in PGM modeling using the near-real time (NRT) and alternative FEIs evaluated in the CRC A-133 study:

- The rapid NOx speciation that speciate fire NOx emissions into less reactive species (e.g., nitric acid and PAN) in addition to NO and NO_2 is recommended over the default fire emissions speciation profile that just speciates fire NOx emissions into NO and NO_2;
- The Sofiev vertical allocation algorithm that uses Fire Radiative Power (FRP) to calculate plume rise is recommended over the PBL500 vertical allocation scheme;
- The RAVE landcover-specific temporal allocation approach for distributing fire emissions over the diurnal cycle is recommended over the default approach that is constant for all landcover types.
- Of the five FEIs that were initially evaluated, the RAVE1.0 generally produced the best ozone and $PM_{2.5}$ model performance and is recommended with the FEER1.0 producing the second best model performance. The FINN2.5 was the worst performing FEI.
- The RAVE2.0 FEI was released near the end of the study that included scaled $PM_{2.5}$ emissions that were evaluated in CAMx and produced large $PM_{2.5}$ overestimations. We conducted further evaluation of RAVE2.0 using the unscaled $PM_{2.5}$ emissions and found similar performance compared to RAVE1.0. Given the improvements of RAVE2.0, it is recommended over the other FEIs evaluated in this study provided the unscaled $PM_{2.5}$ emissions are used.

- Use SOAP3 available in CAMx v7.30+ with POA fire emissions renamed to POA_BB to characterize the evaporation of POA to semi-volatile organic compounds (SVOC) that form SOA.

Ramboll recommends four activities to improve the FEI processor:

- Investigate further refinements to NOx speciation, vertical and temporal allocation using the latest available fire emissions research.
- Evaluate available FEIs and alternatives in FEI processor for CAMx databases other than summer 2021, including EPA fire emissions (Bluesky) as available, and evaluate ozone and $PM_{2.5}$ model performance against observations.
- Develop model-ready fire emissions and modeling platform for summer 2023 using multiple FEIs to evaluate impacts of the Canadian wildfires on central and eastern U.S.

8.0 REFERENCES

Alvarado, M. et al., 2010. Nitrogen oxides and PAN in plumes from boreal fires during ARCTAS-B and their impact on ozone: an integrated analysis of aircraft and satellite observations. *Atmos. Chem. Phys.*, 10, 9739-9760. https://acp.copernicus.org/articles/10/9739/2010/acp-10-9739-2010.pdf.

Boylan, J. W. and A. G. Russell. 2006. PM and light extinction model performance metrics, goals, and criteria for three-dimensional air quality models. *Atmos. Env.* Vol. 40, Issue 26, pp. 4946-4959. August. (https://www.sciencedirect.com/science/article/pii/S1352231006000690).

Darmenov, A. and da Silva, A. 2015. The quick fire emissions dataset (QFED) – Documentation of versions 2.1, 2.2 and 2.4. NASA//TM-2015-104606, Vol. 38, NASA Global Modeling and Assimilation Office, 183 pp., https://gmao.gsfc.nasa.gov/pubs/docs/Darmenov796.pdf

Donahue, N.M., A.L. Robinson, C.O. Stanier, S.N. Pandis. 2006. Coupled partitioning, dilution, and chemical aging of semivolatile organics. *Environ. Sci. Technol.*, **40**, 2635-2643.

Emery, C.E., Z. Liu, A.G. Russell, M.T. Odman, G. Yarwood and N. Kumar. 2016. Recommendations on statistics and benchmarks to assess photochemical model performance. J. of the Air and Waste Management Assoc., Vol. 67, Issue 5. DOI: 10.1080/10962247.2016.1265027. (https://www.tandfonline.com/doi/full/10.1080/10962247.2016.1265027).

EPA. 2016. Treatment of data influenced by Exceptional Events. Federal Register / Vol. 81, No. 191 / Monday, October 3, 2016 / Rules and Regulations. https://www.epa.gov/sites/default/files/2018-10/documents/exceptional_events_rule_revisions_2060-as02_final.pdf.

EPA. 2019. Meteorological Model Performance for Annual 2016 Simulation WRF v3.8. U.S. Environmental Protection Agency, Office of Air Quality Planning and Standards, Air Quality Assessment Division, Research Triangle Park, NC. EPA-454/R-19-010. (https://www3.epa.gov/ttn/scram/reports/Met_Model_Performance-2016_WRF.pdf).

EPA. 2023a. Technical Support Document (TSD): Preparation of Emissions Inventories for the 2016v3 North American Emissions Modeling Platform. U.S. Environmental Protection Agency, Office of Air Quality Planning and Standards, Air Quality Assessment Division, Research Triangle Park, NC. EPA-454/B-23-002. January. (https://www.epa.gov/system/files/documents/2023-03/2016v3_EmisMod_TSD_January2023_1.pdf).

EPA. 2023b. Air Quality Modeling Final Rule Technical Support Document – 2015 Ozone NAAQS Good Neighbor Plan. U.S. Environmental Protection Agency, Office of Air Quality Planning and Standards. (https://www.epa.gov/system/files/documents/2023-03/AQ%20Modeling%20Final%20Rule%20TSD.pdf).

Homer, C., Dewitz, J., Yang, L., Jin, S., Danielson, P., Xian, G., Coulston, J., Herold, N., Wickham, J. and Megown, K., 2015. Completion of the 2011 National Land Cover Database for the conterminous United States–representing a decade of land cover change information. Photogrammetric Engineering & Remote Sensing, 81(5), pp.345-354.

Huang, L., Wu, Z., Liu, H., Yarwood, G., Huang, D., Wilson, G., Chen, H., Ji, D., Tao, J., Han, Z. and Wang, Y., 2024. An improved framework for efficiently modeling organic aerosol (OA) considering primary OA evaporation and secondary OA formation from VOCs, IVOCs, and SVOCs. Environmental Science: Atmospheres.

Ichoku, C. and Ellison, L. 2014. Global top-down smoke-aerosol emissions estimation using satellite fire radiative power measurements, Atmos. Chem. Phys., 14, 6643–6667, https://doi.org/10.5194/acp-14-6643-2014.

Jaffe, D., N. Wigder, N. Downey, G. Pfister, A. Boynard, and S. Reid. 2013. Impact of wildfires on ozone exceptional events in the western U.S. *Environ. Sci. Technol.* 47, 19, 11065-11072. https://pubs.acs.org/doi/abs/10.1021/es402164f.

Jaffe, D., S. O Neill, N. Larkin, A. Holder, D. Peterson, J. Halofsky, and A. Rappold. 2020. Wildfire and prescribed burning impacts on air quality in the United States. *Journal of the Air & Waste Management Association.* 70(6): 583-615. https://doi.org/10.1080/10962247.2020.1749731.

Jaffe, D., B. Schnieder and D. Inouye. 2022. Technical note: Use of PM2.5 to CO ratio as a tracer of wildfire smoke in urban areas. *Atmosphere Chemistry and Physics.* https://acp.copernicus.org/preprints/acp-2022-138/acp-2022-138.pdf.

Kaiser, J. W., Heil, A., Andreae, M. O., Benedetti, A., Chubarova, N., Jones, L., Morcrette, J.-J., Razinger, M., Schultz, M. G., Suttie, M., and van der Werf, G. R. 2012. Biomass burning emissions estimated with a global fire assimilation system based on observed fire radiative power, Biogeosciences, 9, 527–554, https://doi.org/10.5194/bg-9-527-2012.

Li, F., X. Zhang, S. Kondragunta, X. Lu, I. Csiszar, C. C. Schmidt. 2022. Hourly biomass burning emissions product from blended geostationary and polar-orbiting satellites for air quality forecasting applications. Remote Sensing of Environment. https://doi.org/10.1016/j.rse.2022.113237.

Liang, J., and D. Jaffe. 2019. Wildfires are causing extreme PM concentrations in the western United States. Air & Waste Management Association *EM Magazine*. June. https://pubs.awma.org/flip/EM-June-2019/jaffe.pdf.

Lin, J., D. Malia, and A. Kochanski. 2016. Exceptional Events Study: Final Report. University of Utah, Department of Atmospheric Studies. Salt Lake City, Utah. https://documents.deq.utah.gov/air-quality/planning/technical-analysis/research/exceptional-events/DAQ-2017-014408.pdf.

Malecha, K.T., Cai, Z. and Nizkorodov, S.A. 2018. Photodegradation of Secondary Organic Aerosol Material Quantified with a Quartz Crystal Microbalance. *Environmental Science & Technology Letters*, **5**(6), pp.366-371.

McDonald-Buller, E., Y. Kimura, C. Wiedinmyer, C. Emery, Z. Liu and G. Yarwood. 2015. Targeted Improvements in the Fire INventory from NCAR (FINN) Model for Texas Air Quality Planning. Prepared for David Sullivan, Texas Air Quality Research Program and The University of Texas at Austin. August.

NASA, 2023. Ozone Mapping and Profiler Suite (OMPS) HTTPS site. https://ozonewatch.gsfc.nasa.gov/data/omps

NCAR, 2011. The Tropospheric Visible and Ultraviolet (TUV) Radiation Model web page. National Center for Atmospheric Research, Atmospheric Chemistry Division, Boulder, Colorado, https://www2.acom.ucar.edu/modeling/tropospheric-ultraviolet-and-visible-tuv-radiation-model.

Posner, L.N., G. Theodoritsi, A. Robinson, G. Yarwood, B. Koo, R. Morris, M. Mavko, T. Moore and S. Pandis. 2019. Simulation of Fresh and Chemically-Aged Biomass Burning Organic Aerosol. *Atmos. Env.* 196 (2019) 27-37.

Ramboll. 2022. Develop Tools to Process and Evaluate Options for Improved Fire Emission Inventories. Ramboll US Consulting, Inc., Novato CA. Prepared for the Texas Commission on Environmental Quality. June 24.

Ramboll, 2023. Fire Emission Inventory Processing. Prepared for the Texas Commission on Environmental Quality. June.

Ran, L., Gilliam, R., Binkowski, F. S., Xiu, A., Pleim, J., & Band, L. (2015). Sensitivity of the Weather Research and Forecast/Community Multiscale Air Quality modeling system to MODIS LAI, FPAR, and albedo. Journal of Geophysical Research: Atmospheres, 120(16), 8491-8511.

Randles, C. A., da Silva, A. M., Buchard, V., Colarco, P. R., Darmenov, A., Govindaraju, R., Smirnov, A., Holben, B., Ferrare, R., Hair, J., Dhinozuka, Y., and Flynn, C. J. 2017. The MERRA-2 aerosol reanalysis, 1980 onward. Part I: system description and data assimilation evaluation, J. Climate, 30, 6823–6850, https://doi.org/10.1175/JCLI-D-16-0609.1.

Rémy, S., Veira, A., Paugam, R., Sofiev, M., Kaiser, J. W., Marenco, F., Burton, S. P., Benedetti, A., Engelen, R. J., Ferrare, R., and Hair, J. W. 2017. Two global data sets of daily fire emission injection heights since 2003, Atmos. Chem. Phys., 17, 2921–2942, https://doi.org/10.5194/acp-17-2921-2017.

Rienecker, M. M., Suarez, M. J., Gelaro, R., Todling, R., Bacmeister, J., Liu, E., Bosilovich, M. G., Schubert, S. D., Takacs, L., Kim, G.-K., Bloom, S., Chen, J., Collins, D., Conaty, A., da Silva, A., Gu, W., Joiner, J., Koster, R. D., Lucchesi, R., Molod, A., Owens, T., Pawson, S., Pegion, P., Redder, C. R., Reichle, R., Robertson, F. R., Ruddick, A. G., Sienkiewicz, M., and Woollen, J. 2011. MERRA – NASA's Modern-Era Retrospective Analysis for Research and Applications, J. Climate, 24, 3624–3648.

Robinson, A.L., N.M. Donahue, M.K. Shrivastava, E.A. Weitkamp, A.M. Sage, A.P. Grieshop, T.E. Lane, J.R. Pierce, S.N. Pandis. 2007. Rethinking organic aerosols: semivolatile emissions and photochemical aging. *Science*, **315**, 1259-1262.

Simon, H., K. Baker and S. Phillips. 2012. Compilations and Interpretation of Photochemical Model Performance Statistics Published between 2006 and 2012. *Atmos. Env.* 61 (2012) 124-139. December. (http://www.sciencedirect.com/science/article/pii/S135223101200684X).

Sofiev, M., Ermakova, T., and Vankevich, R. 2012. Evaluation of the smoke-injection height from wild-land fires using remote-sensing data. Atmospheric Chemistry and Physics, 12(4), 1995–2006. https://doi.org/10.5194/acp-12-1995-2012.

Strader, R., F. Lurmann, and S.N. Pandis. 1999. Evaluation of secondary organic aerosol formation in winter. *Atmos. Environ.,* **33**, 4849-4863.

Theodoritsi, G.N., L.N. Posner, A.L. Robinson, G. Yarwood, B. Koo, R. Morris, M. Mavko, T. Moore and S.N. Pandis. Biomass Burning Organic Aerosol from Prescribed Burning and Other Activities in the United States. *Atmos. Env.* 25 July 2020, 11753. (https://www.sciencedirect.com/science/article/abs/pii/S1352231020304854?via%3Dihub).

Wiedinmyer, C., Y. Kimura, E. McDonald-Buller, L. Emmons, R. Buchholz, W. Tang, K. Seto, M. Joseph, K. Barsanti, A. Carlton and R. Yokelson. 2023. The Fire Inventory from NCAR version 2.5: an updated global fire emissions model for climate and chemistry applications. Geoscientific Model Development, Volume 16, Issue 13, 3873-3891. July 12. (https://gmd.copernicus.org/articles/16/3873/2023/).

APPENDIX A

FEI EMISSIONS COMPARISON MAPS AND SUMMARIES

APPENDIX A: FEI EMISSIONS COMPARISON MAPS AND SUMMARIES

In this Appendix, we provide spatial maps of fire emissions for the five FEIs in Figure A-1 (VOC), Figure A-2 ($PM_{2.5}$) and Figure A-3 (CO). We provide bar charts comparing FEI emissions estimates and five-FEI averages for the ten case study wildfires in Figure A-4 (VOC), Figure A-5 ($PM_{2.5}$) and Figure A-6 (CO).

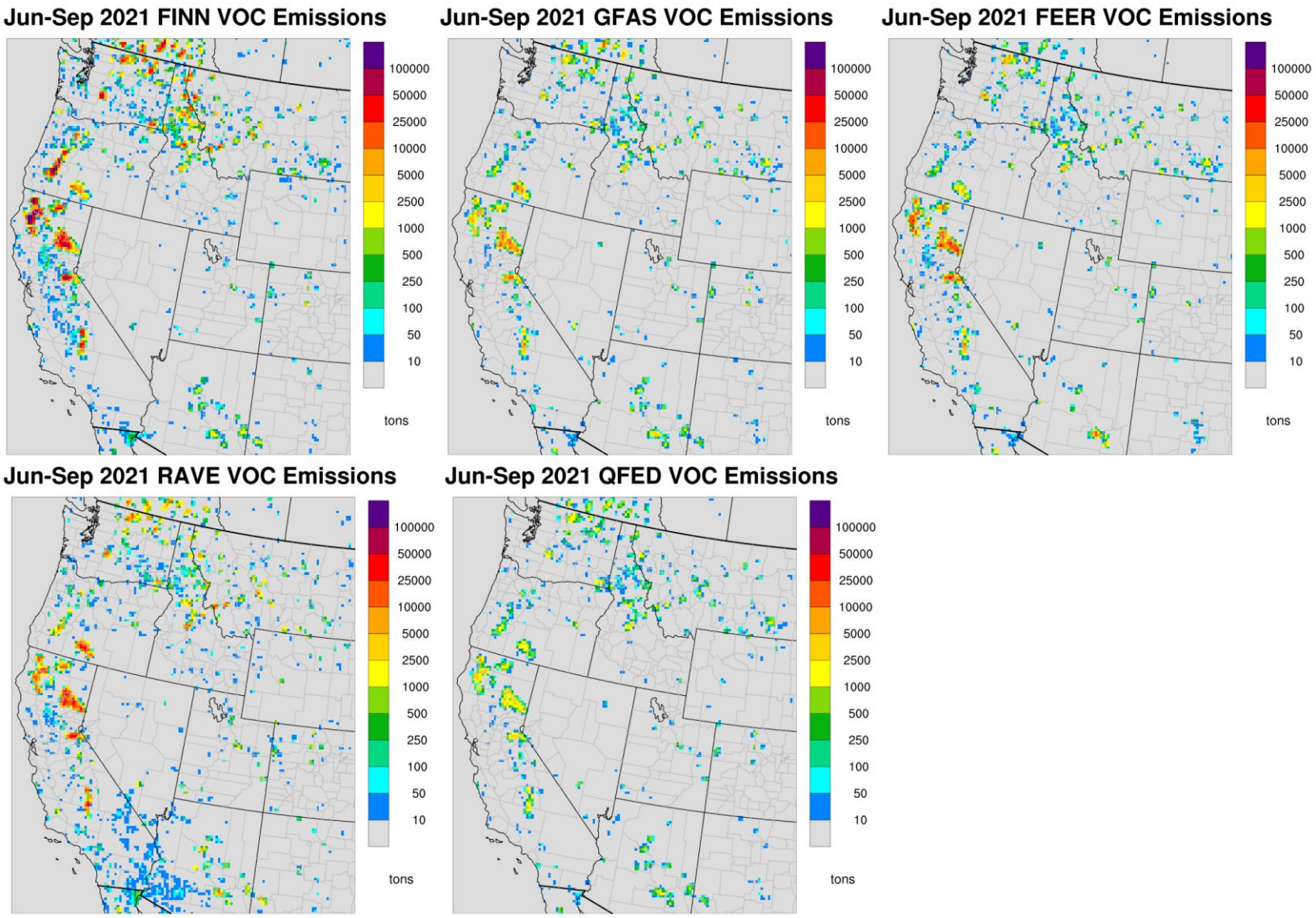

Figure A-1. VOC emissions for June – September 2021 across a subsection of the western 12 km CAMx domain for FINN2.5 (top left), GFAS1.2 (top middle), FEER1.0 (top right), RAVE1.0 (bottom left) and QFED2.5 (bottom middle).

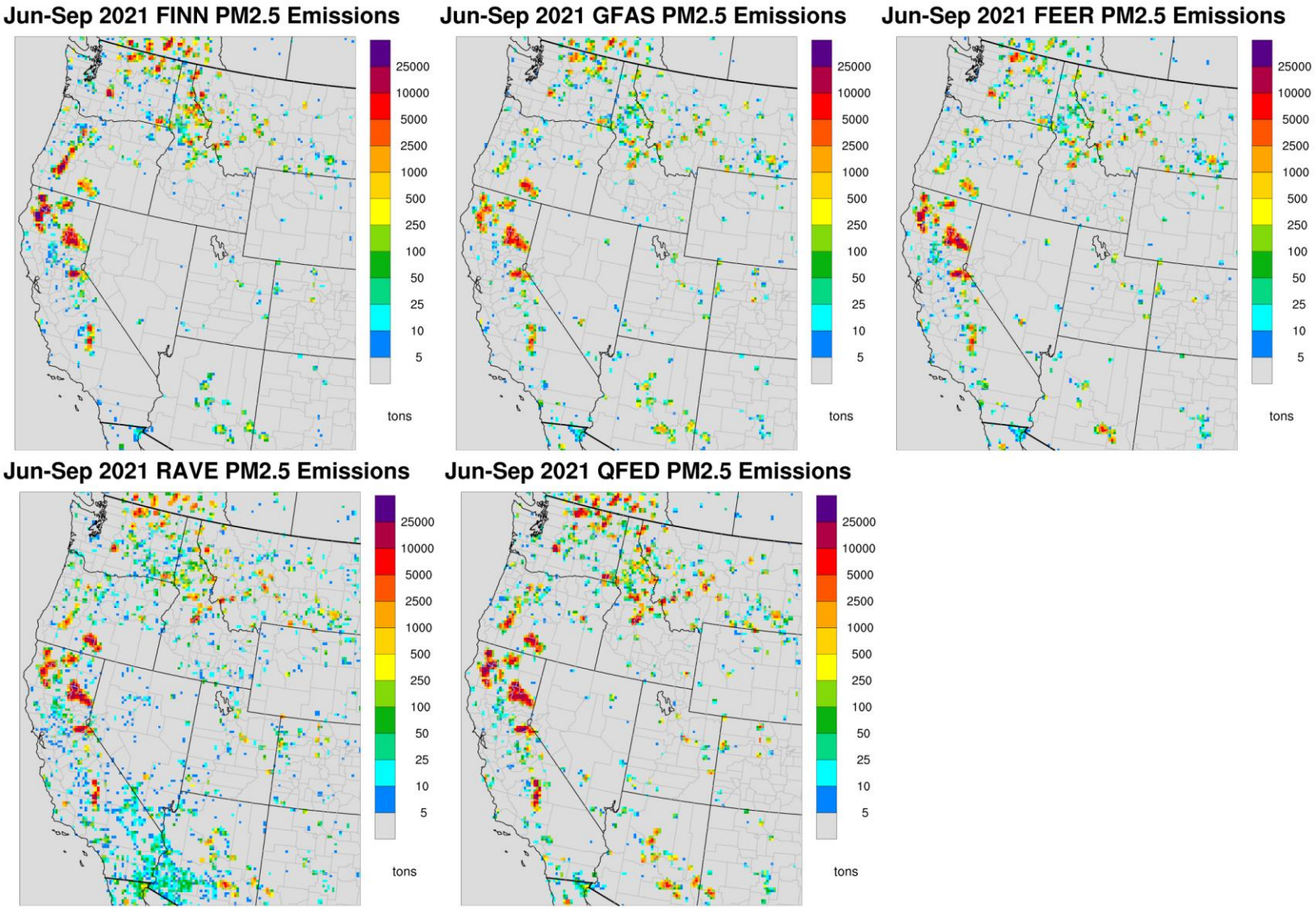

Figure A-2. $PM_{2.5}$ emissions for June – September 2021 across a subsection of the western 12 km CAMx domain for FINN2.5 (top left), GFAS1.2 (top middle), FEER1.0 (top right), RAVE1.0 (bottom left) and QFED2.5 (bottom middle).

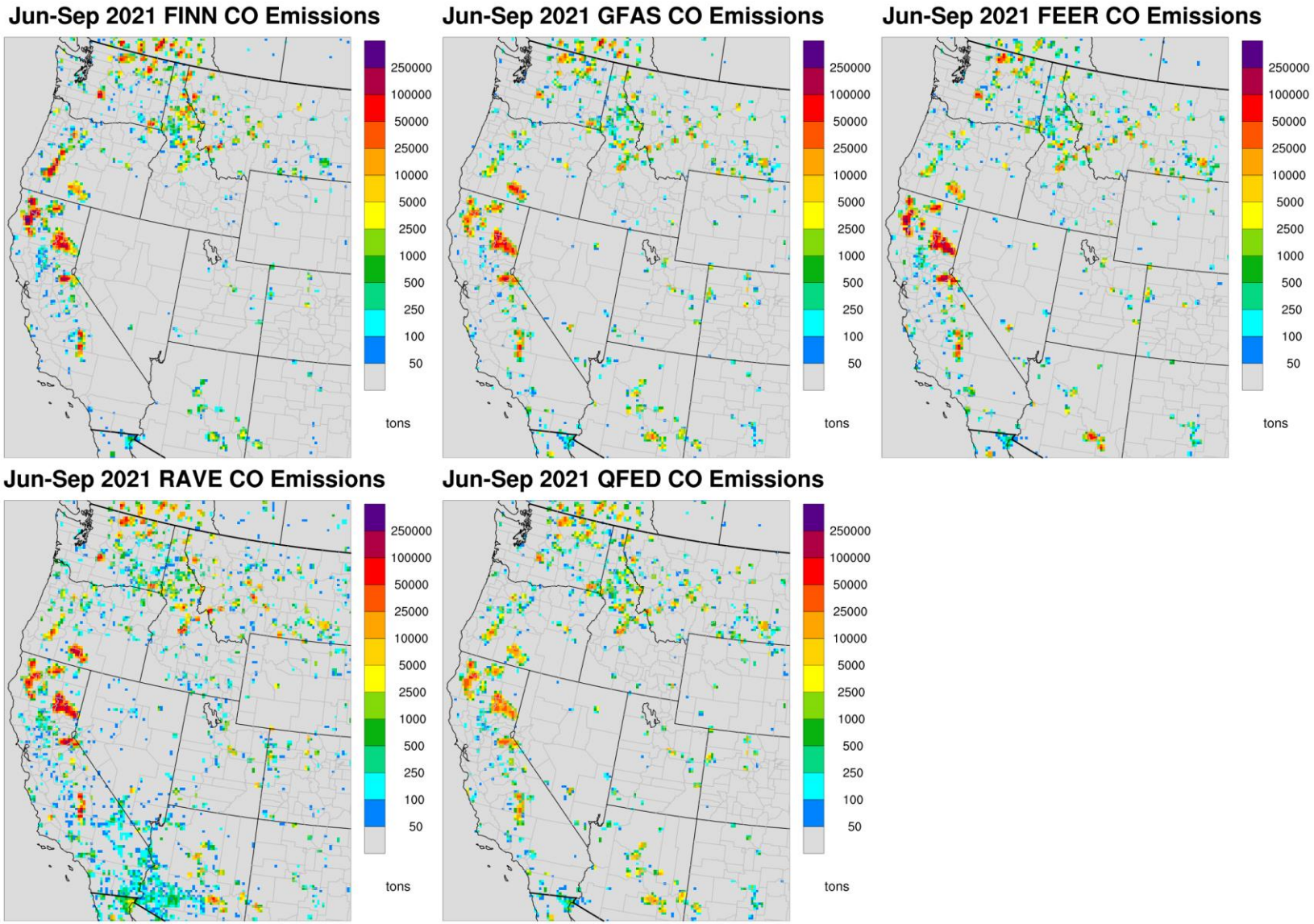

Figure A-3. CO emissions for June – September 2021 across a subsection of the western 12 km CAMx domain for FINN2.5 (top left), GFAS1.2 (top middle), FEER1.0 (top right), RAVE1.0 (bottom left) and QFED2.5 (bottom middle).

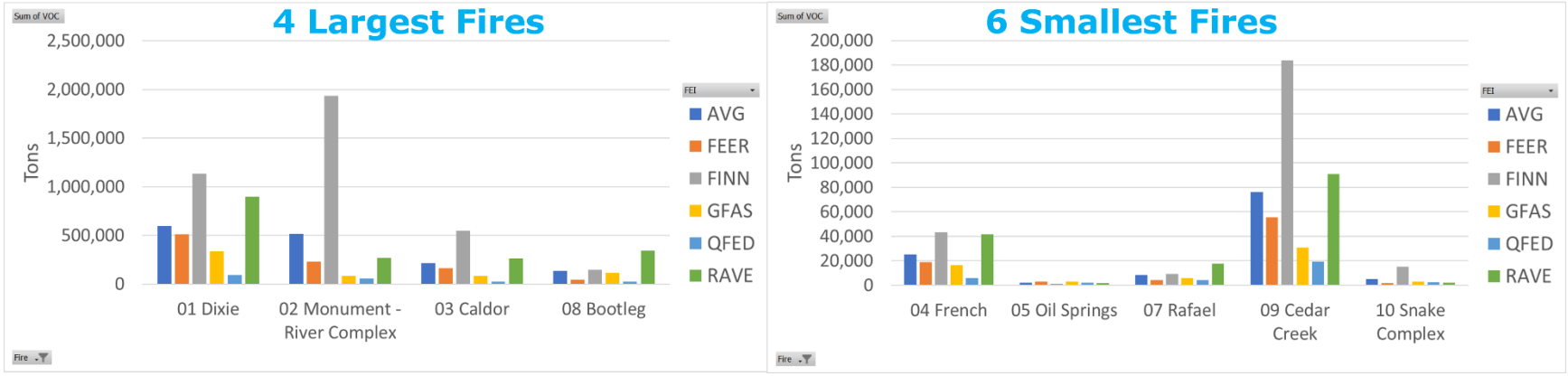

Figure A-4. VOC emissions for the ten case study fires for FEER1.0 (orange), FINN2.5 (grey), GFAS1.2 (yellow), QFED2.5 (light blue), RAVE1.0 (green) and 5-FEI average (dark blue). Emissions for largest four fires shown in left panel; six smallest fires shown in right panel.

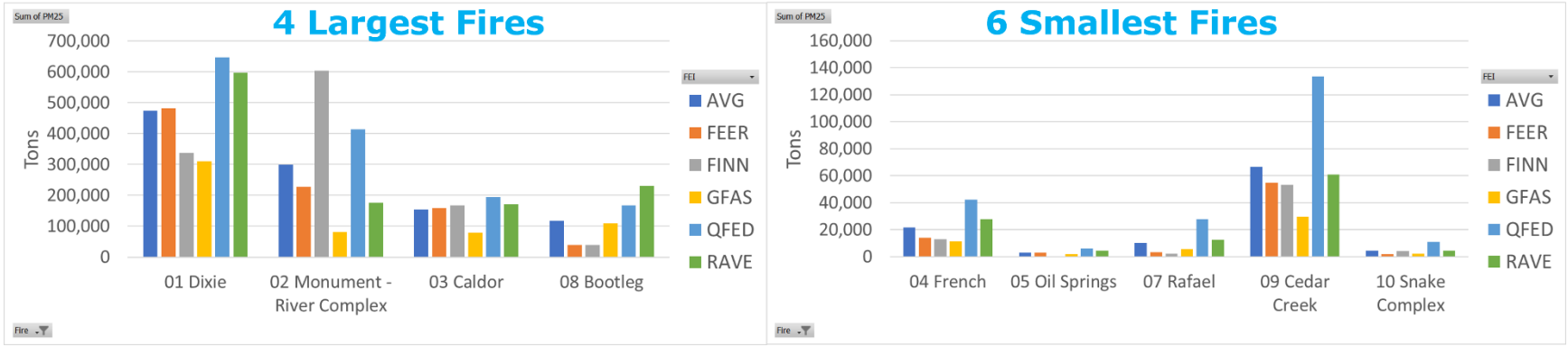

Figure A-5. $PM_{2.5}$ emissions for the ten case study fires for FEER1.0 (orange), FINN2.5 (grey), GFAS1.2 (yellow), QFED2.5 (light blue), RAVE1.0 (green) and 5-FEI average (dark blue). Emissions for largest four fires shown in left panel; six smallest fires shown in right panel

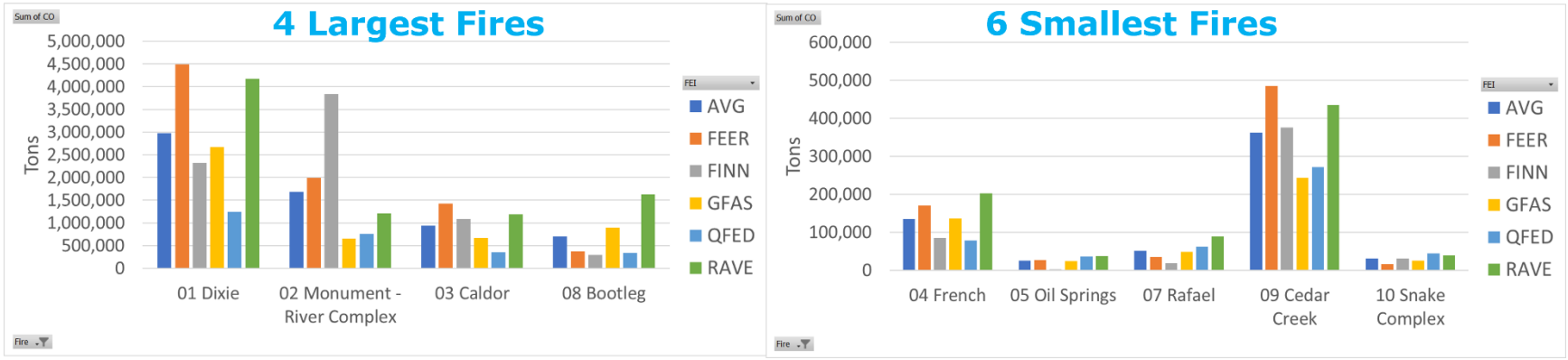

Figure A-6. CO emissions for the ten case study fires for FEER1.0 (orange), FINN2.5 (grey), GFAS1.2 (yellow), QFED2.5 (light blue), RAVE1.0 (green) and 5-FEI average (dark blue). Emissions for largest four fires shown in left panel; six smallest fires shown in right panel.